TECHNICAL DOCUMENTATION

LOCOMOTIVE RESPONSE MODEL

E. H. Chang
V. K. Garg
P. W. Hartmann

MATHEMATICAL MODEL

MATHEMATICAL MODEL

national Government-Industry
h Program on Track Train Dynamics

TECHNICAL DOCUMENTATION

LOCOMOTIVE RESPONSE MODEL

E. H. Chang
V. K. Garg
P. W. Hartmann

MATHEMATICAL MODEL

MATHEMATICAL MODEL

An International Government-Industry Research Program on Track Train Dynamics

1. REPORT NO.	2. REPORT DATE	3. PERIOD COVERED
R-295	February 1978	

4. TITLE AND SUBTITLE

TECHNICAL DOCUMENTATION, LOCOMOTIVE RESPONSE MODEL

5. AUTHOR(S)

E. H. Chang, V. K. Garg , and P. W. Hartmann

6. PERFORMING ORGANIZATION NAME AND ADDRESS

Association of American Railroads
3140 South Federal Street
Chicago, Illinois 60616

7. TYPE OF REPORT
Computer Program Documentation

8. CONTRACT OR GRANT NO.

9. SPONSORING AGENCY NAME AND ADDRESS

Association of American Railroads
3140 South Federal Street
Chicago, Illinois 60616

10. NO. OF PAGES
97

11. NO. OF REFERENCES
6

12. SUPPLEMENTARY NOTES

13. ABSTRACT

This report represents the technical manual documentation for the Locomotive Response Model, a mathematical model, for analyzing the dynamic response of a six-axle locomotive on tangent track, and is developed using a numerical integration technique. The locomotive is represented by a thirty-nine (39) degree-of-freedom model. The excitation includes vertical and lateral rail input. The wheel-rail interaction based on the linear theory proposed by Wicken, Joly and Blader is also considered in the model. The dynamic response of a representative six-axle locomotive subject to the selected vertical and/or lateral track irregularities is analyzed. The effects of primary and secondard stiffnesses on the dynamic characteristics of a locomotive are studied. It is also demonstrated that the model can be used as an effective tool in designing and selecting the "optimum" suspension system for the locomotive.

14. SUBJECT TERMS
dynamic response
numerical integration
time-domain analysis
tangent track

15. AVAILABILITY STATEMENT
Director Technical Center
Association of American Railroads
3140 South Federal Street
Chicago, Illinois 60616

Steering Committee for the Track Train Dynamics Program

Chairman
J. L. Cann
Vice President
Operations
Canadian National Railways

Vice Chairman
W. J. Harris, Jr.
Vice President
Research and Test Department
Association of American Railroads

E. F. Lind
Manager
Track Train Dynamics
Southern Pacific Transportation Co.

W. S. Autrey
Chief Engineer
Atchison, Topeka & Santa Fe Railway Co.

Peter Detmold
Chairman
Canadian Railway Advisory Committee

M. Ephraim
Chief Engineer
Electro Motive Division
General Motors Corporation

J. G. German
Vice President
Engineering
Missouri Pacific Co.

W. S. Hansen
President
A. Stucki Co.

S. B. Hobbs
Deputy Director
Systems Development
Department of Transportation
Transportation Systems Center

W. P. Manos
Vice President
Research and Development
Pullman-Standard

G. C. Martin
Assistant Director of
Rail & Equipment Technology
ConRail

E. R. Mathews
Director
Transportation Test Center
Federal Railroad Administration

R. A. Matthews
Vice President
Railway Progress Institute

W. McLaren
Chief Current Technology Division
Transport Canada-
Research & Development Centre

D. K. McNear
President
Southern Pacific Transportation Co.

L. A. Peterson
Director
Office of Rail Safety Research
Federal Railroad Administration

G. E. Reed
Director
Railroad Sales
AMCAR Division
ACF Industries

R. E. Rinehart
Manager, Systems Analysis
General Electric Company

D. V. Sartore
Chief Engineer Design
Burlington Northern, Inc.

J. J. Schmidt
Assistant Vice President
Equipment Engineering
National Railroad Passenger Corp.

P. S. Settle
Vice-President Commercial
Transportation Product Group
Portec, Inc.

W. W. Simpson
Vice President
Engineering
Southern Railway Company

W. K. Smith
Vice President and
Director of Transportation
General Mills, Inc.

***R. D. Spence** (Chairman)
President
ConRail

***L. S. Crane** (Chairman)
President and Chief
Executive Officer
Southern Railway Company

***D. Y. Clem**
President
McConway & Torley Corporation

***C. Bruce Ward**
President
Gunderson, Inc.

***Edward J. Ward**
Senior Railroad Transport Specialist
Transportation Research Board
National Research Council

***J. B. Stauffer**
Former Director
Transportation Test Center
Federal Railroad Administration

***R. G. Maughan**
Chairman
Railroad Advisory Committee
Transportation Development Agency

***Former members of this committee**

BACKGROUND INFORMATION on the TRACK-TRAIN DYNAMICS PROGRAM

The Track-Train Dynamics Program encompasses studies of the dynamic interaction of a train consist with track as affected by operating practices, terrain, and climatic conditions.

Trains cannot move without these dynamic interactions. Such interactions, however, frequently manifest themselves in ways climaxing in undesirable and costly results. While often differing and sometimes necessarily so, previous efforts to reasonably control these dyanmic interactions have been reflected in the operating practices of each railroad and in the design and maintenance specifications for track and equipment.

Although the matter of track-train dynamics is by no means a new phenomena, the increase in train lengths, car sizes and loadings has emphasized the need to reduce wherever possible excessive dynamic train action. This, in turn, requires a greater effort to achieve more control over the stability of the train as speeds have increased and railroad operations become more systemized.

The Track-Train Dynamics Program is representative of many new programs in which the railroad industry is pooling its resources for joint study and action.

A major planning effort on track-train dynamics was initiated in July 1971 by the Southern Pacific Transporation Company under Contract to the AAR and carried out with AAR staff support. Completed in early 1972, this paln clearly indicated that no individual railroad has both the resources and the incentive to undertake the entire program. Therefore, the AAR was authorized by its Board to proceed with the Track-Train Dynamics Program.

In the same general period, the FRA signaled its interest in vehicle dynamics by development of plans for a major test facility. The design of a track loop for train dynamic testing and the support of related research programs were also pursued by the FRA.

In organizing the effort, it was recognized that a substantial body of information and competence on this problem resided in the railroad supply industry and that significant technical and financial resources were available in government.

Through the Railway Progress Institute, the supply industry coordinated its support for this program and has made available men, equipment, data from earlier proprietary studies, and monetary contributions.

Through the FRA, contractor personnel and direct financial resources have been made available.

Through the Transportation Development Agency, the Canadian Government has made a major commitment to work on this problem and to coordinate that work with the United States' effort.

Through the Office de Recherches et D'Essais, the research arm of the Union Internationale des Chemins de Fer, the basis for a full exchange of information with European groups active in this field had been arranged.

The Track-Train Dynamics Program is managed by the Research and Test Department of the Association of American Railroads under the direction of an industry-government steering committee. Railroad emembers are designated by elected members of the AAR's Operation-Transportation General committee, supply industry members by the Railway Progress Institute, U. S. Government members by the Federal Railroad Administration, and Canadian Government members by the Transportation Development Agency. Appropriate task forces and advisory groups are established by the steering committee on an ad hoc basis, as encessary to pursue and resolve elements of the program.

The staff of the program comprises AAR employeed, personnel contributed on a full-or part-time basis by railroad or members of the supply industry, and personnel under contract to the Federal Railroad Administration or the Transportation Development Agency.

The program plan as presented in 1972 comprised:

1) Phase I -- 1972-1974

   Analysis of and interim action regarding the present dynamic aspects of track, equipment, and operations to reduce excessive train action.

2) Phase II -- 1974-1977

   Development of improved track and equipment specifications and operating practices to increase dynamic stability.

3) Phase III -- 1977-1982

   Application of more advanced scientific principles to railroad track, equipment, and operations to improve dynamic stability.

Phase I officially ended in December of 1974. The major technical elements of Phase I included:

a) The establishment of the dynamic characteristics of track and equipment.

b) The development and validation of mathematical models to permit the rapid analysis of the effects on dynamic stability of modifications in designs, maintenance, and use of equipment and track structures.

c) The development of interim guidelines for train handling, makeup, track structures, and engineer training to reduce excessive train action.

The attached report represents the Technical Manual documentation for the Locomotive Response Model, which was developed as an element of Task 10 TTD Phase II.

ACKNOWLEDGEMENT

This program was developed as part of an effort in Task #7, mathematical modelling of Phase I of the Track-Train Dynamics Research Program. The model has been developed by Mr. Edward H. Chang with technical advice and assistance from Mr. V. K. Garg, Manager Dynamics Division, AAR.

Also, the authors wish to acknowledge Mr. Edward F. Lind, Director, Phase I of the Track-Train Dynamics Research Program. Mr. Lind's leadership has been a major contributing factor to the entire success of the Track-Train Dynamics Research Program - A program which has and will continue ot produce significant contributions to the railroad industry for years to come.

TABLE OF CONTENTS

ABSTRACT

A mathematical model, for analyzing the dynamic response of a six-axle locomotive on tangent track, is developed using a numerical integration technique. The locomotive is represented by a thirty-nine (39) degree-of-freedom model. The excitation includes vertical and lateral rail input. The wheel-rail interaction based on the linear theory proposed by Wicken, Joly and Blader is also considered in the model. The dynamic response of a representative six-axle locomotive subject to the selected vertical and/or lateral track irregularities is analyzed. The effects of primary and secondary stiffnesses on the dynamic characteristics of a locomotive are studied. It is also demonstrated that the model can be used as an effective tool in designing and selecting the 'optimum' suspension system for the locomotive.

NOMENCLATURE

$\{U^b\}$	Carbody generalized displacements
$\{U^t\}$	Truck frame generalized displacements
$\{U^a\}$	Wheel-axle set generalized displacements
$[M^b]$	Mass matrix for carbody
$[M^t]$	Mass matrix for truck frame
$[M^a]$	Mass matrix for a wheel-axle set
$[M]$	Total mass matrix for the system
$[K]$	Total stiffness matrix for the system
$[C]$	Total damping matrix for the system
$[K_g]$	Lateral gravitational stiffness matrix
$[C_g]$	Damping matrix for creep force
m_B	Carbody mass
m_t	Truck frame mass
m_a	Wheel-axle set mass
I_B	Carbody yaw moment of inertia
I_t	Truck frame yaw moment of inertia
I_a	Wheel-axle set yaw moment of inertia
J_B	Carbody roll moment of inertia
J_t	Truck frame roll moment of inertia
J_a	Wheel-axle set roll moment of inertia
$\bar{J}_B$	Carbody pitch moment of inertia
$\bar{J}_t$	Truck frame pitch moment of inertia
K_{xt}	Longitudinal stiffness of secondary suspension per truck side.

K_{yt}	Vertical stiffness of secondary suspension per truck side
K_{zt}	Lateral stiffness of secondary suspension per truck side
K_{xa}	Longitudinal stiffness of primary suspension per axle side
K_{ya}	Vertical stiffness of primary suspension per axle side
K_{za}	Lateral stiffness of primary suspension per axle side
C_{xt}	Longitudinal damping of secondary suspension per truck side
C_{yt}	Vertical damping of secondary suspension per truck side
C_{zt}	Lateral damping of secondary suspension per truck side
C_{xa}	Longitudinal damping of primary suspension per axle side
C_{ya}	Vertical damping of primary suspension per axle side
C_{za}	Lateral damping of primary suspension per axle side
K_g^k	Lateral gravitational stiffness for kth wheel-axle set
C_g^k	Yaw gravitational stiffness for kth wheel-axle set
K_{yr}	Vertical rail stiffness
K_{zr}	Lateral rail stiffness
C_{yr}	Vertical rail damping
C_{zr}	Lateral rail damping
y^b	Carbody vertical displacement
z^b	Carbody lateral displacement
ϕ^b	Carbody roll
ψ^b	Carbody yaw

θ^b	Carbody pitch
y^t	Truck frame vertical displacement
z^t	Truck frame lateral displacement
ϕ^t	Truck frame roll
ψ^t	Truck frame yaw
θ^t	Truck frame pitch
y^a	Wheel-axle set vertical displacement
z^a	Wheel-axle set lateral displacement
ϕ^a	Wheel-axle set roll
ψ^a	Wheel-axle set yaw
a_1	Distance of axle 1 from truck 1 center of gravity
a_2	Distance of axle 2 from truck 1 center of gravity
a_3	Distance of axle 3 from truck 1 center of gravity
a_4	Distance of axle 4 from truck 2 center of gravity
a_5	Distance of axle 5 from truck 2 center of gravity
a_6	Distance of axle 6 from truck 2 center of gravity
b	Half distance between contact points of wheel treads and rails in lateral direction
b_1	Half lateral distance between primary suspension
b_2	Half lateral distance between secondary suspension
h_t	Height of truck frame center of gravity above axle center
h_1	Vertical distance, truck frame center of gravity to secondary suspension
h_2	Vertical distance, carbody center of gravity to secondary suspension
L_1	Distance between truck 1 and carbody center of gravity
L_2	Distance between truck 2 and carbody center of gravity

$\bar{L}$	Distance between truck center of gravity and secondary suspension
r	Wheel tread radius
V	Speed of locomotive
f_L	Lateral creep coefficient
f_T	Longitudinal creep coefficient
f_{s23}	Lateral spin creep coefficient
f_{s33}	Longitudinal spin creep coefficient
W	Axle load
L_R	Rail length
A_o^R	Amplitude of the right rail vertical irregularity
A_o^L	Amplitude of the left rail vertical irregularity
$\bar{A}_o^R$	Amplitude of the right rail lateral irregularity
$\bar{A}_o^L$	Amplitude of the left rail lateral irregularity.
ε	Rate of change of contact plane slope with respect to lateral displacement of wheel-axle set
λ	Effective conicity of wheels
ξ	Rate of change of distance between wheel-axle set center line and contact points with respect to lateral displacement of wheelsets
δ_o	Slope of contact point between wheel and rail at central position
θ	Value used in Wilson Θ integration technique.

LIST OF ILLUSTRATIONS

LIST OF TABLES

1. INTRODUCTION

1.1 General

The dynamic response of a locomotive has been a subject of great interest to locomotive designers, maintenance engineers as well as to track designers for many years. This interest is motivated by desires to improve ride qualities, to reduce wear and damage to locomotive and track components and, most important of all, to ensure safe operation. In the past, many simple or sophisticated analytical models have been developed for analyzing the dynamic behavior of railway vehicles. However, no extensive study has been devoted to the dynamic response of locomotives under deterministic track input. The ever-increasing trailing tonnage and higher operating speeds require that both the locomotive components and its suspension system be improved. Furthermore, safety specifications on the locomotive performance impose strigent design requirements. Consequently, an accurate response history of locomotives under various types of track input and operating conditions would be highly desirable. Thus, necessiated the development of the locomotive response model.

1.2 Objective

The objective of this study is to develop a mathematical model for a six-axle locomotive on tangent track using numerical integration techniques. A time-domain analysis computer program will be developed for analyzing the dynamic

response of a six-axle locomotive subject to various rail input. In addition to a better understanding of the dynamic behavior of a six-axle locomotive, the model will also provide the response information which may be useful to both practicing locomotive and track designers.

2. MATHEMATICAL MODEL AND METHOD OF SOLUTION

2.1 General

The dynamic behavior of a locomotive under track excitations can be analyzed by:

(a) developing a locomotive model with a proper choice of degrees of freedom describing the system in both vertical and lateral directions.

(b) considering the wheel-rail interaction.

In this section the theoretical development of a six-axle locomotive is presented first; then the wheel-rail interaction is considered using geometrical (effective conicity and gravitational stiffnesses) and dynamic (creep forces) relationships.

A kinematic model representing the six-axle locomotive system is shown in Figure 1. This model consists of a carbody, two truck frames and six wheel-axle sets. In the model, the wheel-axle sets and truck frames are connected together by a primary suspension system consisting of linear springs and viscous damping elements. Another set of linear springs and viscous damping elements, referred to as the secondary suspension system, is provided between the truck frames and carbody.

In the analyses, all displacements, are assumed to be small and the lateral clearance between the wheel-axle sets and truck frames has negligible effects on the locomotive response. In addition, non-linearities inherent in the suspension elements are assumed to be negligible.

In the model, the carbody, truck frames and wheel-axle sets are assumed to be rigid. The carbody and each truck frame are assigned five degrees of freedom corresponding to vertical, lateral , roll, yaw and pitch motions. Each wheel-set is provided with four degrees of freedom in the vertical, lateral, roll and yaw directions. Thus, the total number of degrees of freedom of the six-axle locomotive model is thirty-nine (39) (Table 1).

The equations of motion are derived by applying Lagrange's equation on the generalized coordinates. The following assumptions are made in deriving equations of motion for the model:

(a) The axles, truck frame and carbody are rigid and their stiffnesses are lumped into the suspension elements.

(b) The axles run freely in the journal bearing without bearing friction.

(c) No free lateral clearance between the wheel sets and truck frame exists.

(d) All displacements are assumed to be small.

(e) All springs are considered to be linear.

(f) Non-linearities resulting from suspension bottoming, wheel flange contact and dry friction in suspension elements are neglected.

2.2 Equation of Motion

With the coordinate system defined in Figure 2, the generalized displacements of a six-axle locomotive system can be given in matrix notation as

Carbody : $\{U^b\} = [y^b\ z^b\ \phi^b\ \psi^b\ \theta^b]^T$

Trucks : $\{U_j^t\} = [y_j^t\ z_j^t\ \phi_j^t\ \psi_j^t\ \theta_j^t]^T \quad , j = 1,2$

Axles : $\{U_k^a\} = [y_k^a\ z_k^a\ \phi_k^a\ \psi_k^a\ \ ]^T \quad , k = 1,6$

in which $[arg]^T$ indicates matrix transpose. The relative displacements between the carbody and the two trucks are:

$$\{U_1\} = [T_1^t]\ \{U_1^t\} - [T_1^b]\ \{U^b\} \tag{1}$$

$$\{U_2\} = [T_2^t]\ \{U_2^t\} - [T_2^b]\ \{U^b\} \tag{2}$$

Writing Eq(1) and Eq(2) in compact form yields

$$\{U_{B-T_j}\} = [T_j^t]\ \{U_j^t\} - [T_j^b]\ \{U^b\} \qquad j = 1,2 \tag{3}$$

where subscript B-Tj indicates the carbody and truck frame j and $\{U_1\}$ and $\{U_2\}$ are vectors representing the relative displacements, in the x, y and z direction, of the springs between the carbody and truck 1 (leading) and between the carbody and truck 2 (trailing) on the right and left side of the truck.

$$\{U_1\} = [U_{1R}^x\ U_{1R}^y\ U_{1R}^z\ U_{1L}^x\ U_{1L}^y\ U_{1L}^z]^T \tag{3a}$$

$$\{U_2\} = [U_{2R}^x\ U_{2R}^y\ U_{2R}^z\ U_{2L}^x\ U_{2L}^y\ U_{2L}^z]^T \tag{3b}$$

The $[T_1^b]$ and $[T_1^t]$ are the transfer matrices for the leading truck, $[T_2^b]$ and $[T_2^t]$ are the transfer matrices for the trailing truck, in expanded form as shown.

$$[T_1^b] = \begin{bmatrix} 0 & 0 & 0 & b_2 & h_2 \\ 1 & 0 & -b_2 & 0 & L_1 \\ 0 & 1 & -h_2 & -L_1 & 0 \\ 0 & 0 & 0 & -b_2 & h_2 \\ 1 & 0 & b_2 & 0 & L_1 \\ 0 & 1 & -h_2 & -L_1 & 0 \end{bmatrix} \quad (4a)$$

$$[T_2^b] = \begin{bmatrix} 0 & 0 & 0 & b_2 & h_2 \\ 1 & 0 & -b_2 & 0 & -L_2 \\ 0 & 1 & -h_2 & L_2 & 0 \\ 0 & 0 & 0 & -b_2 & h_2 \\ 1 & 0 & b_2 & 0 & -L_2 \\ 0 & 1 & -h_2 & L_2 & 0 \end{bmatrix} \quad (4b)$$

$$[T_1^t] = \begin{bmatrix} 0 & 0 & 0 & b_2 & -h_1 \\ 1 & 0 & -b_2 & 0 & \bar{L} \\ 0 & 1 & h_1 & -\bar{L} & 0 \\ 0 & 0 & 0 & -b_2 & -h_1 \\ 1 & 0 & b_2 & 0 & \bar{L} \\ 0 & 1 & h_1 & -\bar{L} & 0 \end{bmatrix} \quad (4c)$$

$$[T_2^t] = \begin{bmatrix} 0 & 0 & 0 & b_2 & -h_1 \\ 1 & 0 & -b_2 & 0 & -\bar{L} \\ 0 & 1 & h_1 & \bar{L} & 0 \\ 0 & 0 & 0 & -b_2 & -h_1 \\ 1 & 0 & b_2 & 0 & -\bar{L} \\ 0 & 1 & h_1 & \bar{L} & 0 \end{bmatrix} \quad (4d)$$

Similarly, the relative displacement vector between truck frame and the kth axle is

$$\{\bar{U}_k\} = [T^a]\{U_k^a\} - [T_k^a]\{U_1^t\} \tag{5}$$

where $k = 1, 2, 3$ denotes the leading truck axles. Also

$$\{\bar{U}_k\} = [T^a]\{U_k^a\} - [T_k^a]\{U_2^t\} \tag{6}$$

where k=4, 5, 6 and corresponds to trailing truck axles. Rewritting Eq.(5) and Eq.(6) in compact form yields

$$\{\bar{U}_{Tj-Ak}\} = [T^a]\{U_k^a\} - [T_k^a]\{U_j^t\} \quad \text{for } \begin{matrix} j=1,\ k=1,2,3 \\ j=2,\ k=4,5,6 \end{matrix} \tag{7}$$

The vector $\{\bar{U}_k\}$ represents the relative displacements, in the x, y and z directions, of the springs between the truck and axles on the right and left side of truck frame.

$$\{\bar{U}_k\} = [\bar{U}_{kR}^x \ \bar{U}_{kR}^y \ \bar{U}_{kR}^z \ \bar{U}_{kL}^x \ \bar{U}_{kL}^y \ \bar{U}_{kL}^z]^T \quad k = 1,6 \tag{8}$$

The transfer matrices are:

$$[T^a] = \begin{bmatrix} 0 & 0 & 0 & b_1 \\ 1 & 0 & -b_1 & 0 \\ 0 & 1 & 0 & 0 \\ 0 & 0 & 0 & -b_1 \\ 1 & 0 & b_1 & 0 \\ 0 & 1 & 0 & 0 \end{bmatrix} \tag{9}$$

$$[T_k^a] = \begin{bmatrix} 0 & 0 & 0 & b_1 & h_t \\ 1 & 0 & -b_1 & 0 & a_k \\ 0 & 1 & -h_t & -a_k & 0 \\ 0 & 0 & 0 & -b_1 & h_t \\ 1 & 0 & b_1 & 0 & a_k \\ 0 & 1 & -h_t & -a_k & 0 \end{bmatrix} \quad k = 1,6 \qquad (10)$$

in which, a_k is defined as positive if the kth axle is located in the positive direction relative to the center of gravity of the truck, otherwise it is negative. (see Fig.1)

The relative displacement vector between the kth axle and rails is

$$\{\bar{U}_k^r\} = [T^r] \{U_k^a\} - [I] \{U_k^r\} \qquad (11)$$

where k = 1,6.

The vector $\{\bar{U}_k^r\}$ representing the relative displacement, in vertical y and lateral z directions, between the right and left axle springs and the rail is

$$\{\bar{U}_k^r\} = [\bar{U}_{kR}^{ry} \quad \bar{U}_{kR}^{rz} \quad \bar{U}_{kL}^{ry} \quad \bar{U}_{kL}^{rz}]^T \qquad k = 1,6 \qquad (12)$$

[I] is a 4 x 4 unit matrix and the transfer matrix $[T^r]$ is derived according to the coordinate system defined in Fig.3.

$$[T^r] = \begin{bmatrix} 1 & 0 & -b & 0 \\ 0 & 1 & -r & 0 \\ 1 & 0 & b & 0 \\ 0 & 1 & -r & 0 \end{bmatrix} \qquad (13)$$

The vector $\{U_k^r\}$ representing the rail input displacements in y and z directions on the right and left side of the kth axle is

$$\{U_k^r\} = [U_{kR}^{ry} \quad U_{kR}^{rz} \quad U_{kL}^{ry} \quad U_{kL}^{rz}]^T \tag{14}$$

where k = 1, 6 and corresponds to the six axles.

The kinetic energy, T, of the system translations and rotations is given as

$$T = \tfrac{1}{2} \{\dot{U}^b\}^T [M^b]\{\dot{U}^b\} + \tfrac{1}{2} \{\dot{U}_1^t\}^T[M_1^t] \{\dot{U}_1^t\}$$
$$+ \tfrac{1}{2} \{\dot{U}_2^t\}^T [M_2^t]\{\dot{U}_2\} + \tfrac{1}{2} \sum_{k=1}^{6} \{\dot{U}_k^a\}^T[M_k^a] \{\dot{U}_k^a\} \tag{15}$$

where $[M^b]$, $[M_j^t]$ and $[M_k^a]$ are the mass matrices for the carbody, truck frames and wheel-axle sets respectively.

$$[M^b] = \begin{bmatrix} m_B & & & & & \\ & m_B & & & & \\ & & J_B & & & \\ & & & I_B & & \\ & & & & \bar{J}_B & \end{bmatrix} \tag{16a}$$

$$[M_j^t] = \begin{bmatrix} m_t & & & & & \\ & m_t & & & & \\ & & J_t & & & \\ & & & I_t & & \\ & & & & \bar{J}_t & \end{bmatrix} \qquad j=1,2 \tag{16b}$$

$$[M_k^a] = \begin{bmatrix} m_a^k & & & \\ & m_a^k & & \\ & & J_a^k & \\ & & & I_a^k \end{bmatrix} \qquad k=1,6 \qquad (16c)$$

Similarly, the potential energy, V, of the entire system is given by

$$V = \tfrac{1}{2}\{U_1\}^T[K_s]\{U_1\} + \tfrac{1}{2}\{U_2\}^T[K_s]\{U_2\} + \tfrac{1}{2}\sum_{k=1}^{6}\{\bar{U}_k\}^T[K_p^k]\{\bar{U}_k\} + \tfrac{1}{2}\sum_{k=1}^{6}\{\bar{U}_k^r\}^T[K_R]\{\bar{U}_k^r\} \qquad (17)$$

where $[K_s]$, $[K_p^k]$ and $[K_R]$ are the stiffness matrices for the secondary suspension, primary suspension and the track respectively.

$$[K_s] = \begin{bmatrix} K_{xt} & & & & & \\ & K_{yt} & & & & \\ & & K_{zt} & & & \\ & & & K_{xt} & & \\ & & & & K_{yt} & \\ & & & & & K_{zt} \end{bmatrix} \qquad (18a)$$

$$[K_p^k] = \begin{bmatrix} K_{xa}^k & & & & & \\ & K_{ya}^k & & & & \\ & & K_{za}^k & & & \\ & & & K_{xa}^k & & \\ & & & & K_{ya}^k & \\ & & & & & K_{za}^k \end{bmatrix} \qquad (18b)$$

where k=1,6 for axle 1 to 6

$$[K_R] = \begin{bmatrix} K_{yr} & & & & & \\ & K_{zr} & & & & \\ & & K_{yr} & & & \\ & & & K_{zr} & & \end{bmatrix} \tag{18c}$$

The dissipation energy, D, of the entire system is

$$D = \tfrac{1}{2}\{\dot{U}_1\}^T[C_s]\{\dot{U}_1\} + \tfrac{1}{2}\{\dot{U}_2\}^T[C_s]\{\dot{U}_2\} + \tfrac{1}{2}\sum_{k=1}^{6}\{\dot{U}_k\}^T[C_p^k]\{\dot{U}_k\} + \tfrac{1}{2}\sum_{k=1}^{6}\{\dot{U}_k^r\}^T[C_R]\{\dot{U}_k^r\} \tag{19}$$

where $[C_s]$, $[C_p]$ and $[C_R]$ are the damping matrices for the secondary suspension, primary suspension and the track respectively.

$$[C_s] = \begin{bmatrix} C_{xt} & & & & & \\ & C_{yt} & & & & \\ & & C_{zt} & & & \\ & & & C_{xt} & & \\ & & & & C_{yt} & \\ & & & & & C_{zt} \end{bmatrix} \tag{19a}$$

$$[C_p^k] = \begin{bmatrix} C_{xa}^k & & & & & \\ & C_{ya}^k & & & & \\ & & C_{za}^k & & & \\ & & & C_{xa}^k & & \\ & & & & C_{ya}^k & \\ & & & & & C_{za}^k \end{bmatrix} \quad \text{where } k=1,6 \text{ for axle 1 to 6} \tag{19b}$$

$$[C_R] = \begin{bmatrix} C_{yr} & & & & \\ & C_{zr} & & & \\ & & C_{yr} & & \\ & & & C_{zr} & \end{bmatrix} \qquad (19c)$$

The potential energy, V, of the entire system, in terms of the generalized displacements, is given by

$$\begin{aligned} V = {} & \tfrac{1}{2}\left\{\{U_1^t\}^T[T_1^t]^T - \{U^b\}^T[T_1^b]^T\right\}[K_s]\left\{[T_1^t]\{U_1^t\} - [T_1^b]\{U^b\}\right\} \\ & + \tfrac{1}{2}\left\{\{U_2^t\}^T[T_2^t]^T - \{U^b\}^T[T_2^b]^T\right\}[K_s]\left\{[T_2^t]\{U_2^t\} - [T_2^b]\{U^b\}\right\} \\ & + \tfrac{1}{2}\left[\sum_{k=1}^{3}\left\{\{U_k^a\}^T[T^a]^T - \{U_1^t\}^T[T_k^a]^T\right\}[K_p^k]\left\{[T^a]\{U_k^a\} - [T_k^a]\{U_1^t\}\right\}\right] \\ & + \tfrac{1}{2}\left[\sum_{k=4}^{6}\left\{\{U_k^a\}^T[T^a]^T - \{U_2^t\}^T[T_k^a]^T\right\}[K_p^k]\left\{[T^a]\{U_k^a\} - [T_k^a]\{U_2^t\}\right\}\right] \\ & + \tfrac{1}{2}\left[\sum_{k=1}^{6}\left\{\{U_k^r\}^T[I] - \{U_k^a\}^T[T^r]^T\right\}[K_R]\left\{[I]\{U_k^r\} - [T^r]\{U_k^a\}\right\}\right] \end{aligned} \qquad (20)$$

Expansion of the above expression yields

$$\begin{aligned} V = {} & \tfrac{1}{2}\left[\{U_1^t\}^T[T_1^t]^T[K_s][T_1^t]\{U_1^t\} - \{U^b\}^T[T_1^b]^T[K_s][T_1^t]\{U_1^t\}\right. \\ & \left. - \{U_1^t\}^T[T_1^t]^T[K_s][T_1^b]\{U^b\} + \{U^b\}^T[T_1^b]^T[K_s][T_1^b]\{U^b\}\right] \\ & + \tfrac{1}{2}\left[\{U_2^t\}^T[T_2^t]^T[K_s][T_2^t]\{U_2^t\} - \{U^b\}^T[T_2^b]^T[K_s][T_2^t]\{U_2^t\}\right. \\ & \left. - \{U_2^t\}^T[T_2^t]^T[K_s][T_2^b]\{U^b\} + \{U^b\}^T[T_2^b]^T[K_s][T_2^b]\{U^b\}\right] \\ & + \tfrac{1}{2}\left[\sum_{k=1}^{3}\left\{\{U_k^a\}^T[T^a]^T[K_p^k][T^a]\{U_k^a\} - \{U_1^t\}^T[T_k^a]^T[K_p^k][T^a]\{U_k^a\}\right.\right. \\ & \left.\left. - \{U_k^a\}^T[T^a]^T[K_p^k][T_k^a]\{U_1^t\} + \{U_1^t\}^T[T_k^a]^T[K_p^k][T_k^a]\{U_1^t\}\right\}\right] \\ & + \tfrac{1}{2}\left[\sum_{k=4}^{6}\left\{\{U_k^a\}^T[T^a]^T[K_p^k][T^a]\{U_k^a\} - \{U_2^t\}^T[T_k^a]^T[K_p^k][T^a]\{U_k^a\}\right.\right. \\ & \left.\left. - \{U_k^a\}^T[T^a]^T[K_p^k][T_k^a]\{U_2^t\} + \{U_2^t\}^T[T_k^a]^T[K_p^k][T_k^a]\{U_2^t\}\right\}\right] \\ & + \tfrac{1}{2}\left[\sum_{k=1}^{6}\left\{\{U_k^r\}^T[K_R]\{U_k^r\} - \{U_k^a\}^T[T^r]^T[K_R]\{U_k^r\}\right.\right. \\ & \left.\left. - \{U_k^r\}^T[K_R][T^r]\{U_k^a\} + \{U_k^a\}^T[T^r]^T[K_R][T^r]\{U_k^a\}\right\}\right] \end{aligned} \qquad (21)$$

Similarly, the dissipation energy, D, of the entire system, in terms of the generalized displacements, is given by,

$$
\begin{aligned}
D = {} & \tfrac{1}{2}\left\{\{\dot{U}_1^t\}^T[T_1^t]^T - \{\dot{U}^b\}^T[T_1^b]^T\right\}[C_s]\left\{[T_1^t]\{\dot{U}_1^t\} - [T_1^b]\{\dot{U}^b\}\right\} \\
& + \tfrac{1}{2}\left\{\{\dot{U}_2^t\}^T[T_2^t]^T - \{\dot{U}^b\}^T[T_2^b]^T\right\}[C_s]\left\{[T_2^t]\{\dot{U}_2^t\} - [T_2^b]\{\dot{U}^b\}\right\} \\
& + \tfrac{1}{2}\left[\sum_{k=1}^{3}\left\{\{\dot{U}_k^a\}^T[T^a]^T - \{\dot{U}_1^t\}^T[T_k^a]^T\right\}[C_p^k]\left\{[T^a]\{\dot{U}_k^a\} - [T_k^a]\{\dot{U}_1^t\}\right\}\right] \\
& + \tfrac{1}{2}\left[\sum_{k=4}^{6}\left\{\{\dot{U}_k^a\}^T[T^a]^T - \{\dot{U}_2^t\}^T[T_k^a]^T\right\}[C_p^k]\left\{[T^a]\{\dot{U}_k^a\} - [T_k^a]\{\dot{U}_2^t\}\right\}\right] \\
& + \tfrac{1}{2}\left[\sum_{k=1}^{6}\left\{\{\dot{U}_k^r\}^T[I] - \{\dot{U}_k^a\}^T[T^r]^T\right\}[C_R]\left\{[I]\{\dot{U}_k^r\} - [T^r]\{\dot{U}_k^a\}\right\}\right]
\end{aligned}
\tag{22}
$$

The above expression can be rearranged yielding

$$
\begin{aligned}
D = {} & \tfrac{1}{2}\left[\{\dot{U}_1^t\}^T[T_1^t]^T[C_s][T_1^t]\{\dot{U}_1^t\} - \{\dot{U}^b\}^T[T_1^b]^T[C_s][T_1^t]\{\dot{U}_1^t\}\right. \\
& \left. - \{\dot{U}_1^t\}^T[T_1^t]^T[C_s][T_1^b]\{\dot{U}^b\} + \{\dot{U}^b\}^T[T_1^b]^T[C_s][T_1^b]\{\dot{U}^b\}\right] \\
& + \tfrac{1}{2}\left[\{\dot{U}_2^t\}^T[T_2^t]^T[C_s][T_2^t]\{\dot{U}_2^t\} - \{\dot{U}^b\}^T[T_2^b]^T[C_s][T_2^t]\{\dot{U}_2^t\}\right. \\
& \left. - \{\dot{U}_2^t\}^T[T_2^t]^T[C_s][T_2^b]\{\dot{U}^b\} + \{\dot{U}^b\}^T[T_2^b]^T[C_s][T_2^b]\{\dot{U}^b\}\right] \\
& + \tfrac{1}{2}\left[\sum_{k=1}^{3}\left\{\{\dot{U}_k^a\}^T[T^a]^T[C_p^k][T^a]\{\dot{U}_k^a\} - \{\dot{U}_1^t\}^T[T_k^a]^T[C_p^k][T^a]\{\dot{U}_k^a\}\right.\right. \\
& \left.\left. - \{\dot{U}_k^a\}^T[T^a]^T[C_p^k][T_k^a]\{\dot{U}_1^t\} + \{\dot{U}_1^t\}^T[T_k^a]^T[C_p^k][T_k^a]\{\dot{U}_1^t\}\right\}\right] \\
& + \tfrac{1}{2}\left[\sum_{k=4}^{6}\left\{\{\dot{U}_k^a\}^T[T^a]^T[C_p^k][T^a]\{\dot{U}_k^a\} - \{\dot{U}_2^t\}^T[T_k^a]^T[C_p^k][T^a]\{\dot{U}_k^a\}\right.\right. \\
& \left.\left. - \{\dot{U}_k^a\}^T[T^a]^T[C_p^k][T_k^a]\{\dot{U}_2^t\} + \{\dot{U}_2^t\}^T[T_k^a]^T[C_p^k][T_k^a]\{\dot{U}_2^t\}\right\}\right] \\
& + \tfrac{1}{2}\left[\sum_{k=1}^{6}\left\{\{\dot{U}_k^r\}^T[C_R]\{\dot{U}_k^r\} - \{\dot{U}_k^a\}^T[T^r]^T[C_R]\{\dot{U}_k^r\}\right.\right. \\
& \left.\left. - \{\dot{U}_k^r\}^T[C_R][T^r]\{\dot{U}_k^a\} + \{\dot{U}_k^a\}^T[T^r]^T[C_R][T^r]\{\dot{U}_k^a\}\right\}\right]
\end{aligned}
\tag{23}
$$

Using the generalized displacement vector,

$$\{q\} = \left[\{u^b\}^T \{u_1^t\}^T \{u_2^t\}^T \{u_1^a\}^T \{u_2^a\}^T \{u_3^a\}^T \{u_4^a\}^T \{u_5^a\}^T \{u_6^a\}^T\right]^T$$

for the entire system and apply Largrange's equation (24)

$$\frac{d}{dt}\left[\frac{\partial T}{\partial \dot{q}}\right] - \frac{\partial T}{\partial q} + \frac{\partial V}{\partial q} + \frac{\partial D}{\partial \dot{q}} = Q_m \tag{25}$$

for each of the generalized coordinates, the equation of motion for the system can be written as

$$[M]\{\ddot{q}\} + [C']\{\dot{q}\} + [K']\{q\} = \{\bar{Q}_r\} + \{\bar{Q}_{cp}\} \tag{26}$$

where [M],[C'] and [K'] are 39x39 matrices representing the mass, damping and stiffness matrix of the system. The elements (or submatrices) in the mass, damping and stiffness matrix are given in Table 2, 3 and 4 respectively. The vectors $\{\bar{Q}_r\}$ and $\{\bar{Q}_{cp}\}$ represent the generalized forces due to rail input, and the lateral gravitational stiffness and the wheel-rail interaction, respectively. It will be demonstrated in a later section that, by rearranging the $\{\bar{Q}_{cp}\}$ vector on the left hand side of Eq.(26), the equation of motion can be written in the form of

$$[M]\{\ddot{q}\} + [C]\{\dot{q}\} + [K]\{q\} = \{R\} \tag{27}$$

2.3 FORCING FUNCTIONS

2.3.1 Vertical Rail Input

The dynamic response of a locomotive depends greatly on the rail profiles in both the vertical and lateral directions. This excitation basically results from the periodic irregularities of the track (such as low-joints). The vertical geometry of the half-staggered rails can be represented by a rectified sine

wave, Fig.4, as

$$U^{ry} = A_o \left| \sin(\omega t) \right| \qquad (28)$$

This periodic function has an amplitude A_o and a period of two rail-lengths, $2L_R$ and is the input excitation for one wheel. The angular velocity, ω, is given by

$$\omega = \frac{2\pi V}{2L_R}$$

where V - velocity of the locomotive

The equivalent representation of the rectified sine wave, in terms of a Fourier series, is

$$U^{ry} = A_o \left[\frac{2}{\pi} - \frac{4}{\pi} \left(\frac{\cos 2\omega t}{1x3} + \frac{\cos 4\omega t}{3x5} + \frac{\cos 6\omega t}{5x7} + \ldots \right) \right] \qquad (29)$$

For the steady state solution, the constant (mean-position) term may be ignored. Thus the vertical input at the wheels of each axle can be given as :

$$\text{Right} : U^{ry}_{kR} = -\frac{4A^R_o}{\pi} \sum_{n=1}^{\infty} \frac{1}{(4n^2-1)} \cos n\beta\,(t-t_k) \quad k=1,6 \qquad (30a)$$

$$\text{Left} : U^{ry}_{kL} = -\frac{4A^L_o}{\pi} \sum_{n=1}^{\infty} \frac{(-1)^n}{(4n^2-1)} \cos n\beta\,(t-t_k) \quad k=1,6 \qquad (30b)$$

where A^R_o = Amplitude of the right rail vertical irregularity

A^L_o = Amplitude of the left rail vertical irregularity

$\beta = 2\omega = \frac{2\pi V}{L_R}$

for

$t_1 = o$

$t_2 = x_2/V \quad , x_2 = (a_1 - a_2)$

$$t_3 = x_3/V \quad , x_3 = (a_1 - a_3)$$

$$t_4 = x_4/V \quad , x_4 = (L_1 + L_2 + a_1 - a_4)$$

$$t_5 = x_5/V \quad , x_5 = (L_1 + L_2 + a_1 - a_5)$$

$$t_6 = x_6/V \quad , x_6 = (L_1 + L_2 + a_1 - a_6)$$

where x_2 to x_6 are defined in Figure 5.
and V is velocity of the locomotive.

2.3.2 Lateral Rail Input

In this model, the lateral track irregularity is simulated by a continuous sine function (Fig.6). The irregularity frequency and the amplitude for the left and right rail can be treated as independent input.

$$\text{Right} : U_{kR}^{rz} = \bar{A}_o^R \sin [\bar{\omega}_R(t_k - t_{sR}) + \bar{\theta}_R] \quad k = 1,6 \qquad (31a)$$

$$\text{Left} : U_{kL}^{rz} = \bar{A}_o^L \sin [\bar{\omega}_L(t_k - t_{sL}) + \bar{\theta}_L] \quad k = 1,6 \qquad (31b)$$

where $\bar{A}_o^R$ = Amplitude of the right rail lateral irregularity

$\bar{A}_o^L$ = Amplitude of the left rail lateral irregularity

$\bar{\omega}_R$ = Angular velocity of the right rail lateral irregularity

$\bar{\omega}_L$ = Angular velocity of the left rail lateral irregularity.

$\bar{\theta}_R$, $\bar{\theta}_L$ = phase angle of the lateral irregularities

t_{sR} , t_{sL} = starting time for the lateral irregularities

t_k, k=1,6 are the same as those defined previously.

The generalized forces at each axle resulting from the vertical and lateral rail input at the wheel can be calculated

readily by

$$\{Q_r^k\} = [T^r]^T[K_R]\ \{U_k^r\} \qquad k = 1,6 \tag{32}$$

The complete generalized force vector is given by

$$\{\bar{Q}_r\} = \left[\{o\},\{o\},\{o\},\{Q_r^1\},\{Q_r^2\},\{Q_r^3\},\{Q_r^4\},\{Q_r^5\},\{Q_r^6\}\right]^T \tag{33}$$

in which {o} is 5x1 zero vector.

2.3.3 Wheel-Rail Interaction

The expressions for the generalized forces acting between the wheel and rails are similar to those given by Wicken [6]

$$\{Q_{cp}^k\} = [K_g^k]\ [T^r]^T\{\bar{U}_k^r\} + [C_g^k]\ \{\dot{U}_k^a\}$$

$$= [K_g^k]\ \{U_k^a\} - [K_g^k]\ [T^r]^T\{U_k^r\} + [C_g^k]\ \{\dot{U}_k^a\} \tag{34}$$

where $\{\bar{U}_k^r\}$ is the relative displacement between wheel-set, k and the rails.

The $[K_g^k]$ and $[C_g^k]$ are matrices which include the effects of gravity and creep forces resulting from the difference in strain rates of wheel and rails in the contact region. They are given as

$$[K_g^k] = \begin{bmatrix} 0 & 0 & 0 & 0 \\ 0 & -k_g^k & 0 & +2f_L \\ 0 & -k_g^k r & 0 & +2f_L r \\ 0 & -2f_T\frac{\lambda b}{r} + \frac{2f_{s23}}{br}\varepsilon & 0 & k_{gw}^k \end{bmatrix} \qquad k = 1,6 \tag{35a}$$

$$[C_g^k] = \begin{bmatrix} 0 & 0 & 0 & 0 \\ 0 & \frac{-2f_L}{v} & 0 & \frac{-2f_{s23}}{v} \\ 0 & \frac{-2f_L}{v}r & 0 & 0 \\ 0 & 0 & 0 & -\frac{2f_T b^2}{v} \\ & & & -\frac{2f_{s33}}{v} \end{bmatrix} \quad k = 1,6 \qquad (35b)$$

in which, $[K_g^k]$ = lateral gravitational stiffness for wheel-axle set, k

$[C_g^k]$ = Yaw gravitational stiffness for wheel-axle set, k

f_L = Lateral creep coefficient

f_T = Tangential creep coefficient

f_{s23}, f_{s33} = lateral and longitudinal spin creep coefficient

r = wheel tread radius

v = locomotive speed

ϵ = rate of change of contact plane slope with respect to the lat displacement of wheel set

λ = effective wheel conicity

b = Half distance between contact points of wheel treads and rails in lateral direction

The derivations of the lateral gravitational stiffnesses, k_g and the yaw gravitational stiffnesses, k_{gw} for the wheel-axle set can be found in references [4, 6].

The expressions are given as:

$$k_g^k = \frac{W_k}{b} \quad (\xi \delta_o + \varepsilon) \tag{36a}$$

for k = 1,6

$$k_{gw}^k = - W_k \; b \; \delta_o \tag{36b}$$

where W_k = axle load of the wheel-set, k

δ_o = slope of contact point between wheel and rail at central position.

ξ = Rate of change of distance between axle center line and contact points with respect to lateral displacement of wheelset.

In the model, the calculations of the wheel-rail contact geometry parameters ε, ξ and the effective conicity λ are based on the expressions given by Wicken[6] and Blader [2,3]. Either expression (as given in Eq.(37) and (38)) can be used by the users.

According to Wicken [6], the expressions for ε, ξ and λ are

$$\varepsilon = \frac{b}{(R-R')} \quad \frac{b + R\delta o}{b - r\delta o} \tag{37a}$$

$$\xi = \frac{R}{R - R'} \quad \frac{b + R'\delta o}{b - r\delta o} \tag{37b}$$

$$\lambda = \frac{R\delta o}{(R-R')} \quad \frac{b + R'\delta o}{b - r\delta o} \tag{37c}$$

The expressions used by Blader [2] are

$$\varepsilon = \frac{b}{R-R'} \tag{38a}$$

$$\xi = \frac{2\ (1 + \frac{r}{R})}{(1 - \frac{R'}{R})} \tag{38b}$$

$$\lambda = \frac{R\delta o}{(R-R')} \quad \frac{b + R'\delta o}{b - r\delta o} \tag{38c}$$

The complete generalized force vector due to the wheel-rail interaction is given by

$$\{\bar{Q}_{cp}\} = \left[\{o\},\{o\},\{o\},\{Q^1_{cp}\},\{Q^2_{cp}\},\{Q^3_{cp}\},\{Q^4_{cp}\},\{Q^5_{cp}\},\{Q^6_{cp}\}\right]^T \tag{39}$$

in which {o} is a 5x1 zero vector.

By substituting Eq (34) into Eq (26), the generalized equation of motion can be rewritten as

$$[M]\ \{\ddot{q}\} + [C]\ \{\dot{q}\} + [K]\ \{q\} = \{\bar{Q}_r\} + \{\bar{Q}_{wr}\} = \{R\} \tag{40}$$

where

$$\{\bar{Q}_{wr}\} = \left[\{o\},\{o\},\{o\},\{Q^1_{wr}\},\{Q^2_{wr}\},\{Q^3_{wr}\},\{Q^4_{wr}\},\{Q^5_{wr}\},\{Q^6_{wr}\}\right]^T$$

$$\{Q^k_{wr}\} = -[K^k_g]\ [T^r]^T\{U^r_k\} \qquad k = 1,\ 6$$

2.4 Relative Spring Forces and Damping Forces

In calculating the relative forces (with reference to the nominal forces) in the spring elements and dampers, the relative displacement vectors, Eq(3) and Eq(7), and velocity vectors are used. The orientation of the spring and dmaping elements are shown in Fig.7.

Recall that Eq.(3) and Eq.(7) are in the form of

$$\{U_{B-Tj}\} = [T_j^t]\{U_j^t\} - [T_j^b]\{U^b\} \quad \text{for } j = 1,2 \tag{41a}$$

$$\{\bar{U}_{Tj-Ak}\} = [T^a]\{U_k^a\} - [T_k^a]\{U_j^t\} \quad \text{for } \begin{matrix} j = 1,2 \\ k = 1,6 \end{matrix} \tag{41b}$$

and

$$\{\dot{U}_{B-Tj}\} = [T_j^t]\{\dot{U}_j^t\} - [T_j^b]\{\dot{U}^b\} \quad \text{for } j = 1,2 \tag{42a}$$

$$\{\dot{\bar{U}}_{Tj-Ak}\} = [T^a]\{\dot{U}_k^a\} - [T_k^a]\{\dot{U}_j^t\} \quad \text{for } \begin{matrix} j = 1,2 \\ k = 1,6 \end{matrix} \tag{42B}$$

By defining the spring in tension as positive, the relative spring force vectors between carbody and trucks, and between trucks and axles are

$$\{SF_{B-Tj}\} = [S_{Tj}][K_s]\{U_{B-Tj}\} \quad \text{for } j = 1,2 \tag{43a}$$

$$\{SF_{Tj-Ak}\} = [S_{Ak}][K_p^k]\{\bar{U}_{Tj-Ak}\} \quad \text{for } \begin{matrix} j = 1,2 \\ k = 1,6 \end{matrix} \tag{43b}$$

$[S_{Tj}]$ and $[S_{Ak}]$ are the sign indication matrices expanded as

$$[S_{Tj}] = \begin{bmatrix} TS_j & & & & & \\ & -1 & & & & \\ & & -1 & & & \\ & & & TS_j & & \\ & & & & -1 & \\ & & & & & 1 \end{bmatrix} \tag{44a}$$

where $$TS_j = \begin{cases} +1 & j = 1 \\ -1 & j = 2 \end{cases}$$

$$[S_{Ak}] = \begin{bmatrix} AS^k & & & & & \\ & -1 & & & & \\ & & -1 & & & \\ & & & AS^k & & \\ & & & & -1 & \\ & & & & & 1 \end{bmatrix} \tag{44b}$$

where

$$AS^k = \begin{cases} +1 & k = 1,4 \\ -1 & k = 3,6 \end{cases}$$

$$AS^2 = \begin{cases} +1 & \text{if } a_2 \geq 0 \\ -1 & \text{otherwise} \end{cases}$$

$$AS^5 = \begin{cases} +1 & \text{if } a_5 \geq 0 \\ -1 & \text{otherwise} \end{cases}$$

Assuming all the dampers provide only viscous damping to the system, the relative damping force vectors between the carbody and trucks, and between trucks and axle are:

$$\{DF_{B-Tj}\} = - [S_{Tj}] [C_s] \{\dot{U}_{B-Tj}\} \quad \text{for } j = 1,2 \tag{45a}$$

$$\{DF_{Tj-Ak}\} = - [S_{Ak}] [C_p^k] \{\dot{U}_{Tj-Ak}\} \quad \text{for } j = 1,2 \quad \text{for } k = 1,6 \tag{45b}$$

Therefore, the total forces between the carbody and trucks, and between trucks and axles are given by

$$\{TF_{B-Tj}\} = \{SF_{B-Tj}\} + \{DF_{B-Tj}\} \tag{46a}$$

$$\{TF_{Tj-Ak}\} = \{SF_{Tj-Ak}\} + \{DF_{Tj-Ak}\} \tag{46b}$$

2.5 Numerical Integration of Equation of Motion

For integrating the equations of motion, the Wilson-θ method is used. It is essentially an extension of the linear acceleration method, in which a linear variation of acceleration from time t to time t + Δt is assumed. In the Wilson θ method, the acceleration is assumed to be linear from time t to time t + θΔt, Fig.8, where $\theta \geq 1.0$ [1]. When θ = 1.0, the method reduces to the linear acceleration scheme. It has been shown that for unconditional stability, $\theta \geq 1.37$ must be used. In common practice, θ = 1.40 is usually employed.

Let τ denote the increase in time, where $0 \leq \tau \leq \theta\Delta t$; then for the time interval t to t + θΔt, it is assumed that

$$\ddot{q}_{t+\tau} = \ddot{q}_t + \frac{\tau}{\theta\Delta t}(\ddot{q}_{t+\theta\Delta t} - \ddot{q}_t) \tag{47}$$

Integrating (47) yields

$$\dot{q}_{t+\tau} = \dot{q}_t + \ddot{q}_t\tau + \frac{\tau^2}{2\theta\Delta t}(\ddot{q}_{t+\theta\Delta t} - \ddot{q}_t) \tag{48}$$

and

$$q_{t+\tau} = q_t + \dot{q}_t\tau + \tfrac{1}{2}\ddot{q}_t\tau^2 + \frac{1}{6\theta\Delta t}\tau^3(\ddot{q}_{t+\theta\Delta t} - \ddot{q}_t) \tag{49}$$

By substituting $\tau = \theta\Delta t$ into (48) and (49), it is found that

$$\dot{q}_{t+\theta\Delta t} = \dot{q}_t + \frac{\theta\Delta t}{2}(\ddot{q}_{t+\theta\Delta t} + \ddot{q}_t) \tag{50}$$

$$q_{t+\theta\Delta t} = q_t + \theta\Delta t\,\dot{q}_t + \frac{\theta^2\Delta t^2}{6}(\ddot{q}_{t+\theta\Delta t} + 2\ddot{q}_t) \tag{51}$$

Then, $\ddot{q}_{t+\theta\Delta t}$ and $\dot{q}_{t+\theta\Delta t}$ can be solved in terms of $q_{t+\theta\Delta t}$

$$\ddot{q}_{t+\theta\Delta t} = \frac{6}{\theta^2\Delta t^2}(q_{t+\theta\Delta t} - q_t) - \frac{6}{\theta\Delta t}\dot{q}_t - 2\ddot{q}_t \tag{52}$$

and

$$\dot{q}_{t+\theta\Delta t} = \frac{3}{\theta\Delta t}(q_{t+\theta\Delta t} - q_t) - 2\dot{q}_t - \frac{\theta\Delta t}{2}\ddot{q}_t \tag{53}$$

To obtain the solution for the displacements, velocities, and accelerations at time t +Δt, the equilibrium equation (40) is considered at time t + θΔt. However, because the accelerations are assumed to vary linearly, a linearly projected generalized load vector is used;

$$[M]\{\ddot{q}_{t+\theta\Delta t}\} + [C]\{\dot{q}_{t+\theta\Delta t}\} + [K]\{q_{t+\theta\Delta t}\} = \{R_{t+\theta\Delta t}\} \tag{54}$$

$$\text{where } \{R_{t+\theta\Delta t}\} = \{R_t\} + \theta\{R_{t+\Delta t} - R_t\} \tag{55}$$

Substituting Eq(52) and (53) into Eq(54), an equation is obtained from which $q_{t+\theta\Delta t}$ can be solved. The $\ddot{q}_{t+\theta\Delta t}$ can be obtained by substituting $q_{t+\theta\Delta t}$ into Eq(52). Consequently, the $\ddot{q}_{t+\Delta t}$, $\dot{q}_{t+\Delta t}$ and $q_{t+\Delta t}$ can be achieved by substituting $\tau = \Delta t$ and $\ddot{q}_{t+\theta\Delta t}$ into Eq(47), (48) and (49) respectively.

As an alternative, the Newmark method is also provided for integrating the generalized equation of motion. It is also an extension of the linear acceleration method. The following assumptions are used [1] :

$$\dot{q}_{t+\Delta t} = \dot{q}_t + [(1-\delta)\ddot{q}_t + \delta\dot{q}_{t+\Delta t}]\Delta t \tag{56}$$

$$q_{t+\Delta t} = q_t + \dot{q}_t\Delta t + [(\tfrac{1}{2} - \alpha)\ddot{q}_t + \alpha\ddot{q}_{t+\Delta t}]\Delta t^2 \tag{57}$$

where α and δ are parameters that can be determined to obtain integration accuracy and stability. When $\delta=\frac{1}{2}$ and $\alpha=1/6$, relation (56) and (57) correspond to the linear acceleration method (which is also obtained using θ=1 in the Wilson-θ

method). Newmark originally proposed as an unconditionally stable scheme the constant-average-acceleration method, in which case $\delta=\frac{1}{2}$ and $\alpha=\frac{1}{4}$ (see Fig.8).

In addition to Eq(56) and (57), for solution of the displacements, velocities and accelerations at time $t+\Delta t$, the equilibrium equations (40) at time $t+\Delta t$ are also considered:

$$[M]\ \{\ddot{q}_{t+\Delta t}\} + [C]\ \{\dot{q}_{t+\Delta t}\} + [K]\ \{q_{t+\Delta t}\} = \{R_{t+\Delta t}\} \qquad (58)$$

Solving from Eq(57) for $\ddot{q}_{t+\Delta t}$ in terms of $q_{t+\Delta t}$, and then substituting for $\ddot{q}_{t+\Delta t}$ into Eq(56), equations for $\ddot{q}_{t+\Delta t}$ and $\dot{q}_{t+\Delta t}$, each in terms of the unknown displacements $q_{t+\Delta t}$ only, can be obtained. These two relations for $\dot{q}_{t+\Delta t}$ and $\ddot{q}_{t+\Delta t}$ are substituted into Eq(58) to solve for $q_{t+\Delta t}$, after which, using Eq(56) and (57), $\ddot{q}_{t+\Delta t}$ and $\dot{q}_{t+\Delta t}$ can also be calculated.

The complete algorithms using the Wilson-θ and the Newmark integration scheme have been presented by Bathe [1]. The close relationship between the computer implementation of the Wilson-θ and the Newmark method should be noted, which makes it possible to conveniently use both integration schemes in one single computer subprogram. However, in the computer simulation program developed for the model, these two integration schemes are handled seperately. In doing so, it is believed that the program would be easier to structure in future extension for the non-linear analysis of the six-axle locomotive.

3. SIMULATION RESULTS AND ANALYSIS

3.1 Effects of Stiffness Ratio on Locomotive Performance

A representative, hypothetical 6-axle locomotive has been selected in this study. A simulation methodology has been developed to analyze the effect of suspension ratio, η on locomotive performance. The stiffness ratio, η, is defined as the secondary vertical stiffness per truck side to the primary vertical stiffness per truck side. The simulation data used to represent the locomotive is given in Table 5. Basically, the locomotive has a stiff secondary suspension and a relatively soft primary journal suspension. The base value of the stiffness ratio, η, for the locomotive is 12.63. The performance of locomotive is normalized with respect to the base value throughout the study, the stiffnesses of the secondary suspension were varied without changing the primary suspension parameters in order to investigate the influence of stiffness ratio on locomotive performance. Table 6 summarizes the range of stiffness ratio and the associated suspension stiffnesses. The results of the study are presented in non-dimensional form. The scope of the study is limited to the locomotive running on tangent track. Both vertical and/or lateral rail inputs are provided as excitation. The simulations were made at both low and high operating speeds - 18 mph (28.96 km/h) and 80 mph (128.72 km/h). They correspond to the critical speeds for the carbody and the truck hunting, respectively. Three types of wheel profile are considered. Their effective conicities are 1 in 40, 1 in 20 and 1 in 10, respectively. Wheel profile with effective conicity of

1 in 40 is often used for modern high-speed locomotive. The 1 in 20 taper wheel is representive for the locomotive equipped new AAR wheels. A worn wheel profile is characterized by the 1 in 10 wheel taper. Half-staggered vertical irregularities of 1 in (2.54 cm) and 2 in. (5.08 cm) amplitude with a half-wavelength of 39 feet (11.89 m) and parallel lateral irregularities of 3/4 in. (1.81 cm) and 3 in. (7.62 cm) amplitude with half-wavelengths of 39 ft. (11.89 m), 42.5 feet (12.95 m) and 62 feet (18.90 m), respectively were simulated. It is the intent of the study to investigate the performance of locomotive running on the class 2 and class 5 track. It is obvious that by staggering the lateral irregularities of left rail with respect to right rail or vice versa, gage error, can also be simulated. However, only alignment error is investigated in this study. It may be pointed out that the simulation results presented in the following section are corresponding to the steady state condition.

Maximum Carbody Displacements

In Figures 9(a), 9(b) and 9(c), the plots of transmissibility versus stiffness ratio, η, at 18 mph (28.9 km/h) are shown for the various rail irregularities. It may be observed from Figures 9(a) and 9(b) that the maximum vertical displacement of the carbody due to the vertical rail input is only slightly influenced by the choice of η. However, the maximum lateral displacement of the carbody is quite sensitive to the variation of the stiffness ratio. A comparison between the responses with various wheel profiles shows that in all cases, the worn wheels exhibits

a higher transmiissibility factor than the new wheels. It is evident that the effect of the stiffness ratio, η on carbody response is more pronounced in the case with combined vertical and lateral rail irregularities, Fig.9(c). The transmissibility of the maximum carbody vertical displacement decreases slightly as the stiffness ratio increases from 1 to 6 and increases rather slowly when the stiffness ratio becomes greater than 6. The transmissibility of the maximum carbody lateral displacement decreases slightly and then increases fairly linearly as a function of stiffness ratio. Its worth mentioning that the lateral irregularities wavelength affects substantially the transmissibility of the lateral displacement of carbody, especially at high stiffness ratio range. Since the human body in general is more sensitive to lateral oscillations, locomotives with a large stiffness ratio may exhibit poor ride quality. It is interesting to observe that the transmissibilities are minimum, in all cases, at low stiffness ratio.

Figures 10(a), 10(b) and 10(c) show transmissibility versus stiffness ratio at 80 mph (128.72 km/h) speed for the various rail irregularities. The resulting behavior of the carbody is very similar to the behavior observed at 18 mph (28.96 km/h). The maximum vertical response of the carbody remains constant with respect to stiffness ratio. Maximum lateral response of the carbody is, on the other hand, very much influenced by the choice of stiffness ratio. It should be pointed out that the carbody lateral displacements at

80 mph (128.72 km/h) are small. These displacements are arbitrarily normalized with respect to η=8 in order to review their relative variations as a function of stiffness ratio. The effects of lateral irregularities wavelength on carbody lateral displacement are shown in Fig.10(c). At low stiffness ratio, sudden excessive carbody lateral displacement can be expected if the predominant lateral irregularity half wavelength increases from 42.5 ft (12.95 m) to 62.0 ft.(18.90 m) At the speed of 80 mph (128.72 km/h) (approximately truck hunting speed), relatively small carbody lateral displacements is expected due to the linearity assumption used in the model. In reality, the inherent non-linear characteristics of the locomotive-track system could be expected to induce a higher level of carbody lateral displacement and acceleration. Thus, the ride quality may also deteriorate.

L/V Consideration

As discussed in earlier section, the developed model, beside being capable of predicting the locomotive's performance under prescribed track input, also calculates the relative spring and damping forces in the primary and secondary suspension systems. At steady state condition, the maximum change in vertical spring force (relative to norminal static spring force) in the primary suspension system could review accurately the minimum vertical wheel load. Correspondingly, the maximum lateral spring force in the primary suspension would provide insight into the maximum lateral wheel load.

The normalized maximum change in vertical spring force and maximum lateral spring force in primary suspension at

18 mph (28.96 km/h) resulting from various rail irregularities are presented in Figures 11(a), 11(b) and 11(c). The maximum lateral spring force (or maximum lateral wheel load) due to 1 in (2.54 cm) vertical rail input increases as a function of stiffness ratio, Fig.11(a). The maximum change in vertical spring force is the smallest between stiffness ratio of 1 to 3. It also reveals that the minimum vertical wheel load is the largest at stiffness ratio of 2. By assuming the maximum lateral and the minimum vertical occur simultaneously; the smallest L/V ratio can be expected at stiffness ratio of 2. When the vertical rail input is increased from 1 in.(2.54 cm) to 2 in (5.08 cm), similar observations can be made for the maximum lateral wheel load and the minimum vertical wheel load, Fig.11 (b). It is obvious that the L/V ratio decreases as stiffness ratio decreases. In the case for 2.0 inch (5.08 cm) vertical coupled with 3 inch (7.62 cm) lateral rail input, the variations observed for the change in vertical spring force are more drastic. However, the decrease in minimum vertical wheel load (or the increase in maximum change in vertical spring force) is also accompanied by a decrease in the maximum lateral wheel load (or the maximum lateral spring force), Fig.11 (c). As a result, the L/V ratios are kept approximately at the same level as that for η = 12.63.

In Figures 12(a), 12(b) and 12(c), the effects of various rail input on the maximum lateral wheel load and the minimum vertical wheel load at the speed of 80 mph (128.72 km/h) are presented. Based on the philosophy developed previously,

low and high stiffness ratio could be undesirable for the track with 1 inch (2.54 cm) vertical rail input and the track with 2 inch (5.08 cm) vertical rail input, respectively, (see Fig.12(a) and Fig.12(b)). Throughout this report, stiffness ratio, η ranges from 1 to 4 is referred to as low. High stiffness ratio is referred as to values from 8 to 12.63. Any values, from 4 to 8, is classified as intermediate stiffness ratio. In Fig.12(c), the effects of lateral irregularity wavelengths on the maximum lateral wheel load and the maximum vertical wheel load are demonstrated. The results suggest that the lowest L/V ratio occurs at the intermediate stiffness ratio.

Carbody Rotations

In Figures 13(a), 13(b) and 13(c), the normalized carbody rotation versus stiffness ratio at 18 mph (28.96 km/h) are shown. The rotations considered include carbody roll, yaw and pitch. The results suggest that stiffness ratios of 4 or high would be desirable as far as the carbody rotation is concerned.

The normalized carbody rotation at 80 mph (128.72 km/h) due to 1 in (2.54 cm), 2 in (5.08 cm) vertical rail input and 1 in (2.54 cm) vertical coupled with 3/4 in (1.91 cm) lateral rail input are illustrated in Figures 14(a), 14(b) and 14(c), respectively. In contrast to the carbody behavior at the speed of 18 mph (28.96 km/h), the yaw and pitch at 80 mph (128.72 km/h) are more responsive to vertical and/or

lateral irregularities. The carbody roll decreases exponentially as a function of the stiffness ratio for a 1 in (2.54 cm) vertical rail input. However, it increases exponentially for 2 in (5.08 cm) vertical rail excitation. (see Fig.14(a) and Fig.14(b)). Similar observation can also be made for the cases of 1 in (2.54 cm) vertical rail input and of 1 in (2.54 cm) vertical coupled with 3/4 in (1.91 cm) lateral rail input. (see Fig.14(a) and Fig.14(c)). Consequently, any transition from a section of track with 1 in (2.54 cm) vertical irregularities to a section of 2 in(5.08 cm) vertical irregularities could possibly cause considerable variation in carbody roll if the suspension stiffness ratio is small. Similarly, sudden change in carbody roll can also be expected for the transition from a section with 1 in (2.54 cm) vertical irregularities to a section with 1 in (2.54 cm) vertical coupled with 3/4 in (1.91 cm) lateral irregularities if the locomotive suspension system is designed with small stiffness ratio. At low stiffness ratio region, similar observations can be made for carbody yaw and pitch. The above observed behavior for carbody roll, yaw and pitch may induce undesirable performance of the locomotive during a curve entry or exit. In worst case, it may even cause derailments.

Table 7 summarizes the variations of the normalized carbody rotation for the cases considered in Figures 13(a) 13(b), 13(c), 14(a) 14(b) and 14(c). The net variations in normalized carbody roll, yaw and pitch are also given in the table. It is interesting to observe that the smallest

variations correspond to the stiffness ratio ranges from 4 to 8. From the design point of view, yaw rotation should deserve more attention at high operating speed, since the lateral oscillation of the locomotive can be greatly affected by yawing.

Carbody Accelerations

The carbody vertical and lateral accelerations at 18 mph (28.96 km/h) due to various rail input are presented in Figures 15 (a) and 15(b). The vertical accelerations of the carbody are relatively insensitive to the choice of stiffness ratio and the lateral irregularities wavelengths. (see Fig.15(a)). However, the acceleration level is affected considerably by the wheel profile especially at high stiffness ratio range. The carbody lateral accelerations vary fairly linearly as a function of stiffness ratio, Fig.15(b). It can be observed that at high stiffness ratio, the carbody lateral acceleration may have exceeded the human tolerable limits. The effects of the wheel profile on the carbody lateral acceleration level are also demonstrated in Fig.15(b). In all cases, the worn wheel exhibits higher level of acceleration for all stiffness ratio considered. In contrast to carbody vertical acceleration, the lateral irregularity wavelengths have influence on the carbody lateral acceleration, especially at high stiffness ratio.

In Figures 15(c) and 15(d), the carbody vertical and lateral accelerations due to various rail input at 80 mph (128.72 km/h) are shown. It is interesting to observe that the locomotive equipped with new wheels (of effective

conicity 1 in 20)has higher level of acceleration in carbody than the one with worn wheels (of effective conicity 1 in 10). The lateral irregularity wavelengths are more influential to the vertical acceleration at high speed than at low speed. The effects of wheel profile on carbody lateral acceleration at 80 mph (128.72 km/h) are clearly demonstrated in Fig.15(d). Generally speaking, the new wheel exhibits lower level of acceleration than the worn wheel. Once again, the predominant lateral irregularity wavelengths play an important role in dictating the maximum carbody acceleration at high speed. A parallel study of Fig.15(a), 16(a) and 16(b) indicates that both the vertical and lateral carbody accelerations are higher at 18 mph (28.96 km/h) than at 80 mph (128.72 km/h).

Wheel-Axle Set Accelerations

In Figures 16(a) and 16(b), the maximum axle lateral acceleration versus stiffness ratio at the speed of 18 mph (28.96 km/h) and of 80 mph (128.72 km/h) have been plotted. It may be recalled that speeds of 18 mph (28.96 km/h) and 80 mph (128.72 km/h) correspond very closely to the critical conditions concerning carbody and axle hunting respectively. In Fig.16(a) no influence of the stiffness ratio on the maximum axle lateral accelerations is observed. It is due to the fact that the primary suspension is kept constant in all cases.

However, the maximum axle lateral accelerations are significantly increased due to additional vertical and/or lateral rail input. The effects of wheel profile on the

maximum axle lateral acceleration is also illustrated. As indicated, the most critical level of acceleration for the axle depends on the lateral irregularity wavelength as well as the wheel profile. The choice of the wavelengths used in this study is arbitrary. However, it is the intent of this study to demonstrate that a critical and dominant wavelengths at given speed may not necessary be critical at different speed. The maximum axle acceleration for the 80 mph (128.72 km/h) case is given in Fig.16(b). It can be observed that the maximum axle lateral accelerations except for one case, are relatively insensitive to the choice of stiffness ratio. The observed variation is possible due to utilization of wheel with effective conicity of 1 in 40. It is interesting to note that track input of 1 inch (2.54 cm) vertical and 3/4 inch (1.91 cm) lateral with lateral half wavelength being 62.0 ft. (18.90 m) excites the axle's acceleration to higher level than the one with lateral half-wavelengths of 39.0 ft (11.89 m) and 42.5 ft (12.95 m). Again, it has to be pointed out that no intention has been made in locating the most critical lateral irregularity wavelength in this study. However, it has been demonstrated that the operating speed, the wheel profile and the lateral irregularity wavelength are the parameters which affect the maximum axle lateral acceleration for a given vehicle and track with prescribed rail input.

3.2 Effects of Primary Stiffness on Locomotive Performance

In all the previous studies, the secondary suspension is changed without varying the primary suspension system. It is obvious that by varying simultaneously the primary and the secondary suspension, the stiffness ratio can be kept unchanged. In this section, the effects of soft and stiff primary suspension (relative to the one selected in previous studies) on locomotive response are investigated. Table 8 illustrates three types of primary suspension system of interest. Case 2 corresponds to the primary and secondary suspension systems used in all the previous studies. With reference to stiffness values of case 2, case 1 and case 3 represents a relatively soft and stiff primary and secondary suspension, respectively. If stiffnesses of case 2 are considered to 100%, the stiffnesses of case 1 and case 3 corresponds to 70% and 135% of the stiffnesses of case 2, respectively. Only limited simulations are performed in comparing the relative merits of the stiff and soft primary suspension systems. Generalization of the findings based on these limited study would not be recommended. The simulation results are normalized with respect to case 2 stiffness ratio of 12.63 in order to reflect the effects of relative stiffness of primary suspension on the locomotive performance.

In Figure 17 through Figure 21, the performance of locomotive, with different primary and secondary suspension systems,due to 2 inch(5.08 cm) vertical and 3 inch (7.62 cm) lateral rail input at 18 mph (28.96 km/h) speed are shown. The locomotive is equipped with wheels of 40 in. (101.6 cm)

diameter and with effective conicity of 1 in 40. The dominant lateral irregularity half-wavelength is assumed to be 39.0 ft (11.89m).

Figure 17 illustrates the carbody displacements transmissibility for primarly and secondary suspension of various degrees of stiffness. The results indicate that, as far as the carbody displacements are concerned, high (η = 8 to 12.63) and low (η = 1 to 4) stiffness ratio is desirable for the soft and stiff primarly suspension systems respectively.

The effects of primary suspension stiffness on the normalized minimum vertical wheel load and maximum lateral wheel load are presented in Figure 18 . It is interesting to observe that high stiffness ratio is desirable for the soft primary suspension as far as for the derailment tendency is concerned. Similarly, it can be observed that low stiffness ratio is desirable for the locomotive with stiff primary suspension system.

The normalized carbody rotation of the locomotive with primary suspension of various degrees of stiffness are illustrated in Figure 19. Comparisons between the results indicate that the most appropiate range of stiffness ratio for the carbody rotation would be 3 to 8.

As illustrated in Figure 20, the stiffness of the primary suspension has significant influence on the ride quality of the locomotive. The carbody vertical and lateral accelerations for the locomotive with soft primary suspension are relatively insensitive to the choice of stiffness ratio.

However, the carbody lateral acceleration of the locomotive with stiff primary suspension increases significantly as a function of stiffness ratio. Generally speaking, high stiffness ratio is undesirable for locomotive with all the primary suspension considered with respect to ride quality.

The plot of the maximum axle lateral acceleration is shown in Figure 21. The results indicate that the maximum axle lateral acceleration is not influenced by the choice of stiffness ratio. The stiff and soft primary suspension systems exhibit lower acceleration levels than the primary suspension of intermediate stiffness. Since, the lateral irregularity wavelength plays an important role in dictating the maximum axle lateral acceleration level. The above observed axle behavior may not be true in general.

4. SUMMARY AND CONCLUSIONS

A mathematical model, for analyzing the dynamic response of a six-axle locomotive on tangent track, is developed using a numerical integration technique. A thirty-nine (39) degree-of-freedom model is assumed for the locomotive. The excitation includes vertical and lateral rail input. The wheel-rail interaction is also taken into account based on the linear theory proposed by Wicken, Joly and Blader. The dynamic behavior of a typical six-axle locomotive subject to the selected vertical and/or lateral track irregularities is analyzed. The effects of primary and secondary suspension stiffnesses on the dynamic characteristics of the locomotive are studied. The 'optimum' stiffness ratio is selected based on the parametric studies performed.

As demonstrated, the dynamic performance of a locomotive depends greatly on its suspension systems and the track excitation. Proper design of locomotive suspension systems would ensure safe operation. However, the design of locomotive suspension system is, by no means, a straight forward and easy task. Frequently, the design objectives, which require extensive considerations in areas such as curving performance, lateral stability on tangent track, adhesion efficiency, derailment tendency, etc, impose certain potentially conflicting requirements. Consequently, no unique suspension system can be designed to achieve all the objectives simultaneously to the desired level of satisfaction.

Compromise between the objective requirements are often required in order to select an "optimum" suspension stiffness ratio. Based on the results of the limited parametric studies presented in section 3, there exists a region of stiffness ratio, namely between 4 to 8, in which a good compromise is achieved.

For the stiffness ratio greater than 8, the response characteristics of the locomotive at low and high operating speeds are deteriorated, thus results in poor ride quality. The variations on the minimum vertical wheel load and the maximum lateral wheel load become substantial and the safe L/V ratio limit may be exceeded. Consequently, a potential derailment may occur.

A stiffness ratio in the range of 1 to 4 is highly desirable from ride quality point of view, but this tends to cause large variation in the carbody rotation. As a result, it may induce an undesirable initial conditions for locomotive in curve entry on exit conditions. In addition, the large fluctuation in the minimum vertical wheel load may cause a derailment of the locomotive.

The analysis of the maximum axle lateral acceleration indicates that the critical acceleration level depends greatly on the predominant lateral irregularity wavelength, the effective conicity of the wheels and the operating speed for a given set of rail input. The critical lateral irregularity wavelength for a lovomotive at a given speed need not be critical when the speed or the property of the suspension is changed.

The limited study of the effects of primary and secondary suspensions with various degrees of stiffness on locomotive performance indicates that the response characteristics are generally deteriorated if a stiff suspension system is employed. However, the results tend to suggest that the "optimum" range of stiffness ratio also lies between values 4 to 8. Further studies have to be performed before the conclusion can be drawn on the "optimum" stiffness ratio for the locomotive with relatively stiff and soft primary and secondary suspension systems (with respect to the selected base line value).

Some recommended areas for further studies on the optimization of locomotive suspension system or for the future development of the model are given as follows:

1. The combined effects of profile error, alignments errors and gage errors on the locomotive dynamic response.
2. The "optimum" stiffness ratio for the locomotive with stiff and soft primary and secondary suspension systems.
3. The transient response of locomotive during transition from a section of tangent track to another section with different track irregularities.
4. The development of track loading spectrum at steady-state and transient conditions for track design.
5. The incorporation of the effects of wheel-flange clearances, and the non-linearity of primary and/or secondary systems into the model.
6. The incorporation of various integration schemes into the model for integrating the equation of motion. e.g. Euler's

method, Houbolt's method, Runge-Kutta integration technique, central difference method.

REFERENCES

1. Bathe, K.J., and Wilson, E.L., Numerical Methods in Finite Element Analysis, Prentice-Hall, Inc., New Jersey, 1976.

2. Blader, F.B., "Free Lateral Oscillations in Long Freight Trains" Ph.D Thesis, Queen's University at Kingston, Dept., of Mechanical Engineering August, 1972.

3. Blader, F.B. and Kurtz, E.F., Jr."Dynamic Stability of Cars in Long Freight Trains" Rail Transportation Division ASME, presented at the Winter Annual Meeting, Nov.11-15, 1973, Paper No.73-WA/RT-2.

4. Garg,V.K. Martin, G.C. Hartmann, P.W., "Technical Documentation : Locomotive Hunting Model "Track-Train Dynamic, Research Report No.R-219, A.A.R.

5. Joly, R "Study of the Traverse Stability of a Railway Vehicle Running at High Speed" Rail International, Feb. 1972.

6. Wicken, A.H., "The Dynamics of Railway Vehicles on straight tracks : Fundamental Considerations of Lateral Stability" Proc.Inst.Mech.Eng., Vol.180, pt.3F, London, 1965-66.

TABLE 1 GENERALIZED DISPLACEMENT FOR THE SIX-AXLE LOCOMOTIVE

MATRIX	SYMBOL	D.O.F. NO.	DESCRIPTION
$\{U^b\}$	y^b	1	Vehicle Body, vertical
	z^b	2	Vehicle Body, lateral
	ϕ^b	3	Vehicle Body, roll
	ψ^b	4	Vehicle Body, yaw
	θ^b	5	Vehicle Body, pitch
$\{U_1^t\}$	y_1^t	6	Truck 1, vertical
	z_1^t	7	Truck 1, lateral
	ϕ_1^t	8	Truck 1, roll
	ψ_1^t	9	Truck 1, yaw
	θ_1^t	10	Truck 1, pitch
$\{U_2^t\}$	y_2^t	11	Truck 2, vertical
	z_2^t	12	Truck 2, lateral
	ϕ_2^t	13	Truck 2, roll
	ψ_2^t	14	Truck 2, yaw
	θ_2^t	15	Truck 2, pitch
$\{U_1^a\}$	y_1^a	16	Axle 1, vertical
	z_1^a	17	Axle 1, lateral
	ϕ_1^a	18	Axle 1, roll
	ψ_1^a	19	Axle 1, yaw

TABLE 1 (continued)

MATRIX	SYMBOL	D.O.F. No.	DESCRIPTION
$\{U_2^a\}$	y_2^a	20	Axle 2, vertical
	z_2^a	21	Axle 2, lateral
	ϕ_2^a	22	Axle 2, roll
	ψ_2^a	23	Axle 2, yaw
$\{U_3^a\}$	y_3^a	24	Axle 3, vertical
	z_3^a	25	Axle 3, lateral
	ϕ_3^a	26	Axle 3, roll
	ψ_3^a	27	Axle 3, yaw
$\{U_4^a\}$	y_4^a	28	Axle 4, vertical
	z_4^a	29	Axle 4, lateral
	ϕ_4^a	30	Axle 4, roll
	ψ_4^a	31	Axle 4, yaw
$\{U_5^a\}$	y_5^a	32	Axle 5, vertical
	z_5^a	33	Axle 5, lateral
	ϕ_5^a	34	Axle 5, roll
	ψ_5^a	35	Axle 5, yaw
$\{U_6^a\}$	y_6^a	36	Axle 6, vertical
	z_6^a	37	Axle 6, lateral
	ϕ_6^a	38	Axle 6, roll
	ψ_6^a	39	Axle 6, yaw

Body	$[M^b]$								$\{\ddot{U}^b\}$
Front Truck		$[M_1^t]$							$\{\ddot{U}_1^t\}$
Rear Truck			$[M_2^t]$						$\{\ddot{U}_2^t\}$
Axle 1				$[M_1^a]$					$\{\ddot{U}_1^a\}$
Axle 2					$[M_2^a]$				$\{\ddot{U}_2^a\}$
Axle 3						$[M_3^a]$			$\{\ddot{U}_3^a\}$
Axle 4							$[M_4^a]$		$\{\ddot{U}_4^a\}$
Axle 5								$[M_5^a]$	$\{\ddot{U}_5^a\}$
Axle 6									$\{\ddot{U}_6^a\}$

NOTE : Only non-zero entries are shown

TABLE 2 MASS MATRIX, [M]

Body	$[K'_{1,1}]$	$[K'_{1,2}]$	$[K'_{1,3}]$						$\{U^b\}_{5x1}$
Front Truck	$[K'_{2,1}]$	$[K'_{2,2}]$		$[K'_{2,4}]$	$[K'_{2,5}]$	$[K'_{2,6}]$			$\{U^t_1\}_{5x1}$
Rear Truck	$[K'_{3,1}]$		$[K'_{3,3}]$				$[K'_{3,7}]$	$[K'_{3,8}]$	$[K'_{3,9}]$ $\{U^t_2\}_{5x1}$
Axle 1		$[K'_{4,2}]$		$[K'_{4,4}]$					$\{U^a_1\}_{4x1}$
Axle 2		$[K'_{5,2}]$			$[K'_{5,5}]$				$\{U^a_2\}_{4x1}$
Axle 3		$[K'_{6,2}]$				$[K'_{6,6}]$			$\{U^a_3\}_{4x1}$
Axle 4			$[K'_{7,3}]$				$[K'_{7,7}]$		$\{U^a_4\}_{4x1}$
Axle 5			$[K'_{8,3}]$					$[K'_{8,8}]$	$\{U^a_5\}_{4x1}$
Axle 6			$[K'_{9,3}]$						$[K'_{9,9}]$ $\{U^a_6\}_{4x1}$

NOTE : Only non-zero entries are shown

TABLE 3 STIFFNESS MATRIX, [K']

TABLE 3 STIFFNESS MATRIX, [K'] (CONT,D)

SUBMATRICES	SIZE	CONTENTS
$[K'_{1,1}]$	5x5	$[T_1^b]^T[K_s]\ [T_1^b] + [T_2^b]^T[K_s]\ [T_2^b]$
$[K'_{1,2}]$	5x5	$-[T_1^b]^T[K_s]\ [T_1^b]$
$[K'_{1,3}]$	5x5	$-[T_2^b]^T[K_s]\ [T_1^b]$
$[K'_{2,1}]$	5x5	$[K'_{1,2}]^T$
$[K'_{2,2}]$	5x5	$[T_1^t]^T[K_s]\ [T_1^t] + \sum_{k=1}^{3} [T_k^a]^T[K_p^k]\ [T_k^a]$
$[K'_{2,4}]$	5x4	$-[T_1^a]^T[K_p^1]\ [T^a]$
$[K'_{2,5}]$	5x4	$-[T_2^a]^T[K_p^2]\ [T^a]$
$[K'_{2,6}]$	5x4	$-[T_3^a]^T[K_p^3]\ [T^a]$
$[K'_{3,1}]$	5x5	$[K'_{1,3}]^T$
$[K'_{3,3}]$	5x5	$[T_2^t]^T[K_s]\ [T_2^t] + \sum_{k=4}^{6} [T_k^a]^T[K_p^k]\ [T_k^a]$
$[K'_{3,7}]$	5x4	$-[T_4^a]^T[K_p^4]\ [T^a]$
$[K'_{3,8}]$	5x4	$-[T_5^a]^T[K_p^5]\ [T^a]$
$[K'_{3,9}]$	5x4	$-[T_6^a]^T[K_p^6]\ [T^a]$
$[K'_{4,2}]$	4x5	$[K'_{2,4}]^T$
$[K'_{4,4}]$	4x4	$[T^a]^T[K_p^1]\ [T^a] + [T^r]^T[K_R]\ [T^r]$
$[K'_{5,2}]$	4x5	$[K'_{2,5}]^T$
$[K'_{5,5}]$	4x4	$[T^a]^T[K_p^2]\ [T^a] + [T^r]^T[K_R]\ [T^r]$
$[K'_{6,2}]$	4x5	$[K'_{2,6}]^T$
$[K'_{6,6}]$	4x4	$[T^a]^T[K_p^3]\ [T^a] + [T^r]^T[K_R]\ [T^r]$
$[K'_{7,3}]$	4x5	$[K'_{3,7}]^T$

TABLE 3 STIFFNESS MATRIX,[K'] (CONT,D)

SUBMATRICES	SIZE	CONTENTS
$[K'_{7,7}]$	4x4	$[T^a]^T[K^4_p]\ [T^a] + [T^r]^T[K_R]\ [T^r]$
$[K'_{8,3}]$	4x5	$[K'_{3,8}]^T$
$[K'_{8,8}]$	4x4	$[T^a]^T[K^5_p]\ [T^a] + [T^r]^T[K_R]\ [T^r]$
$[K'_{9,3}]$	4x5	$[K'_{3,9}]^T$
$[K'_{9,9}]$	4x4	$[T^a]^T[K^6_p]\ [T^a] + [T^r]^T[K_R]\ [T^r]$

Body	$[C'_{1,1}]$	$[C'_{1,2}]$	$[C'_{1,3}]$						$\{\dot{U}^b\}_{5x1}$
Front Truck	$[C'_{2,1}]$	$[C'_{2,2}]$		$[C'_{2,4}]$	$[C'_{2,5}]$	$[C'_{2,6}]$			$\{\dot{U}^t_1\}_{5x1}$
Rear Truck	$[C'_{3,1}]$		$[C'_{3,3}]$				$[C'_{3,7}]$	$[C'_{3,8}]$	$[C'_{3,9}]$ $\{\dot{U}^t_2\}_{5x1}$
Axle 1		$[C'_{4,2}]$		$[C'_{4,4}]$					$\{\dot{U}^a_1\}_{4x1}$
Axle 2		$[C'_{5,2}]$			$[C'_{5,5}]$				$\{\dot{U}^a_2\}_{4x1}$
Axle 3		$[C'_{6,2}]$				$[C'_{6,6}]$			$\{\dot{U}^a_3\}_{4x1}$
Axle 4			$[C'_{7,3}]$				$[C'_{7,7}]$		$\{\dot{U}^a_4\}_{4x1}$
Axle 5			$[C'_{8,3}]$					$[C'_{8,8}]$	$\{\dot{U}^a_5\}_{4x1}$
Axle 6			$[C'_{9,3}]$						$[C'_{9,9}]$ $\{\dot{U}^a_6\}_{4x1}$

NOTE : Only non-zero entries are shown

TABLE 4 DAMPING MATRIX, [C']

TABLE 4 DAMPING MATRIX, [C'](CONT,D)

SUBMATRICES	SIZE	CONTENTS
$[C'_{1,1}]$	5x5	$[T_1^b]^T[C_s]\ [T_1^b] + [T_2^b]^T[C_s]\ [T_2^b]$
$[C'_{1,2}]$	5x5	$-[T_1^b]^T[C_s]\ [T_1^t]$
$[C'_{1,3}]$	5x5	$-[T_2^b]^T[C_s]\ [T_2^t]$
$[C'_{2,1}]$	5x5	$[C'_{1,2}]^T$
$[C'_{2,2}]$	5x5	$[T_1^t]^T[C_s]\ [T_1^t] + \sum_{k=1}^{3} [T_k^a]^T[C_p^k]\ [T_k^a]$
$[C'_{2,4}]$	5x4	$-[T_1^a]^T[C_p^1]\ [T^a]$
$[C'_{2,5}]$	5x4	$-[T_2^a]^T[C_p^2]\ [T^a]$
$[C'_{2,6}]$	5x4	$-[T_3^a]^T[C_p^3]\ [T^a]$
$[C'_{3,1}]$	5x5	$[C'_{1,3}]^T$
$[C'_{3,3}]$	5x5	$[T_2^t]^T[C_s]\ [T_2^t] + \sum_{k=4}^{6} [T_k^a]^T[C_p^k]\ [T_k^a]$
$[C'_{3,7}]$	5x4	$-[T_4^a]^T[C_p^4]\ [T^a]$
$[C'_{3,8}]$	5x4	$-[T_5^a]^T[C_p^5]\ [T^a]$
$[C'_{3,9}]$	5x4	$-[T_6^a]^T[C_p^6]\ [T^a]$
$[C'_{4,2}]$	4x5	$[C'_{2,4}]^T$
$[C'_{4,4}]$	4x4	$[T^a]^T[C_p^1]\ [T^a] + [T^r]^T[C_R]\ [T^r]$
$[C'_{5,2}]$	4x5	$[C'_{2,5}]^T$
$[C'_{5,5}]$	4x4	$[T^a]^T[C_p^2]\ [T^a] + [T^r]^T[C_R]\ [T^r]$
$[C'_{6,2}]$	4x5	$[C'_{2,6}]^T$
$[C'_{6.6}]$	4x4	$[T^a]^T[C_p^3]\ [T^a] + [T^r]^T[C_R]\ [T^r]$
$[C'_{7,3}]$	4x5	$[C'_{3,7}]^T$

TABLE 4 DAMPING MATRIC, [C'] (CONT,D)

SUBMATRICES	SIZE	CONTENTS
$[C'_{7,7}]$	4x4	$[T^a]^T[C_p^4]\ [T^a] + [T^r]^T[C_R]\ [T^r]$
$[C'_{8,3}]$	4x5	$[C'_{3,8}]^T$
$[C'_{8,8}]$	4x4	$[T^a]^T[C_p^5]\ [T^a] + [T^r]^T[C_R]\ [T^r]$
$[C'_{9,3}]$	4x5	$[C'_{3,9}]^T$
$[C'_{9,9}]$	4x4	$[T^a]^T[C_p^6]\ [T^a] + [T^r]^T[C_R]\ [T^r]$

TABLE 5 INPUT DATA FOR 6-AXLE LOCOMOTIVE

DIMENSIONAL DATA

A1	Distance between front truck center and leading axle (axle 1)	=	79.38 in. (201.63 cm)
A2	Distance between front truck center and middle axle (axle 2)	=	-1.25 in (-3.18 cm)
A3	Distance between front truck center and trailing axle (axle 3)	=	-85.00 in (-215.90 cm)
A4	Distance between rear truck center and leading axle (axle 4)	=	85.00 in (215.90 cm)
A5	Distance between rear truck center and middle axle (axle 5)	=	1.25 in (3.18 cm)
A6	Distance between rear truck center and trailing axle (axle 6)	=	-79.38 in. (-201.63 cm)
B	Half distance between wheel contact points	=	29.5 in (74.9 cm)
B1	Half lateral distance between primary suspension	=	39.5 in (100.3 cm)
B2	Half lateral distance between secondary suspension	=	35.12 in (89.20 cm)
HT	Height of truck frame center of gravity above axle center	=	2.50 in (6.35 cm)
H1	Height of bolster spring center above truck frame center of gravity	=	5.00 in (12.70 cm)
H2	Height of carbody center of gravity above bolster spring center	=	50.20 in (127.50 cm)

XL1	Distance between carbody center and leading truck center	=	276.00 in (701.04 cm)
XL2	Distance between carbody center and trailing truck center	=	276.00 in (701.04 cm)
XLBAR	Distance between truck center and bolster spring center	=	0.00 in (0.00 cm)
RO	Wheel tread radius	=	20.00 in (50.80 cm)

MASS AND INERTIA DATA:

XMB	Carbody mass	=	766 lb-sec^2/in (347 kg)
XMT	Truck frame mass	=	40 lb-sec^2/in (18.2 kg)
XMA	Wheel-axle set mass	=	30 lb-sec^2/in (13.6 kg)
XJB	Carbody roll mement of inertia	=	1,720,000 lb-in-sec^2 (195,000 kg-m^2)
XIB	Carbody yaw mement of inertia	=	39,600,000 lb-in-sec^2 (4,490,000 kg-m^2)
XJBB	Carbody pitch moment of inertia	=	15,000,000 lb-in-sec^2 (17,005,800 kg-m^2)
XJT	Truck frame roll moment of inertia	=	56,000 lb-in-sec^2 (6,350 kg-m^2)
XIT	Truck frame yaw moment of inertia	=	178,000 lb-in-sec^2 (20,200 kg-m^2)
XJBT	Truck frame pitch moment of inertia	=	45,000 lb-in-sec^2 (5,100 kg-m^2)

XJA	Wheel-axle set roll moment of inertia	=	8,000 lb-in-sec^2 (970 kg-m^2)
XIA	Wheel axle set yaw moment of Inertia	=	16,500 lb-in -sec^2 (1,870 kg-m^2)

SPRING RATES AND DAMPING DATA:

XKXT	Longitudinal secondary stiffness per truck side	=	11,000 lb/in (1,930 KN/m)
XKYT	Vertical secondary stiffness per truck side	=	250,000 lb/in (43,750 KN/m)
XKZT	Lateral secondary stiffness per truck side	=	11,000 lb/in (1,930 kN/m)
XKXA	Longitudinal primary stiffness per axle side	=	250,000 lb/in (43,750 kN/m)
XKYA	Vertical primary stiffness per axle side	=	6,600 lb/in (1,155 kN/m)
XKZA	Lateral primary stiffness per axle side	=	2,000 lb/in (350 kN/m)
CXT	Longitudinal damping of secondary suspension per truck side	=	300 lb-sec/in (52.50 kN.s/m)
CYT	Vertical damping of secondary suspension per truck side	=	250 lb-sec/in (43.75 kN.s/m)
CZT	Lateral damping of secondary suspension per truck side	=	300 lb-sec/in (52.50 kN.s/m)
CXA	Longitudinal damping of primary suspension per axle side	=	6.25 lb-sec/in (1.10 kN.s/m)
CYA	Vertical damping of primary suspension per axle side	=	50 lb-sec/in (8.75 kN.s/m)

CZA	Lateral damping of primary suspension per axle side	=	200 lb-sec/in (35 kN.s/m)

MISCELLANEOUS DATA

FL	Lateral creep coefficient per wheel	=	4,000,000 lb (17,800 kN)
FT	Longitudinal creep coefficient per wheel	=	4,000,000 lb (17,800 kN)
FS23	Lateral spin creep coefficient per wheel	=	0.0 lb (0.0 kN)
FS33	Longitudinal spin creep coefficient per wheel	=	0.0 lb (0.0 kN)
W	Axle load	=	66,000 lb (293 kN)
V	Velocity of locomotive	=	Variable
RHO(δ)	Nominal wheel taper in central position	=	0.025, 0.05 or 0.10
XLAMD(λ)	Effective conicity	=	0.025, 0.05 or 0.10
ZETA(ξ)	Rate of change of distance between axle center line and contact points with respect to lateral displacement of wheel-set.	=	1.00
EPSI(ε)	Rate of change of contact plane slope with respect to lateral displacement of wheel-set.	=	0.025, 0.05 or 0.10

TRACK DATA:

XKYR	Vertical rail stiffness	=	120,000 lb/in (21,000 kN/m)
XKZR	Lateral rail stiffness	=	80,000 lb/in (14,000 kN/m)
CYR	Vertical rail damping	=	10 lb-sec/in (1.75 kN.s/m)
CZR	Lateral rail damping	=	10 lb-sec/in (1.75 kN.s/m)
XLR	Rail length	=	468 in (1188.7 cm)
AMPR	Amplitude of vertical input at right rail	=	Variable
AMPL	Amplitude of vertical input at left rail	=	Variable
AMPRL	Amplitude of lateral input at right rail	=	Variable
FRQRL	Frequency of lateral rail input, CPS	=	Variable
ANGRL	Phase angle, degree	=	Variable
AMPLL	Amplitude of lateral input at left rail	=	Variable
FRQLL	Frequency of lateral rail input, CPS	=	Variable
ANGLL	Phase angle, degree	=	Variable
THETA	Value used in the Wilson-θ integration technique.	$\geq$	1.37

TABLE 6 RANGE OF STIFFNESS RATIO, η BEING CONSIDERED IN THE STUDY

UNIT : KIPS/IN

STIFFNESS RATIO, η	12.63	8.0	4.0	2.0	1.0
Secondary Suspension per truck side					
Vertical	250.0	158.4	79.2	39.6	19.8
Lateral	11.0	7.0	3.5	1.75	0.875
Primary suspension per side axle					
Vertical	6.6	6.6	6.6	6.6	6.6
Lateral	2.0	2.0	2.0	2.0	2.0

Base Value

$$\eta = \frac{\text{Secondary Suspension Stiffness per truck side}}{\text{Primary Suspension Stiffness per truck side}}$$

$$= \frac{250.0}{3(6.6)}$$

$$= 12.63$$

NOTE : 1 lb/in = 175.13 N/m

TABLE 7 VARIATIONS IN NORMALIZED CARBODY ROTATION

SPEED : 18 MPH (28.96 km/n)
80 MPH(128.72 km/n)

STIFFNESS RATIO η	1	2	4	6	8
CARBODY ROLL	0.258-2.391	0.400-1.670	0.708-1.391	0.610-1.125	0.597-1.141
	(2.133)*	(1.270)	(0.683)	(0.515)	(0.544)
CARBODY YAW	0.450-1.188	0.511-1.151	0.714-1.550	0.790-1.271	0.930-1.124
	(0.738)	(0.580)	(0.836)	(0.481)	(0.194)
CARBODY PITCH	0.332-1.510	0.378-1.297	0.538-1.432	0.680-1.330	0.775-1.210
	(1.178)	(0.919)	(0.894)	(0.650)	(0.435)

NOTE : Carbody roll, yaw and pitch are normalized with respect to the carbody roll, yaw and pitch with stiffness ratio of 12.63

* The net variation of the normalized carbody rotation is given within the brackets.

TABLE 8 PRIMARY AND SECONDARY SUSPENSION STIFFNESSES

UNIT : KIPS/IN

(Conversion factor 1lb/in.=175.13 N/m)

CASE	STIFFNESS RATIO, η	12.63	8.0	4.0	2.0	1.0
	Secondary Suspension per truck side					
	Vertical	175.0	110.88	55.44	27.720	13.86
(1)	Lateral	7.7	4.90	2.45	1.225	0.613
70%	Primary suspension per axle side.					
	Vertical	4.62	4.62	4.62	4.62	4.62
	Lateral	1.40	1.40	1.40	1.40	1.40
	Secondary Suspension per truck side.					
	Vertical	250.00	158.40	79.20	39.60	19.800
(2)	Lateral	11.00	7.00	3.50	1.75	0.875
100%	Primary Suspension per axle side.					
	Vertical	6.6	6.6	6.6	6.6	6.6
	Lateral	2.0	2.0	2.0	2.0	2.0
	Secondary Suspension per truck side.					
	Vertical	337.50	213.84	106.920	53.460	26.730
(3)	Lateral	14.85	9.45	4.725	2.363	1.181
135%	Primary Suspension per axle side.					
	Vertical	8.91	8.91	8.91	8.91	8.91
	Lateral	2.70	2.70	2.70	2.70	2.70

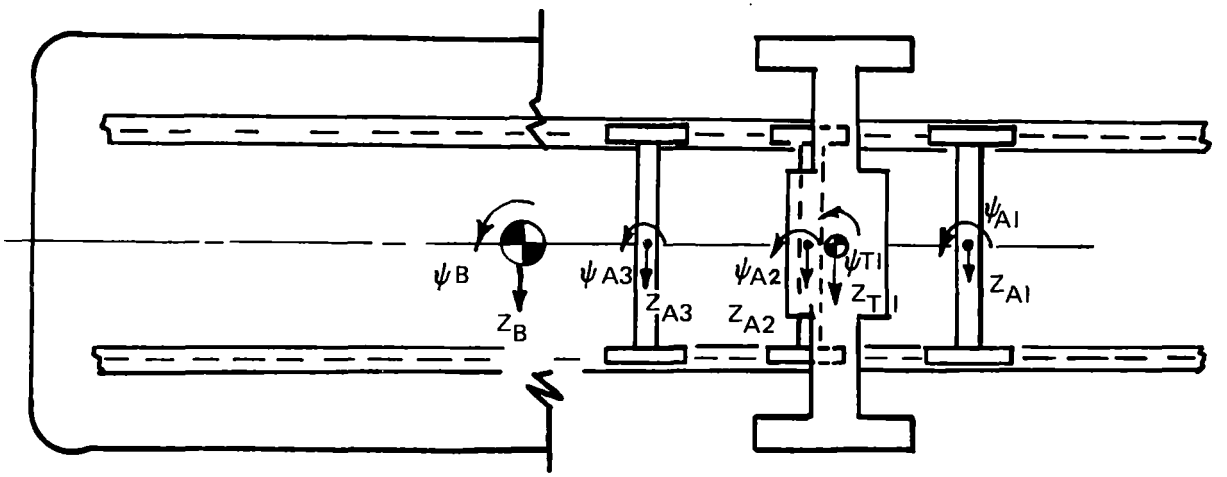

PLAN

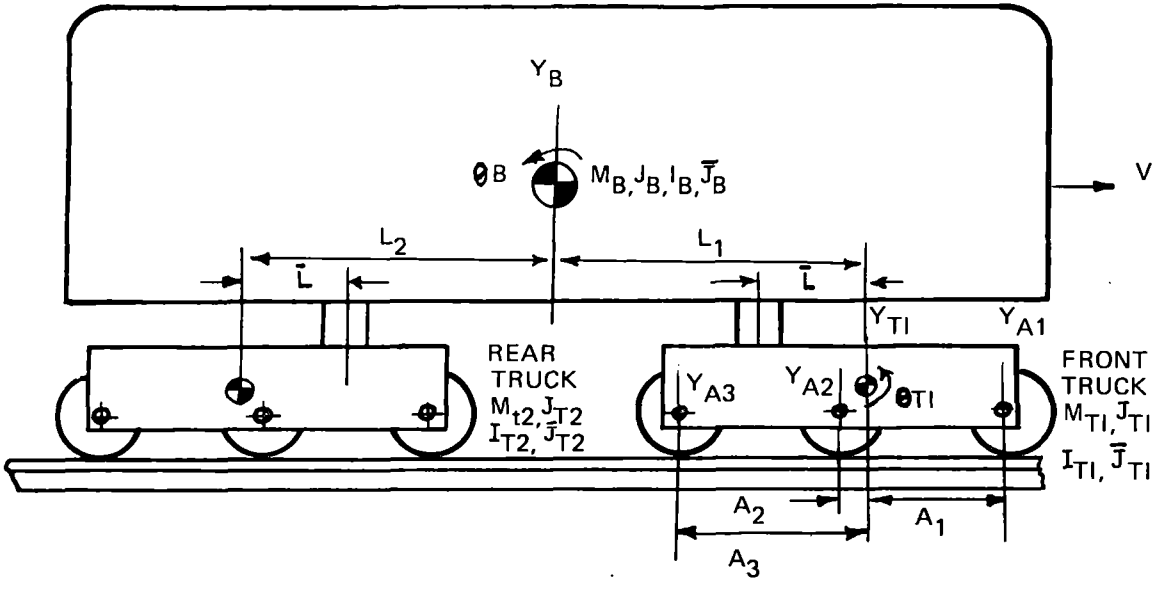

ELEVATION

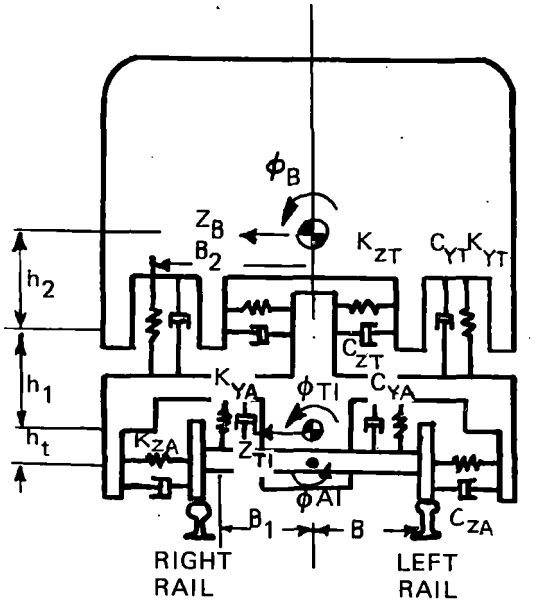

END VIEW

FIGURE 1 SIX-AXLE LOCOMOTIVE MODEL

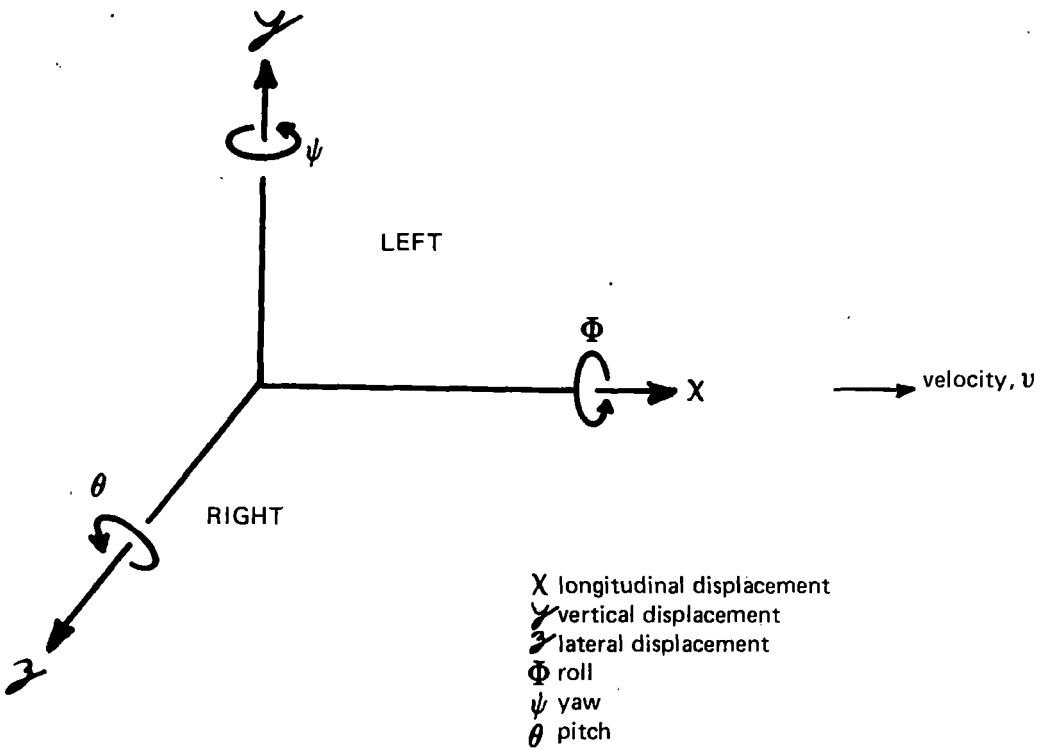

FIGURE 2 CARTESIAN CO-ORDINATES DEFINING THE DISPLACEMENTS OF A SIX-AXLE LOCOMOTIVE SYSTEM

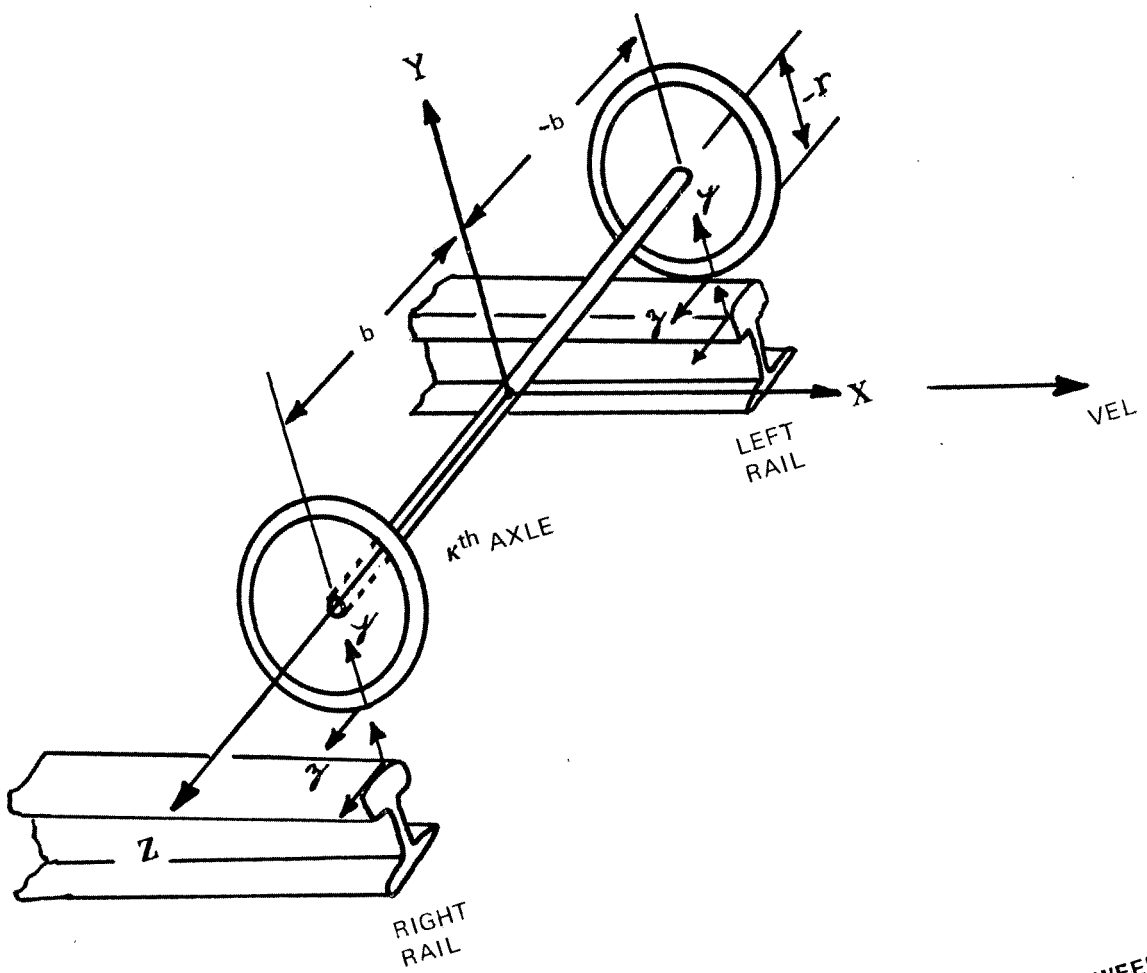

FIGURE 3 CO-ORDINATE SYSTEM FOR RELATIVE DISPLACEMENTS BETWEEN THE κ^{th} AXLE AND RAILS

$$u^{ry} = A_o \left| \sin(\omega t) \right|$$

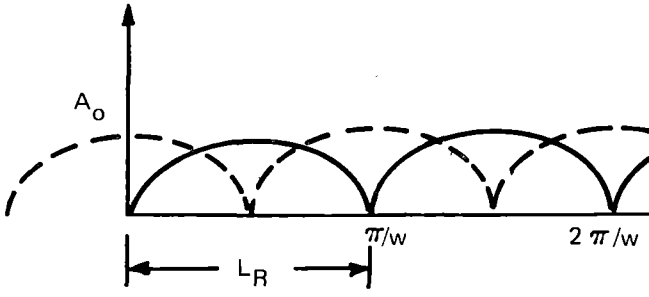

FIGURE 4 VERTICAL RAIL INPUT

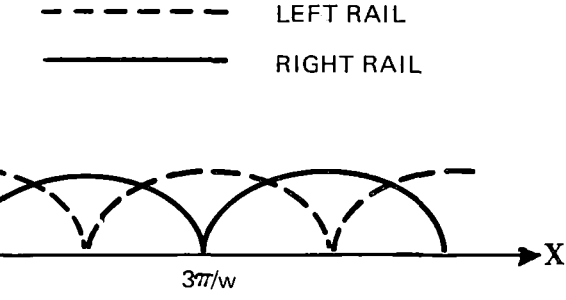
LEFT RAIL
RIGHT RAIL
X
3π/w

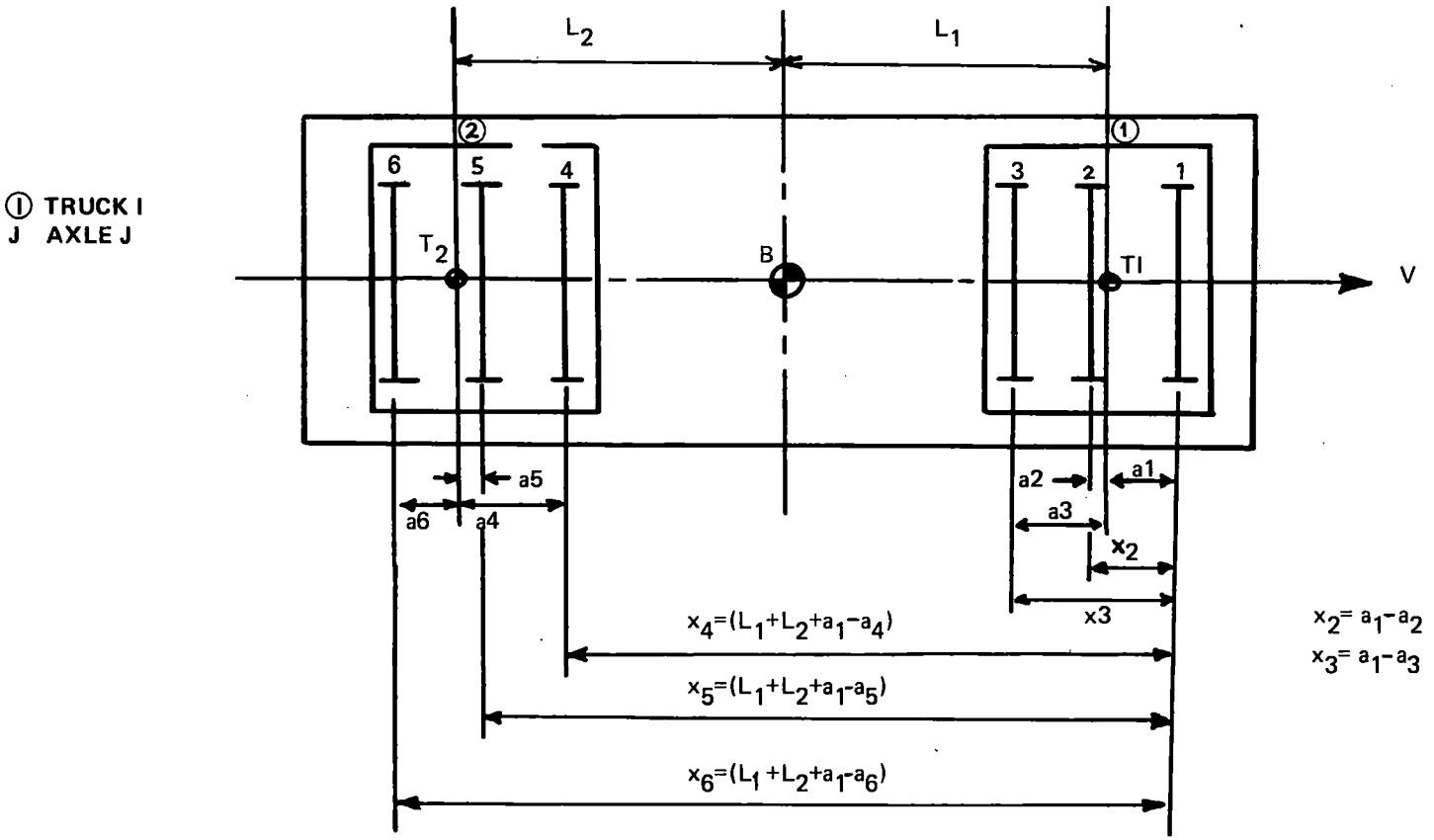

note; a_i is defined to be positive when it is in the positive direction, otherwise it is negative

FIGURE5 RELATIVE POSITIONS OF THE AXLES

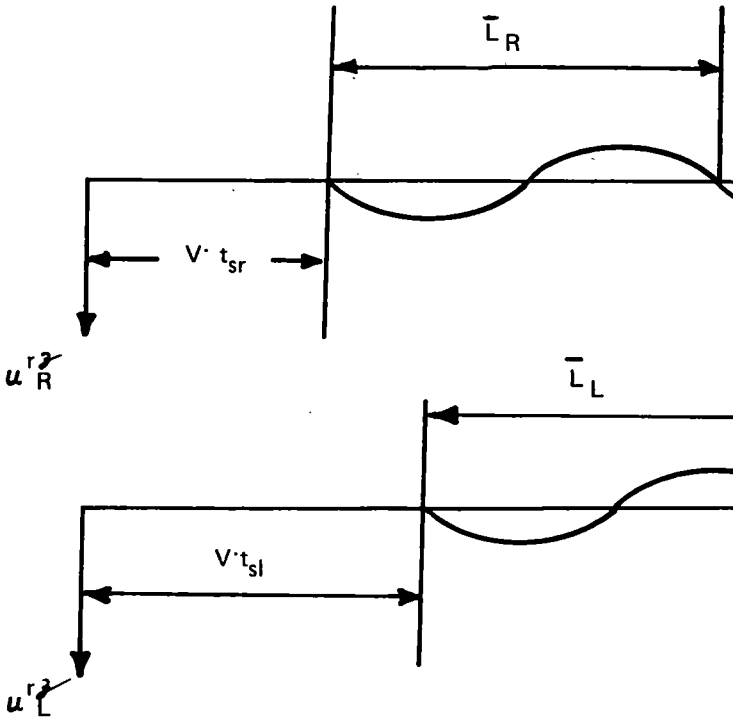

FIGURE 6 LATERAL RAIL INPUT

RIGHT RAIL

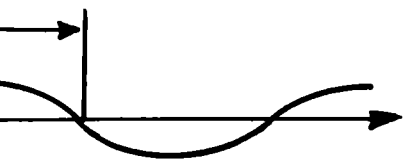

LEFT RAIL

FIGURE 7 VERTICAL, LATERAL AND LONGITUDINAL SPRINGS AND DAMPERS ORIENTATIONS ASSUMED IN THE FORCE CALCULATIONS

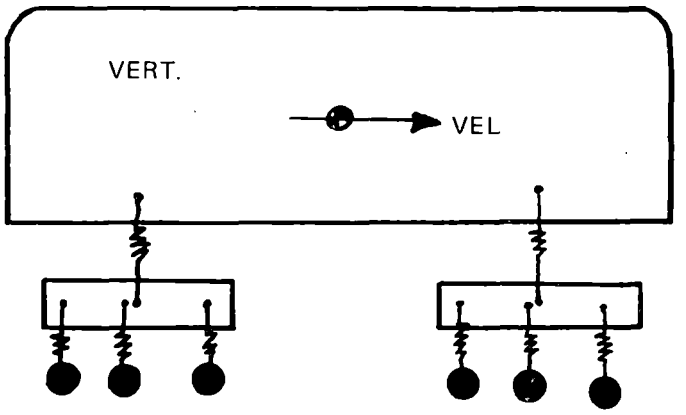

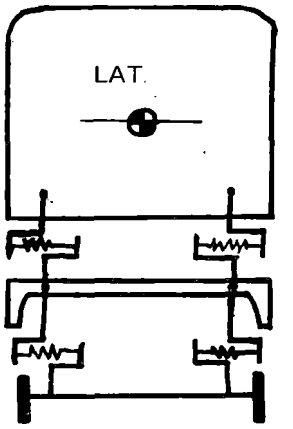

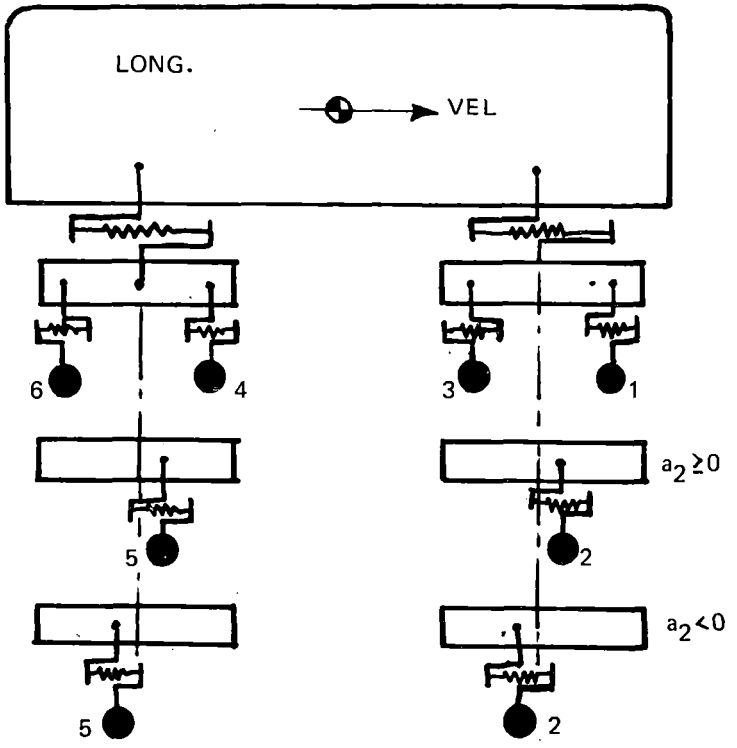

note; the dampers are oriented in the same fashion as those for the vertical, lateral and longitudinal springs.

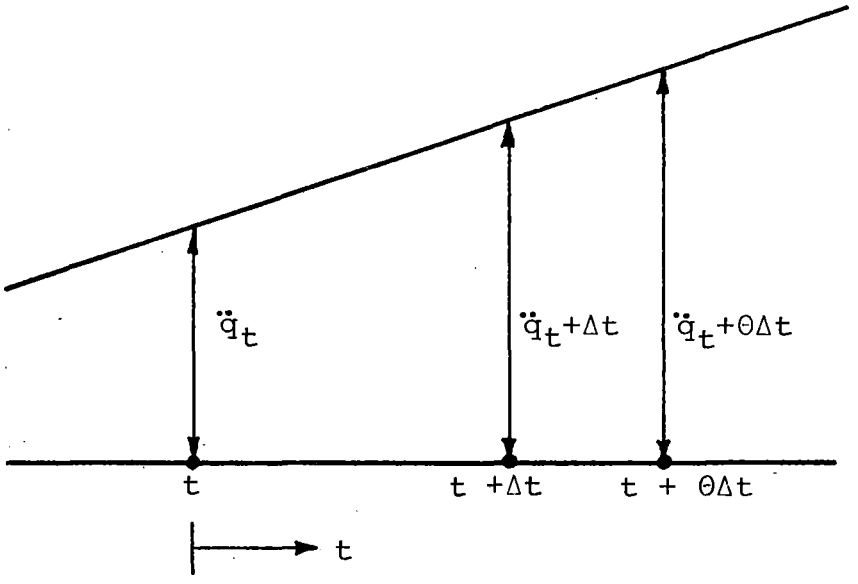

(A) LINEAR ACCELERATION ASSUMPTION OF WILSON-θ METHOD

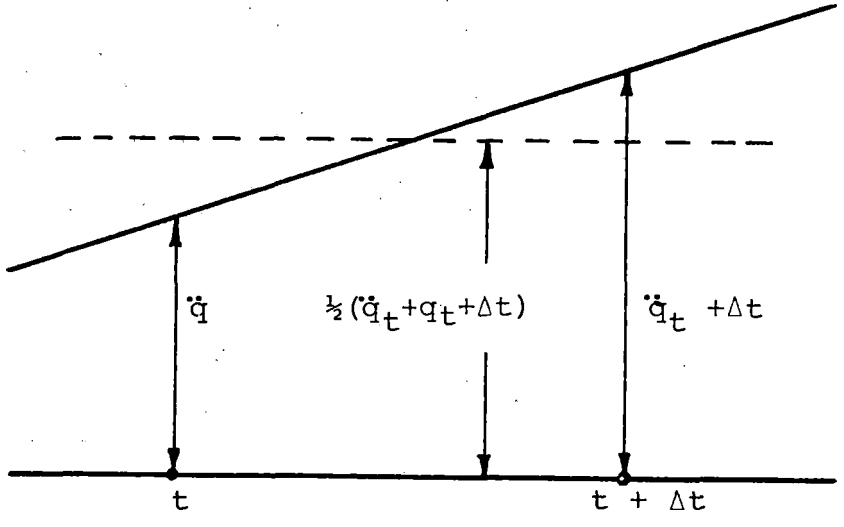

(B) NEWMARK'S CONSTANT-AVERAGE-ACCELERATION SCHEME

FIG 8. NUMERICAL INTEGRATION OF EQUATION OF MOTION [1]

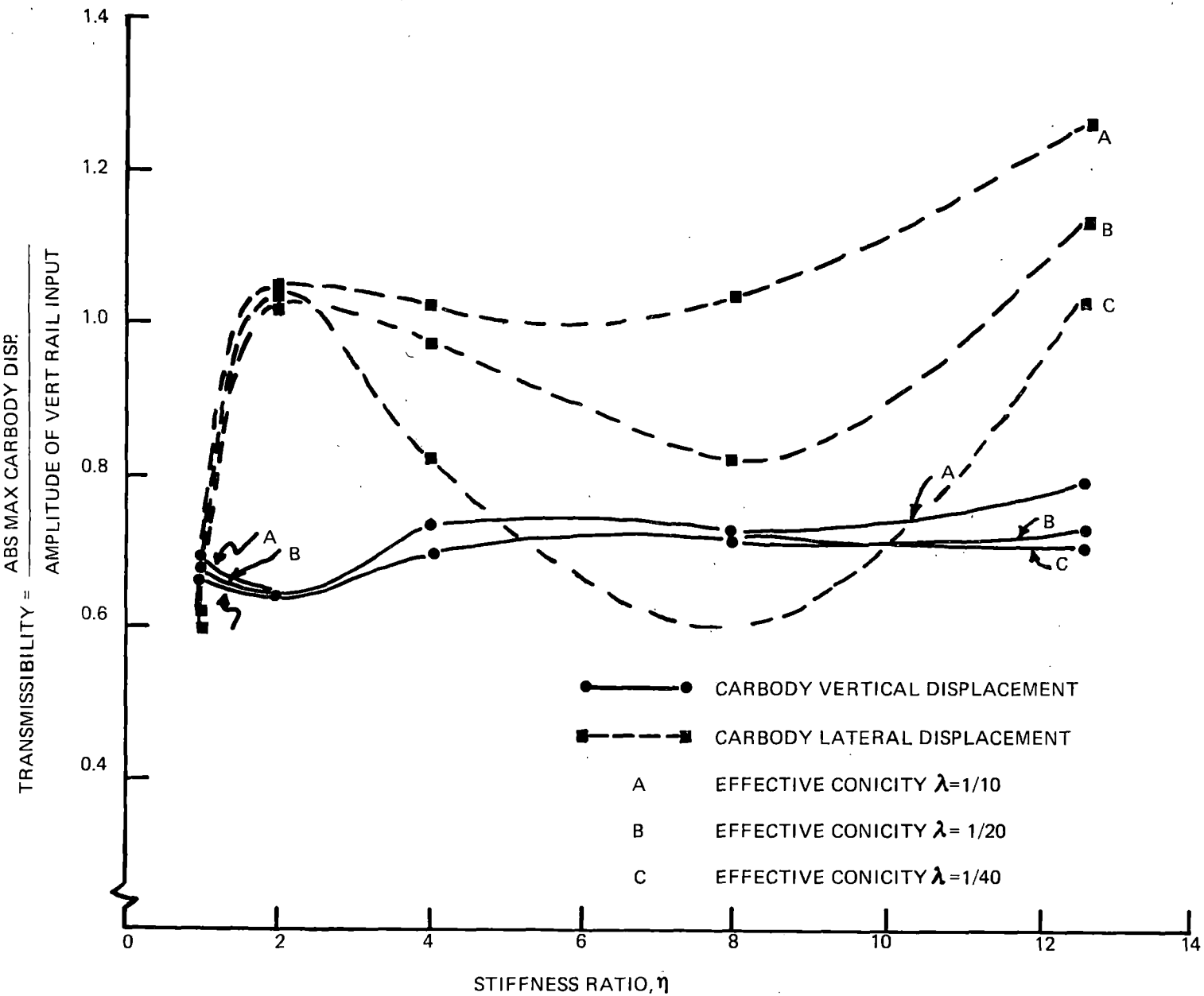

FIGURE 9A – TRANSMISSIBILITY VS. STIFFNESS RATIO, η AT 18 MPH (28.96 KM/H) SPEED DUE TO 1 INCH (2.54 CM) VERTICAL RAIL INPUT

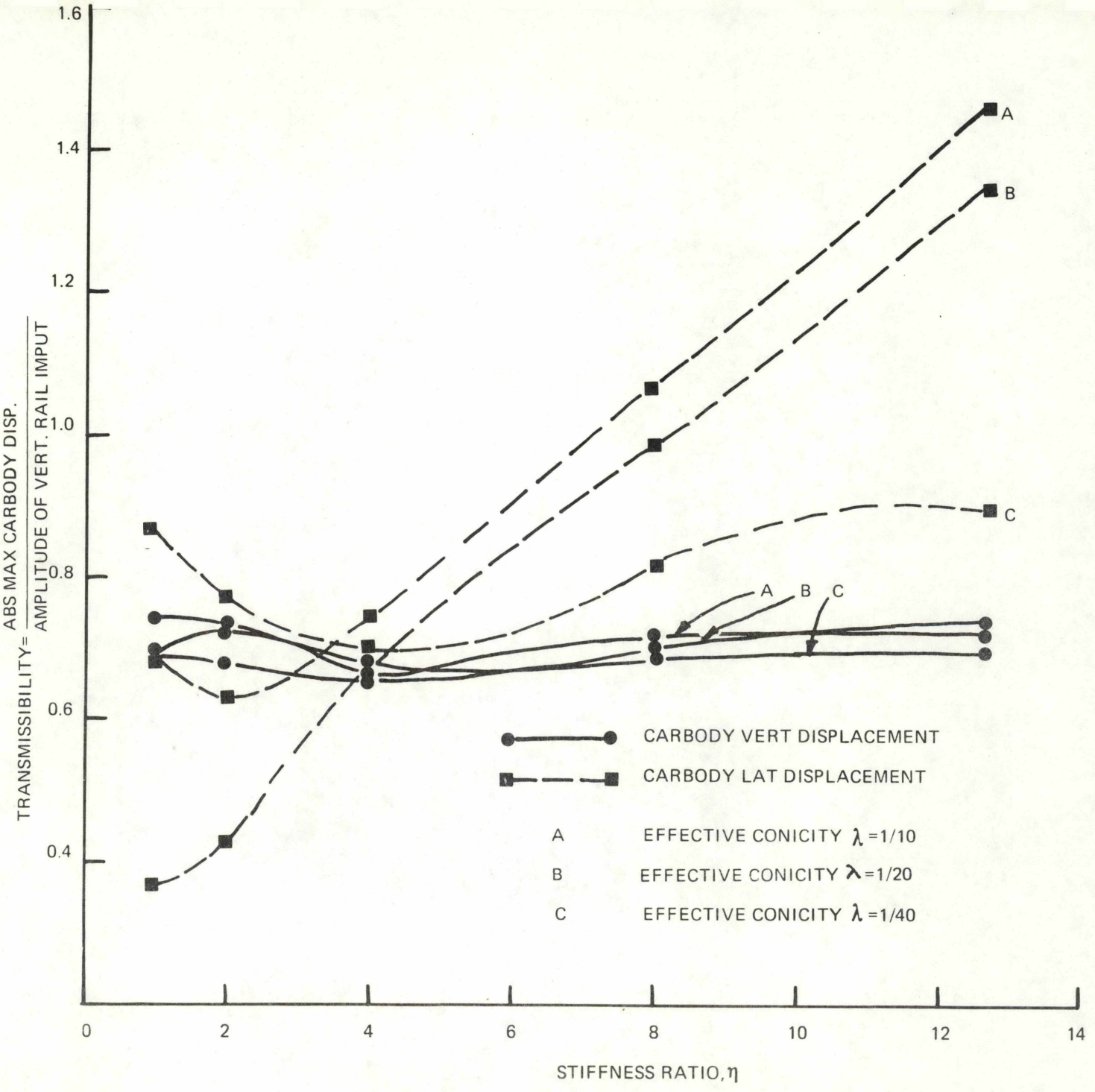

FIGURE 9B – TRANSMISSIBILITY VS. STIFFNESS RATIO, η AT 18 MPH (28.96 KM/H) SPEED DUE TO 2 INCH (5.08 CM) VERTICAL RAIL INPUT

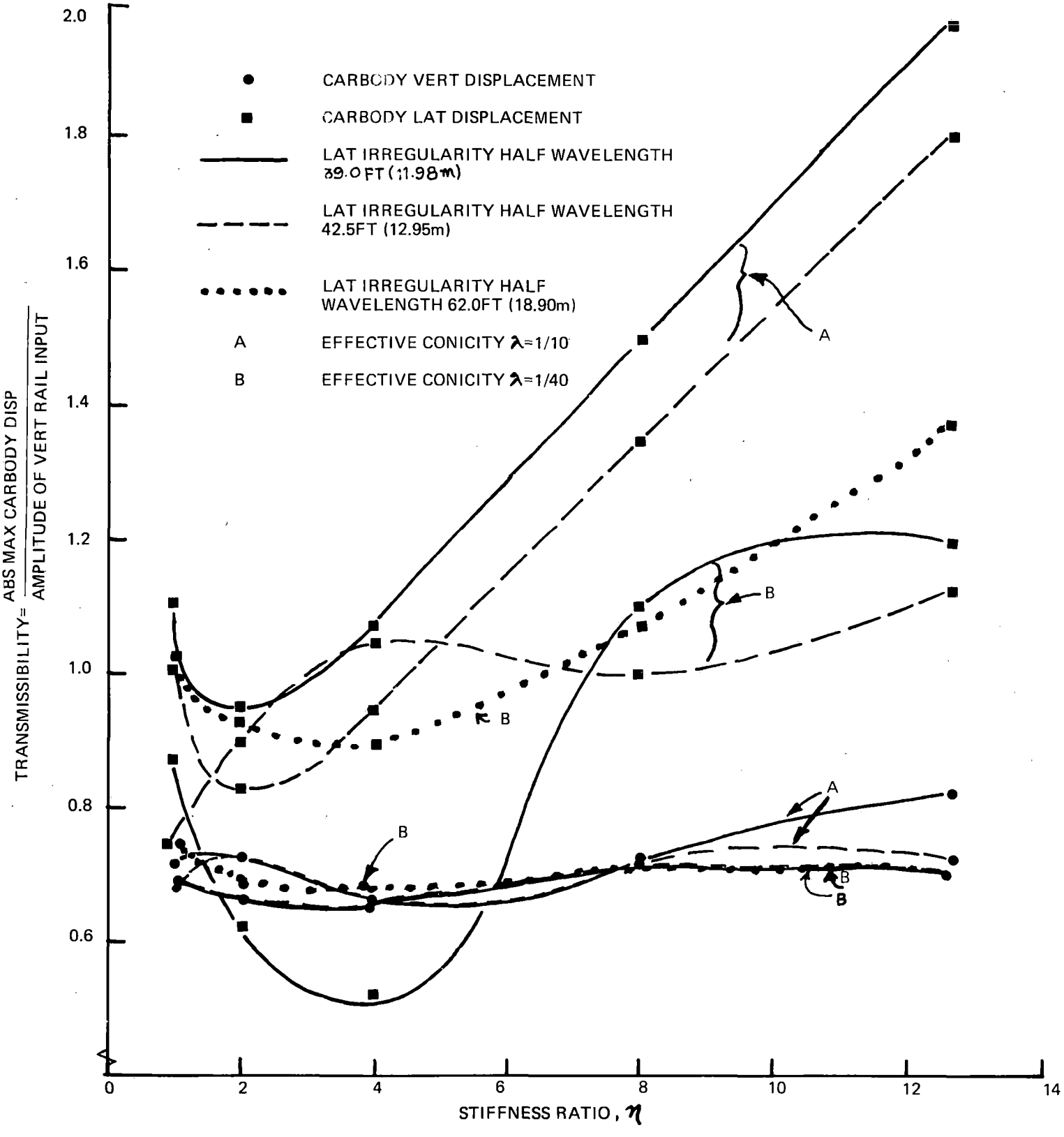

FIGURE 9C TRANSMISSIBILITY VS. STIFFNESS RATIO η AT 18 MPH (28.96 KM/H) SPEED DUE TO 2 INCH (5.08CM) VERTICAL AND 3 INCH (7.62 CM) LATERAL RAIL INPUT

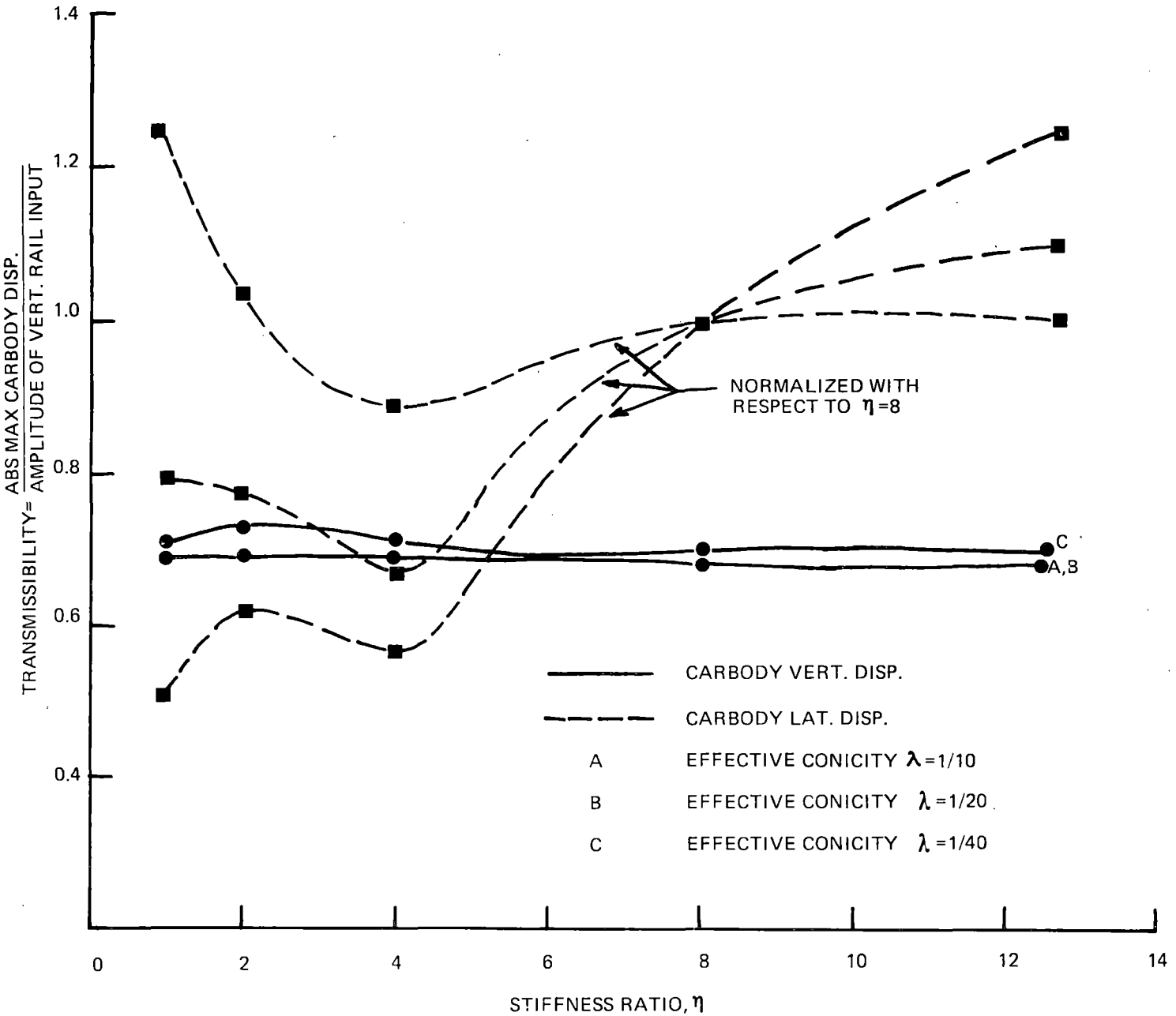

FIGURE 10A – TRANSMISSIBILITY VS. STIFFNESS RATIO, η AT 80 MPH (128.72 KM/H) SPEED DUE TO 1 INCH (2.54 CM) VERTICAL RAIL INPUT

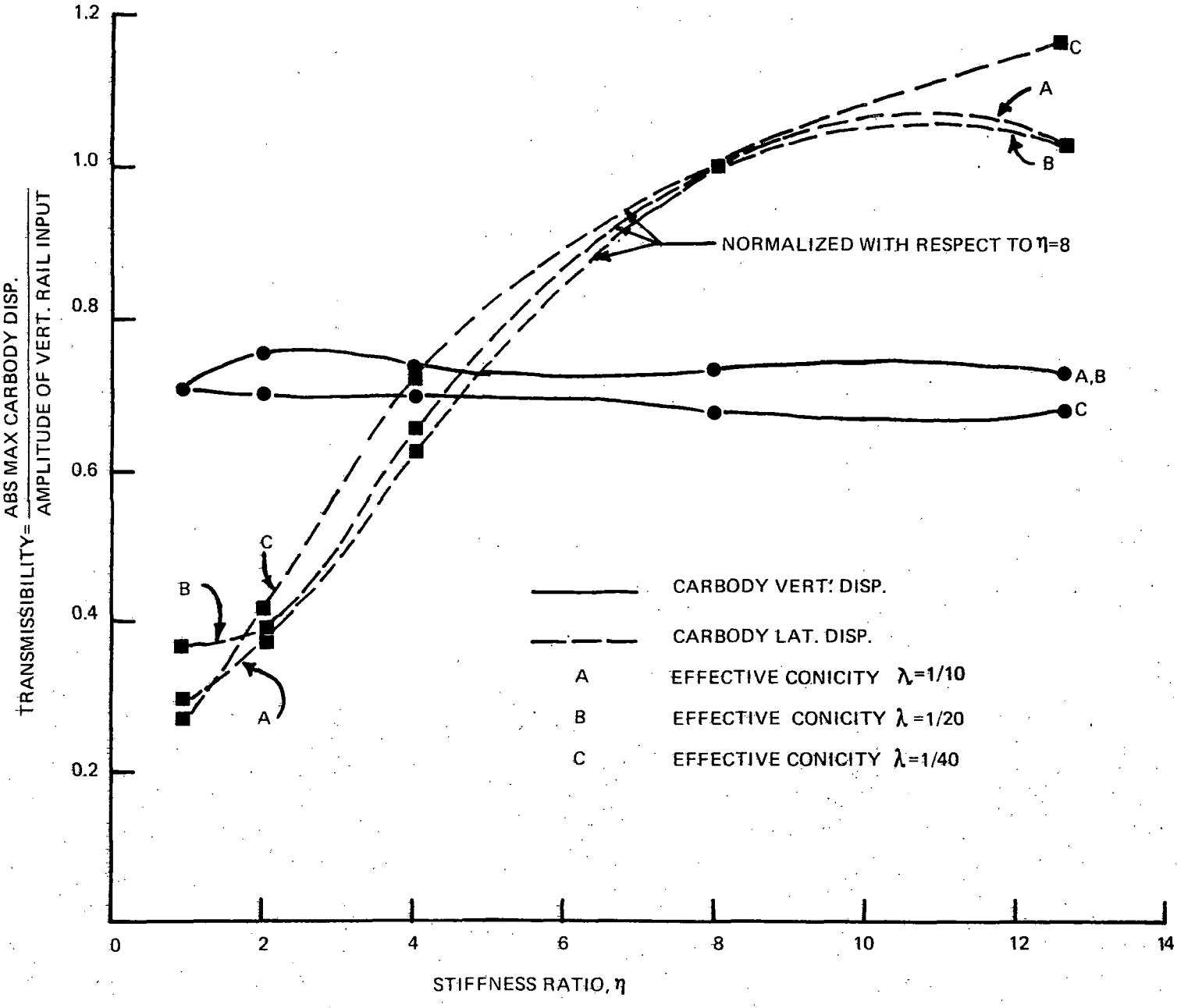

FIGURE 10B – TRANSMISSIBILITY VS. STIFFNESS RATIO, η AT 80 MPH (128.72 KM/H) SPEED DUE TO 2 INCH (5.08 CM) VERTICAL RAIL INPUT

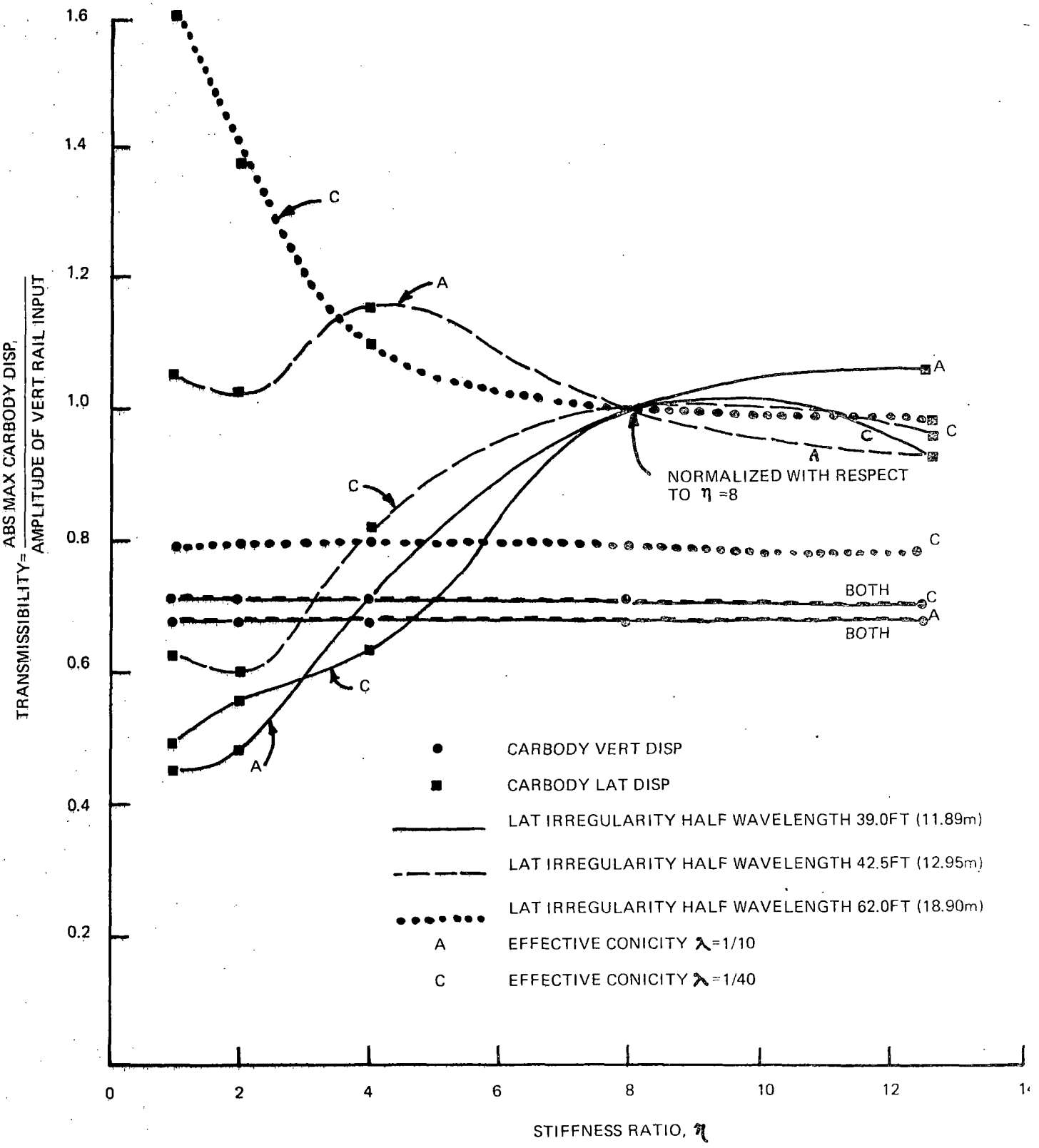

FIGURE 10C – TRANSMISSIBILITY VS. STIFFNESS RATIO, η AT 80 MPH (128.72 KM/H) SPEED DUE TO 1 INCH (2.54 CM) VERTICAL AND ¾ INCH (1.91 CM) LATERAL RAIL INPUT

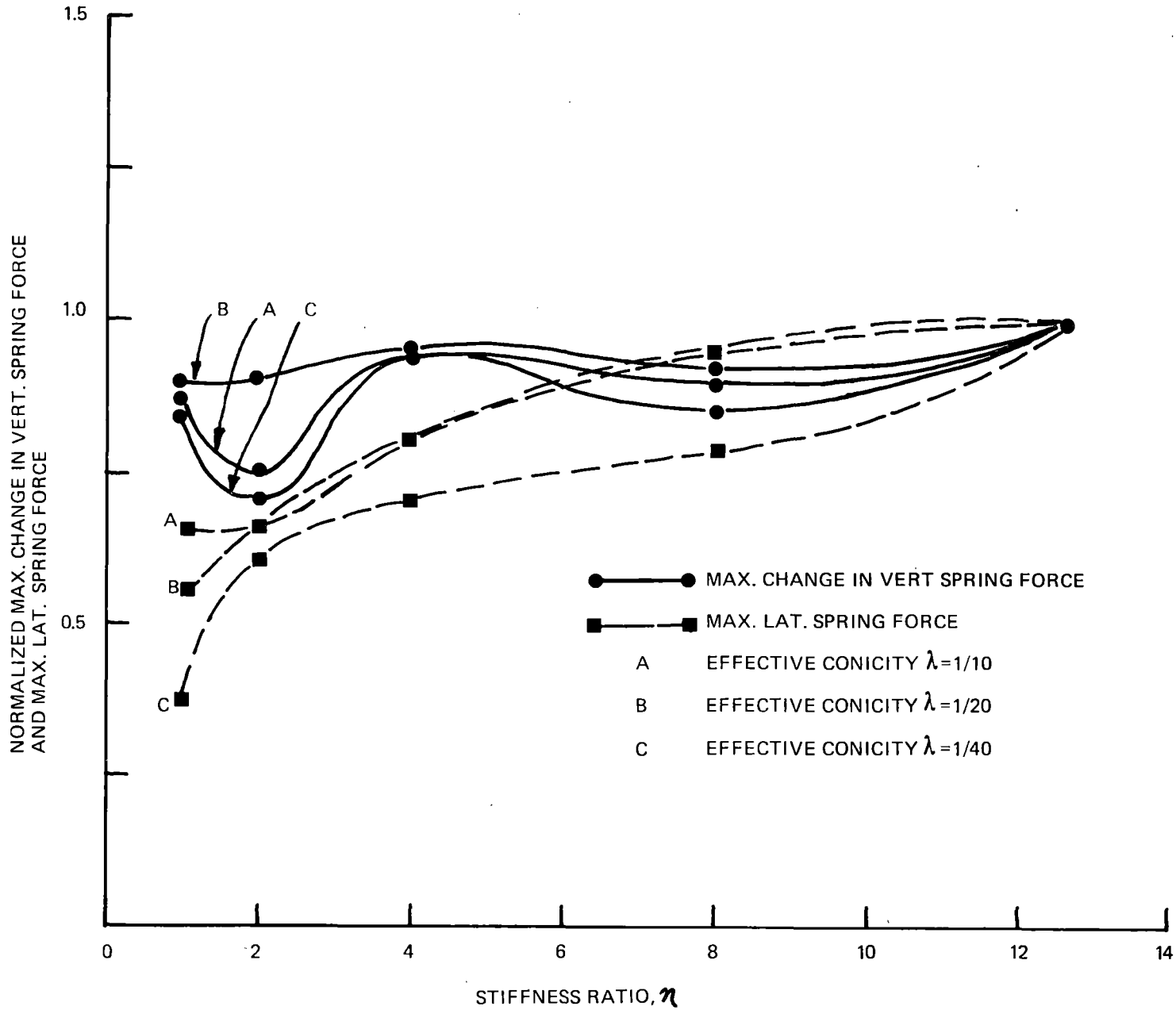

FIGURE 11A – NORMALIZED MAXIMUM CHANGE IN VERTICAL SPRING FORCE AND MAXIMUM LATERAL SPRING FORCE AT WHEEL–AXLE SETS VS. STIFFNESS RATIO, η AT 18 MPH (28.96 KM/H) SPEED DUE TO 1 INCH (2.54 CM) VERTICAL RAIL INPUT

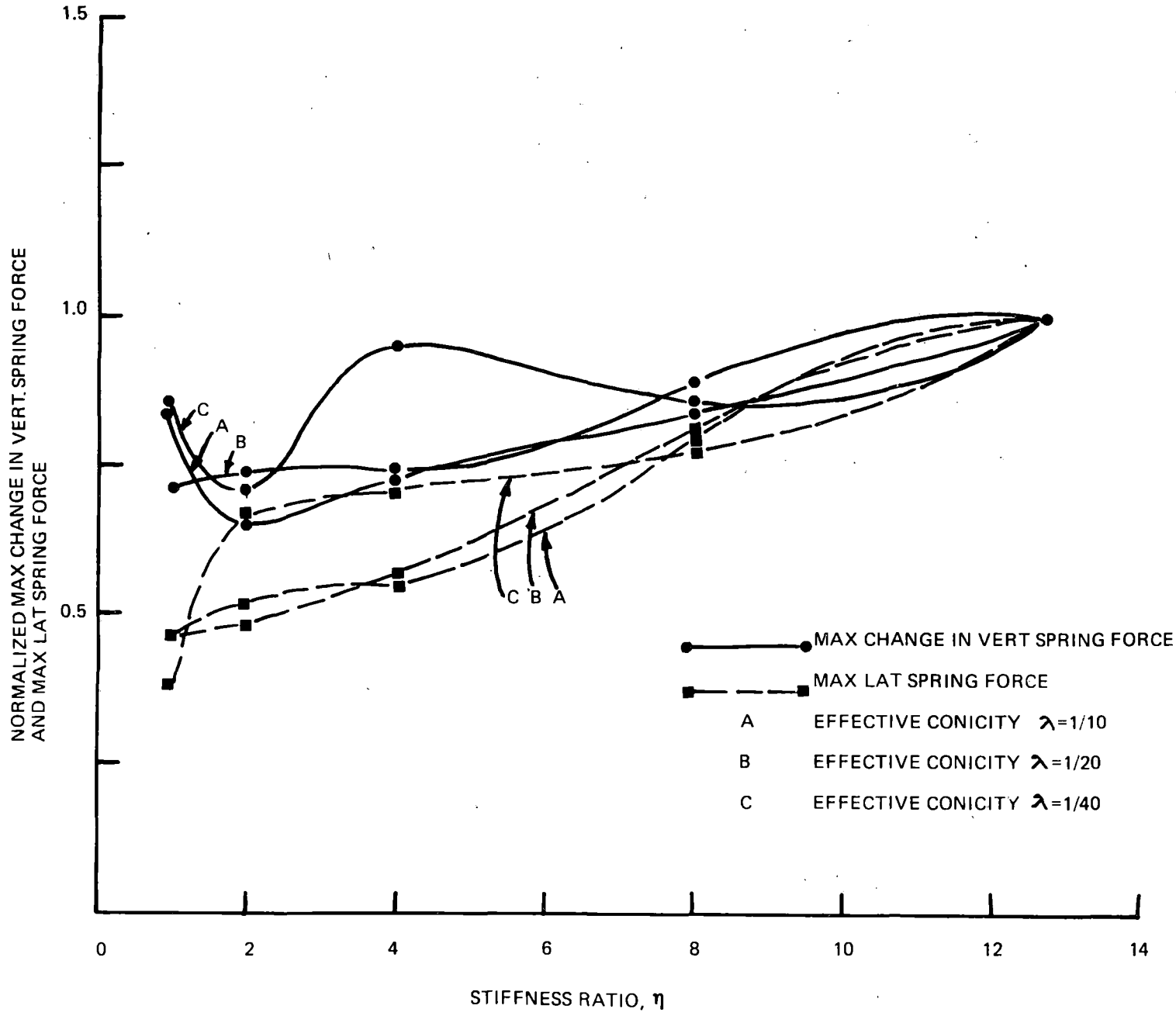

FIGURE 11B – NORMALIZED MAXIMUM CHANGE IN VERTICAL SPRING FORCE AND MAXIMUM LATERAL SPRING FORCE AT WHEEL–AXLE SETS VS. STIFFNESS RATIO, η AT 18 MPH (28.96 KM/H) SPEED DUE TO 2 INCH (5.08 CM) VERTICAL RAIL INPUT

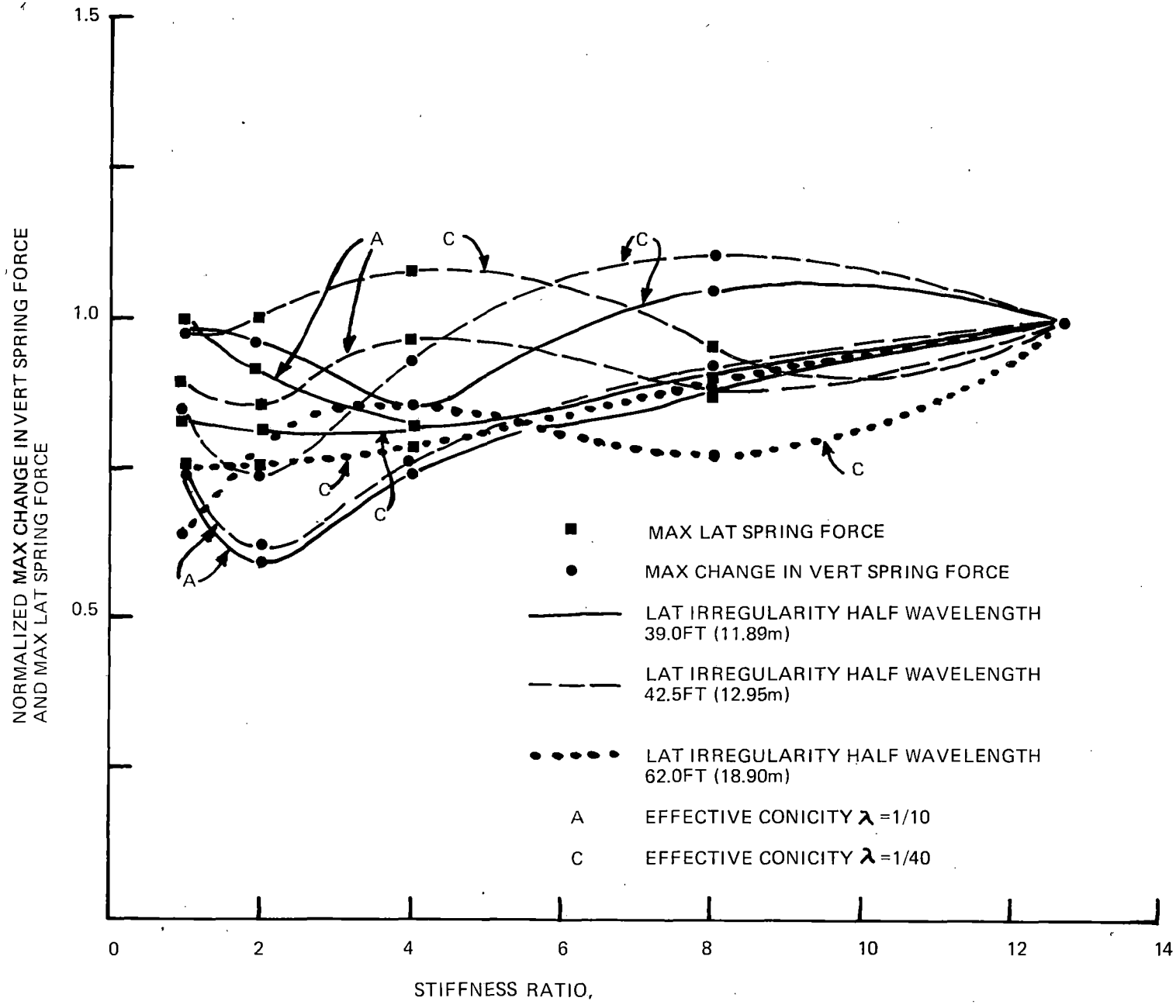

FIGURE 11C – NORMALIZED MAXIMUM CHANGE IN VERTICAL SPRING FORCE AND MAXIMUM LATERAL SPRING FORCE AT WHEEL–AXLE SETS VS. STIFFNESS RATIO, η AT 18 MPH (28.96 KM/H) SPEED DUE TO 2 INCH (5.08 CM) VERTICAL AND 3 INCH (7.62 CM) LATERAL RAIL INPUT

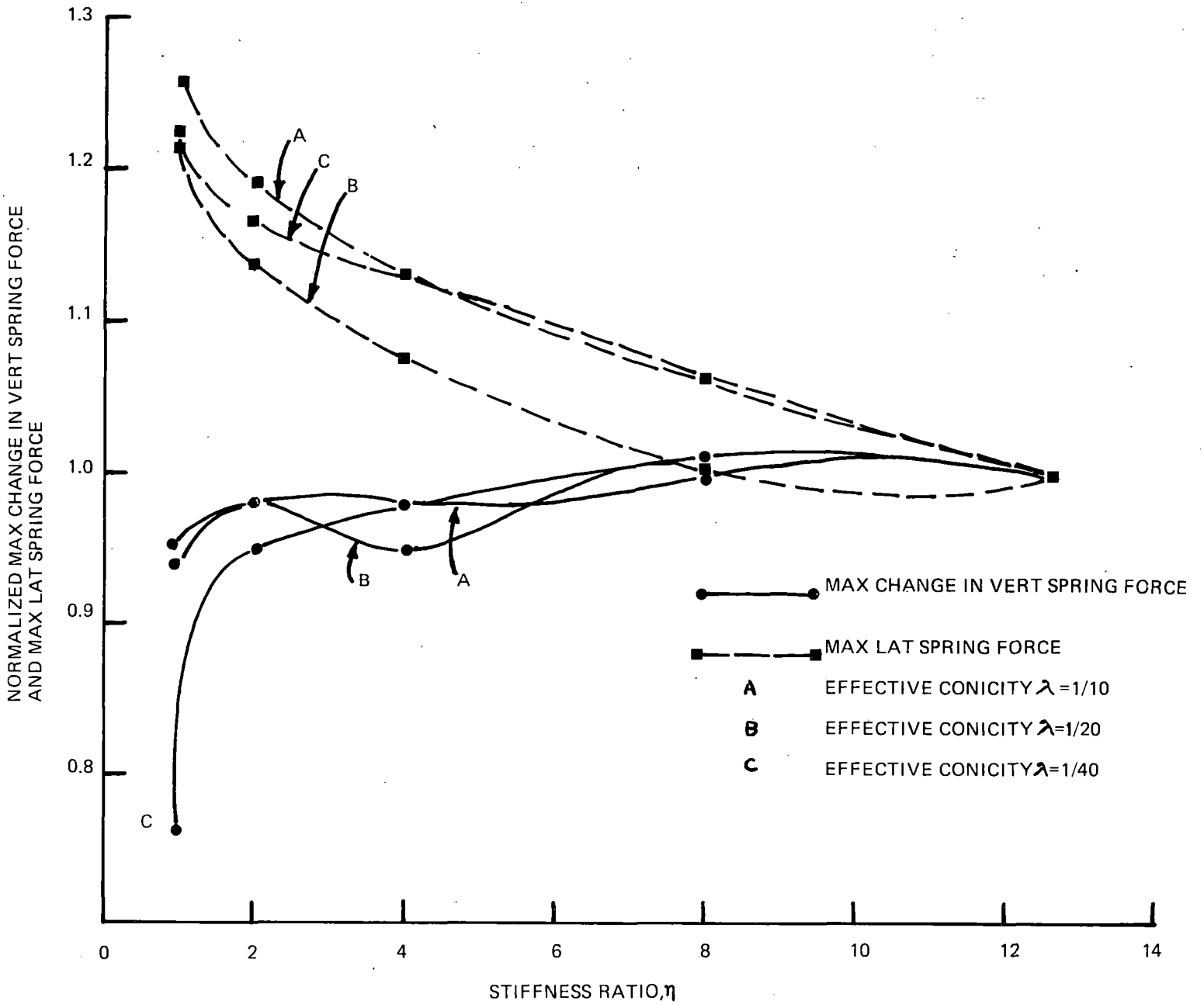

FIGURE 12A – NORMALIZED MAXIMUM CHANGE IN VERTICAL SPRING FORCE AND MAXIMUM LATERAL SPRING FORCE AT WHEEL–AXLE SETS VS. STIFFNESS RATIO, η AT 80 MPH (128.72 KM/H) SPEED DUE TO 1 INCH (2.54 CM) VERTICAL RAIL INPUT

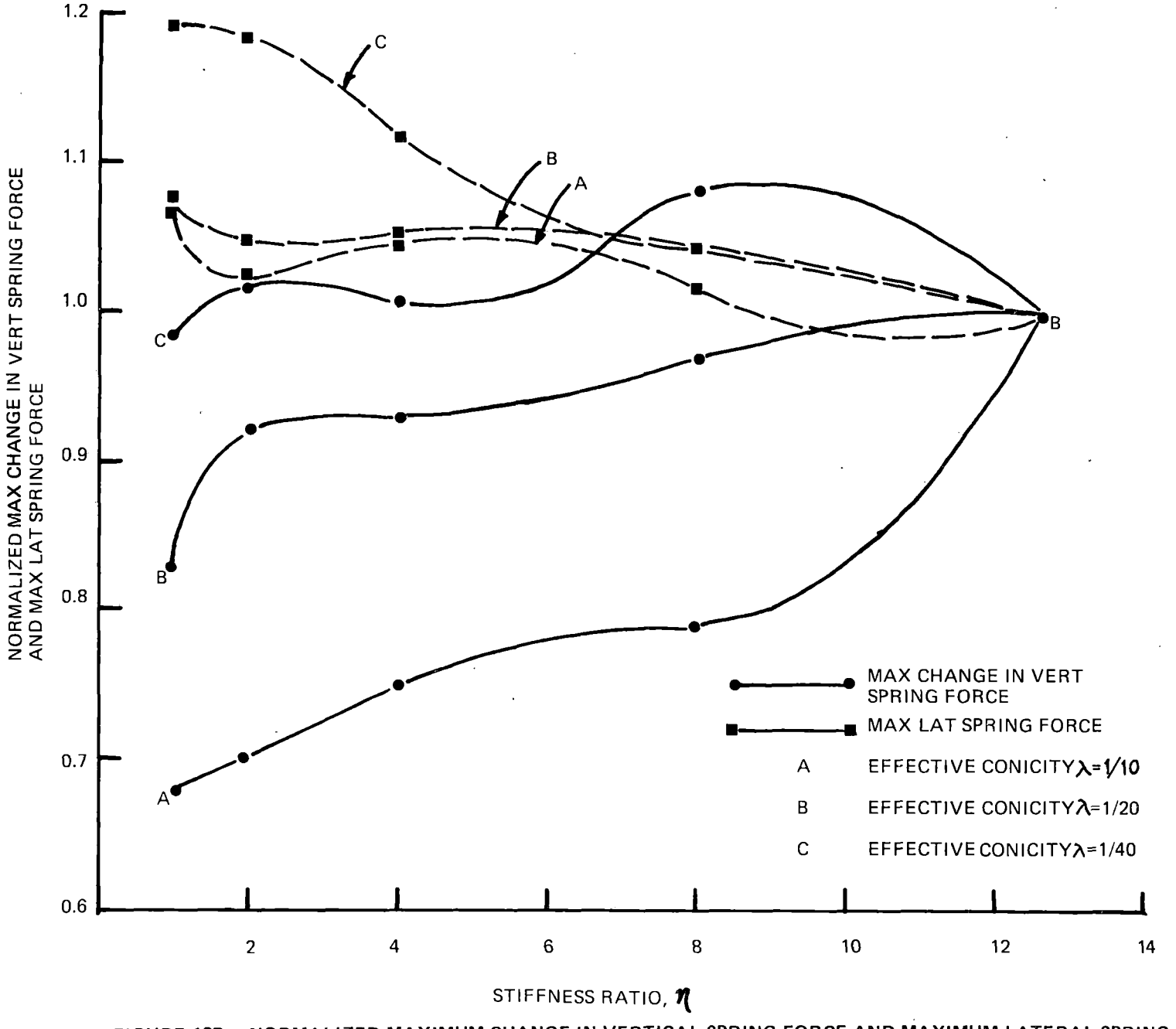

FIGURE 12B – NORMALIZED MAXIMUM CHANGE IN VERTICAL SPRING FORCE AND MAXIMUM LATERAL SPRING FORCE AT WHEEL–AXLE SETS VS. STIFFNESS RATIO, η AT 80 MPH (128.72 KM/H) SPEED DUE TO 2 INCH (5.08 CM) VERTICAL RAIL INPUT

FIGURE 12C NORMALIZED MAXIMUM CHANGE IN VERTICLE SPRING FORCE AND AND MAX LAT. SPRING FORCE AT WHEEL AXIS SETS VS. STIFFNESS RATIO, AT 80 MPH (128.72KM/H) SPEED DUE TO 1 INCH(2.54 CM) VERTICAL AND 3/4 INCH (1.91 CM) LATERAL RAIL INPUT'

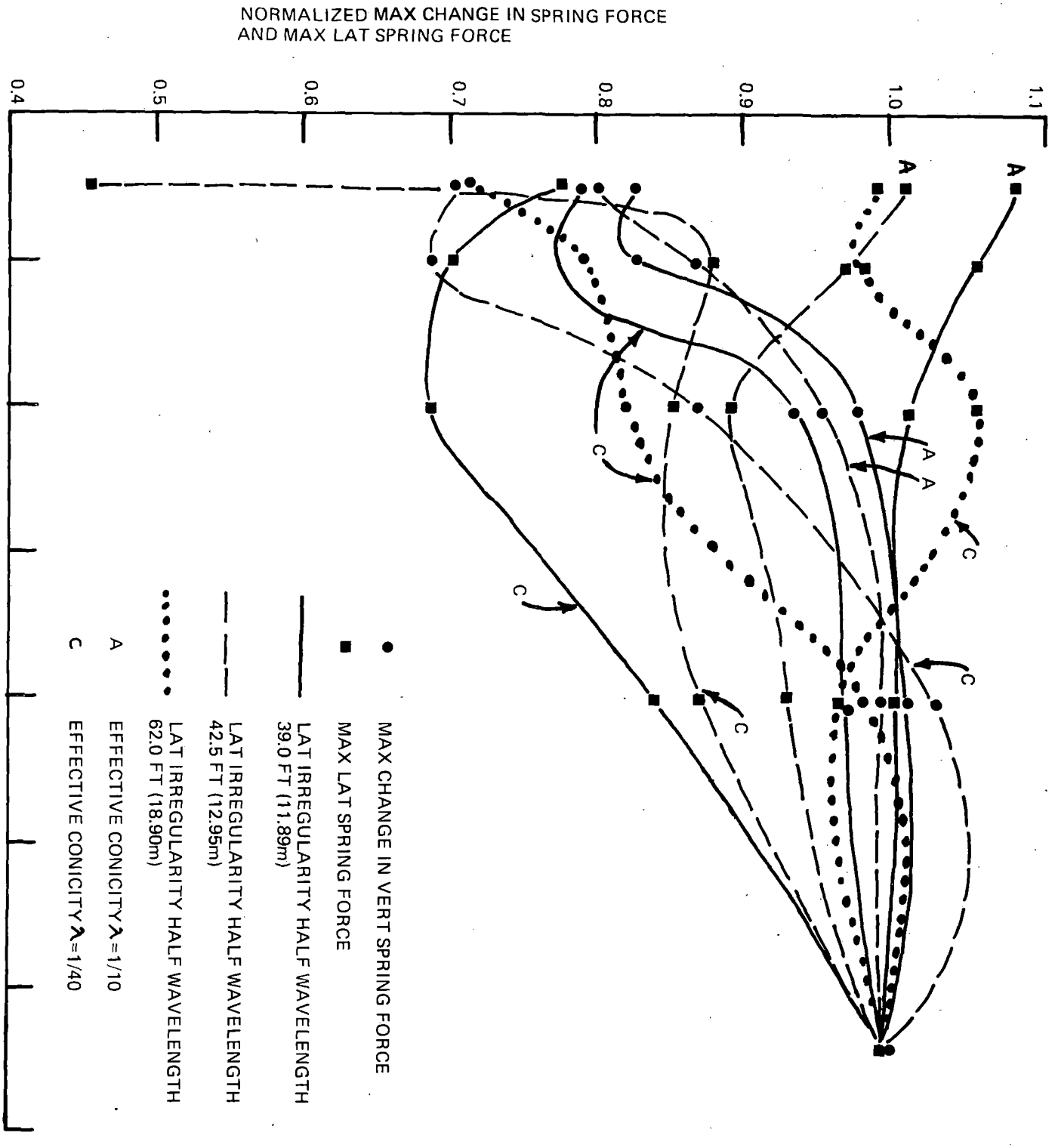

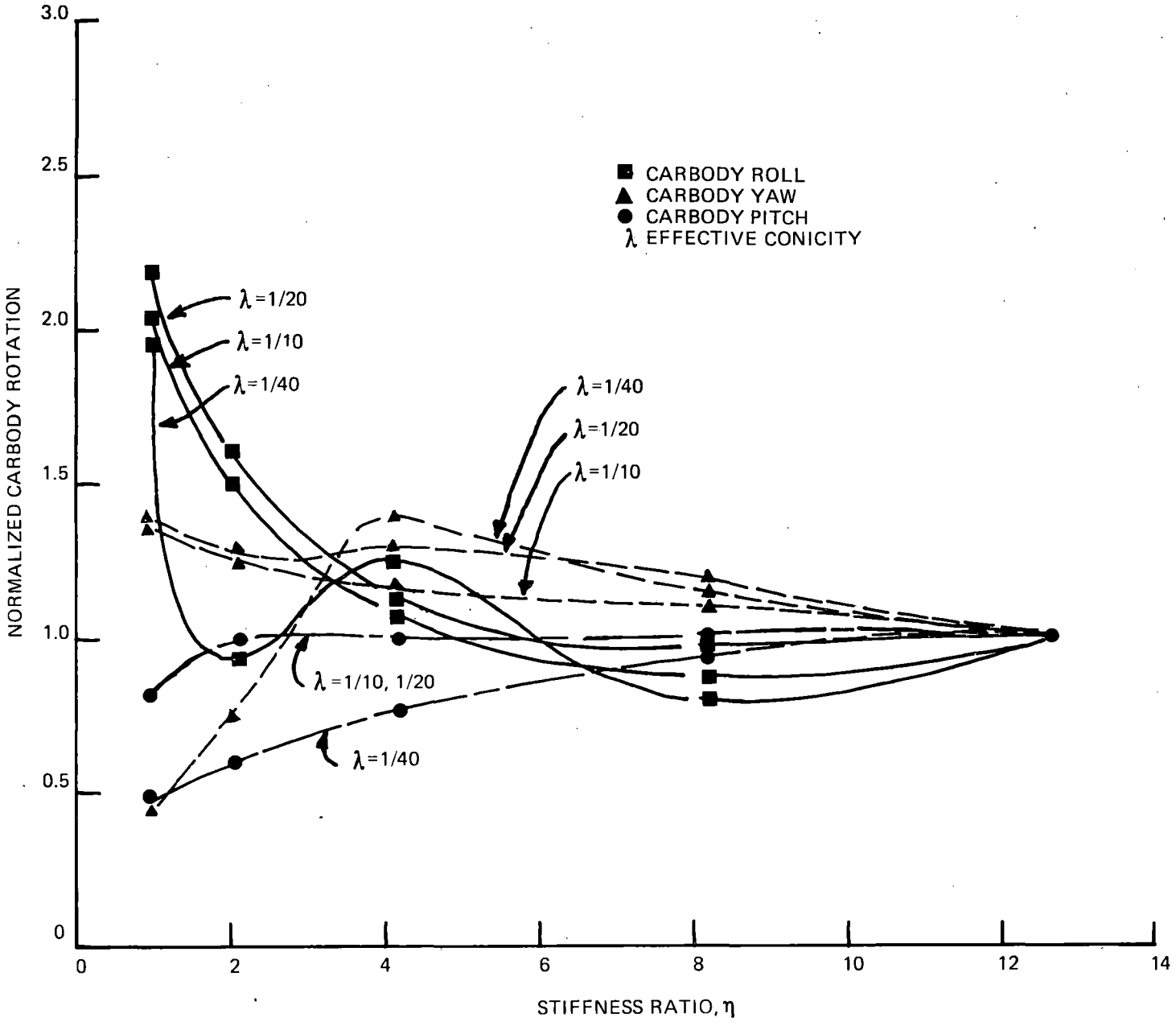

FIGURE 13A – NORMALIZED CARBODY ROTATION VS. STIFFNESS RATIO, η AT 18 MPH (28.96 KM/H) SPEED DUE TO 1 INCH (2.54 CM) VERTICAL RAIL INPUT

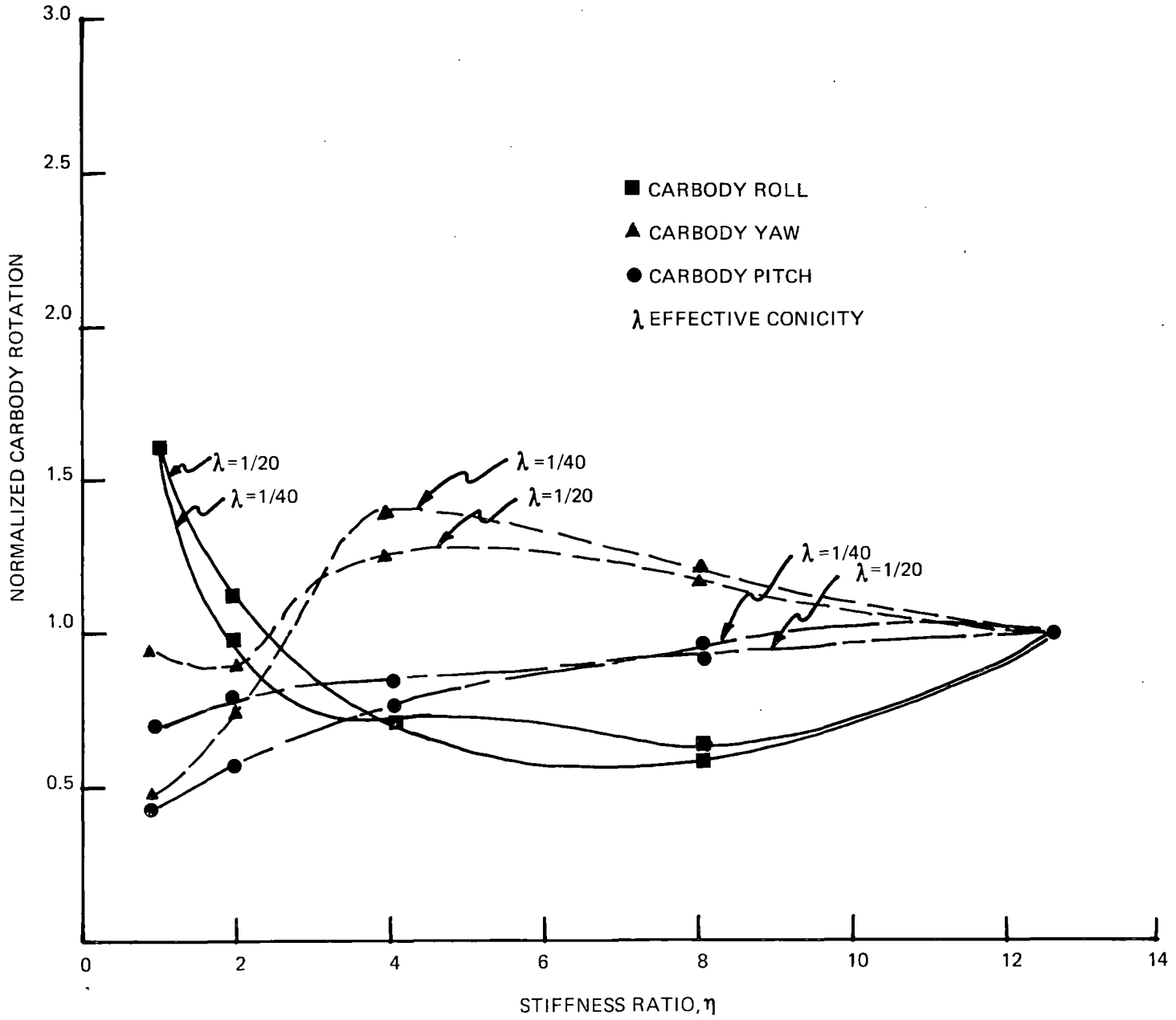

FIGURE 13B – NORMALIZED CARBODY ROTATION VS. STIFFNESS RATIO, η AT 18 MPH (28.96 KM/H) SPEED DUE TO 2 INCH (5.08 CM) VERTICAL RAIL INPUT

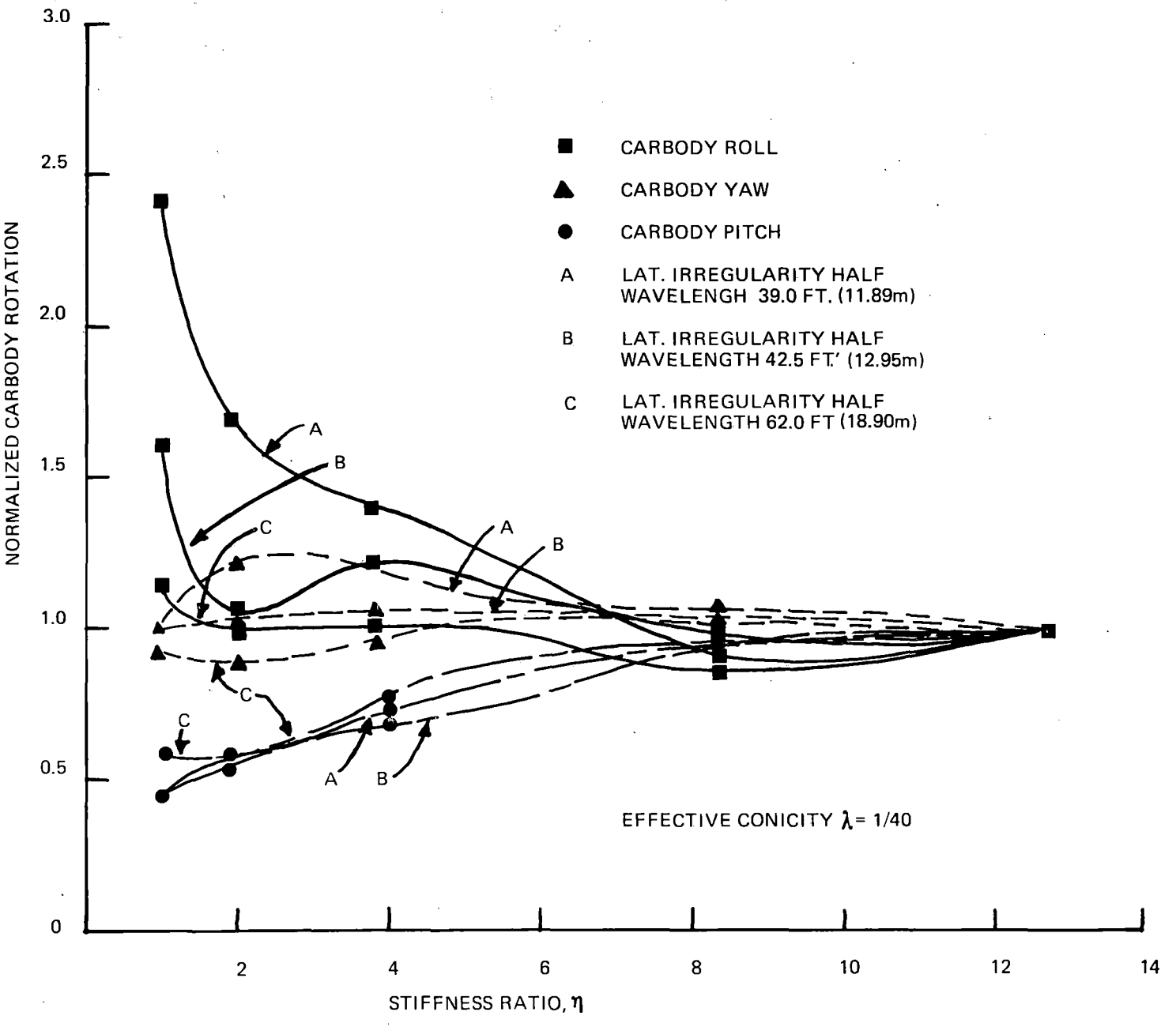

FIGURE 13C – NORMALIZED CARBODY ROTATION VS. STIFFNESS RATIO, η AT 18 MPH (28.96KM/H) SPEED DUE TO 2 INCH (5.08 CM) VERTICAL AND 3 INCH (7.62 CM) LATERAL RAIL INPUT

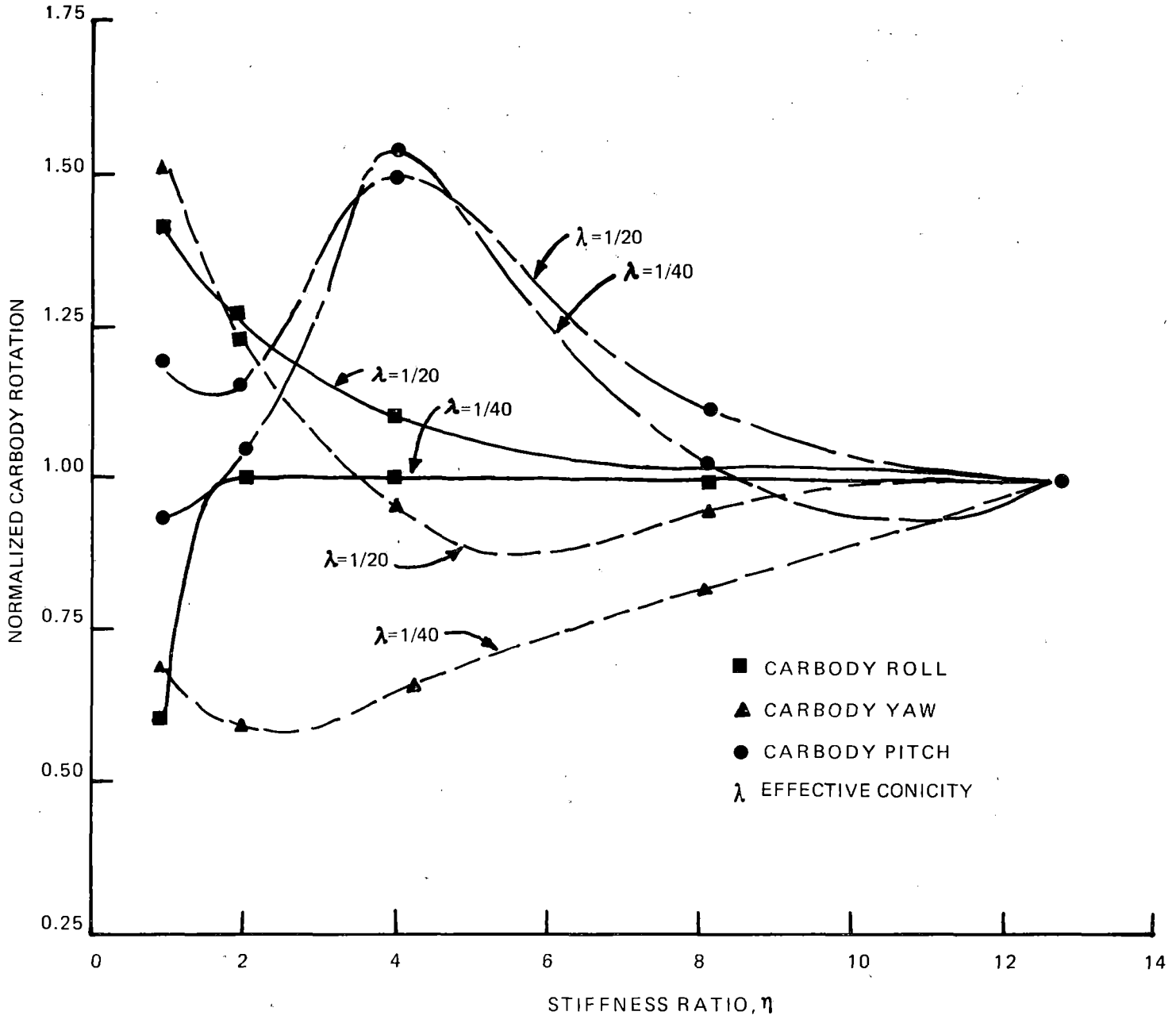

FIGURE 14A – NORMALIZED CARBODY ROTATION VS. STIFFNESS RATIO, η AT 80 MPH (128.72 KM/H)SPEED DUE TO 1 INCH (2.54CM) VERTICAL RAIL INPUT

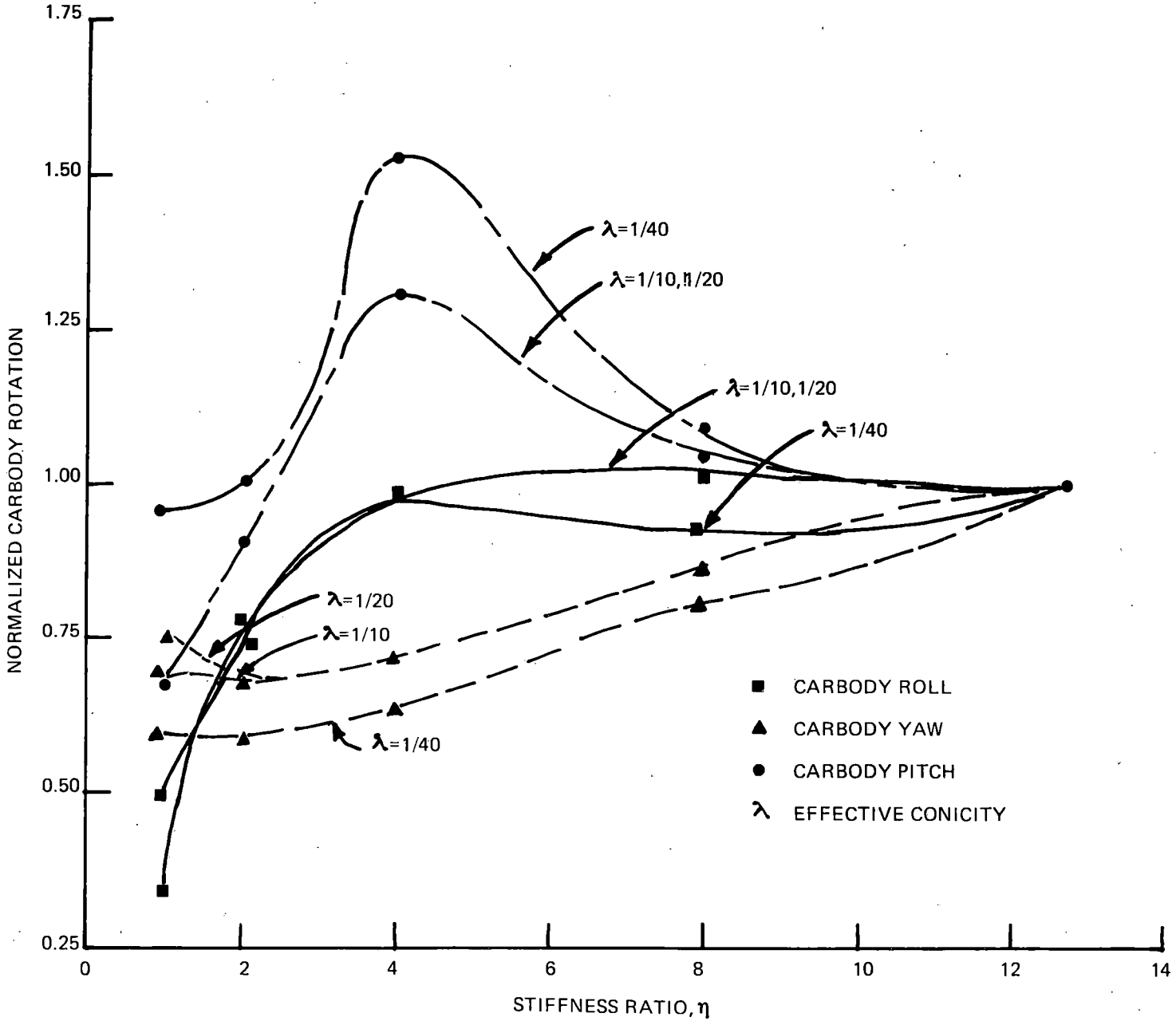

FIGURE 14B – NORMALIZED CARBODY ROTATION VS. STIFFNESS RATIO, η AT 80 MPH (128.72 KM/H) SPEED DUE TO 2 INCH (5.08 CM) VERTICAL RAIL INPUT

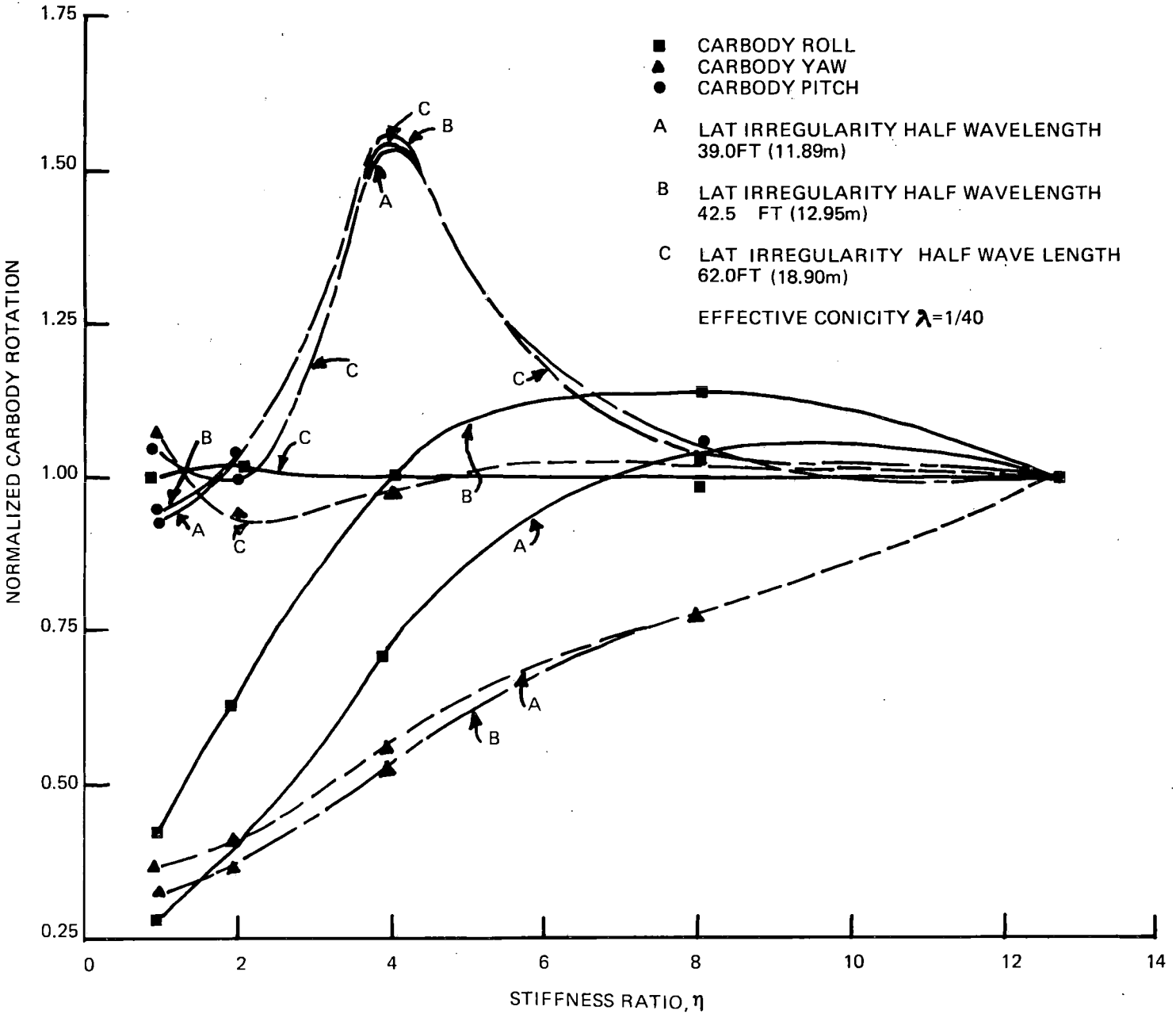

FIGURE 14C – NORMALIZED CARBODY ROTATION VS. STIFFNESS RATIO, η AT 80 MPH (128.72 KM/H) SPEED DUE TO 1 INCH (2.54 CM) VERTICAL AND ¾ INCH (1.91 CM) LATERAL RAIL INPUT

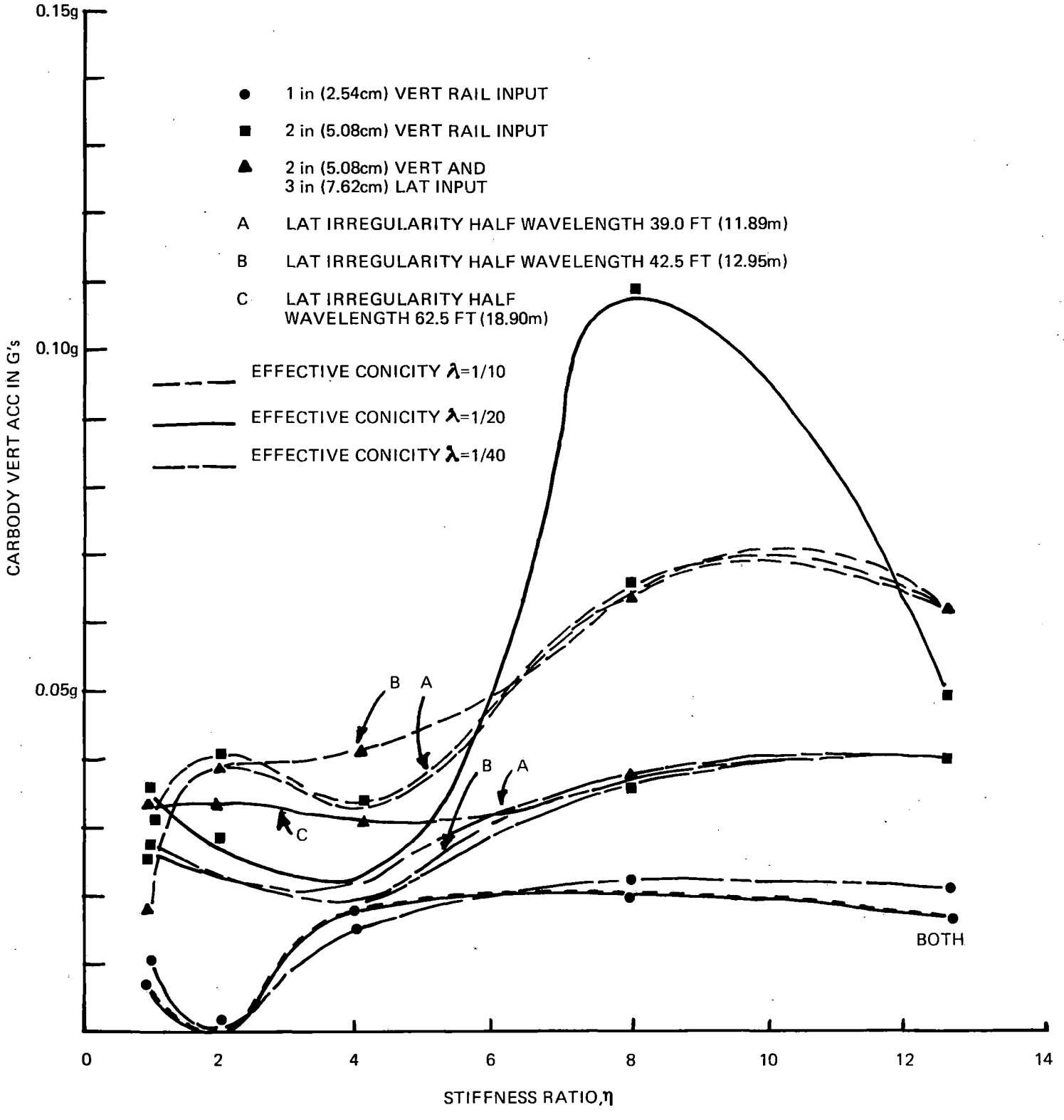

FIGURE 15A – MAXIMUM CARBODY VERTICAL ACCELERATION AT 18 MPH (28.96 KM/H) VS. STIFFNESS RATIO, η

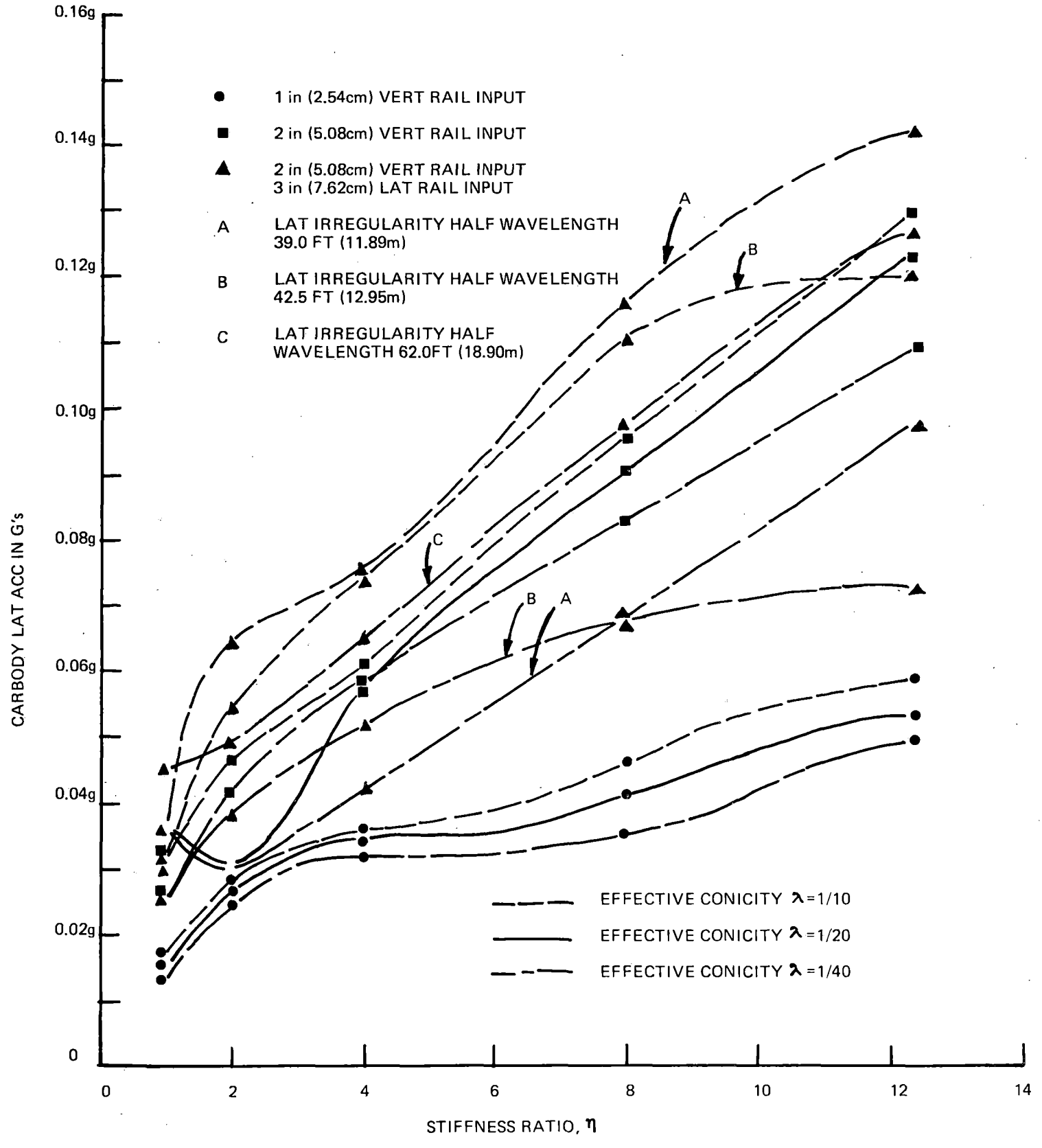

FIGURE 15B – MAXIMUM CARBODY LATERAL ACCELERATION AT 18 MPH (28.96 KM/H) VS. STIFFNESS RATIO, η

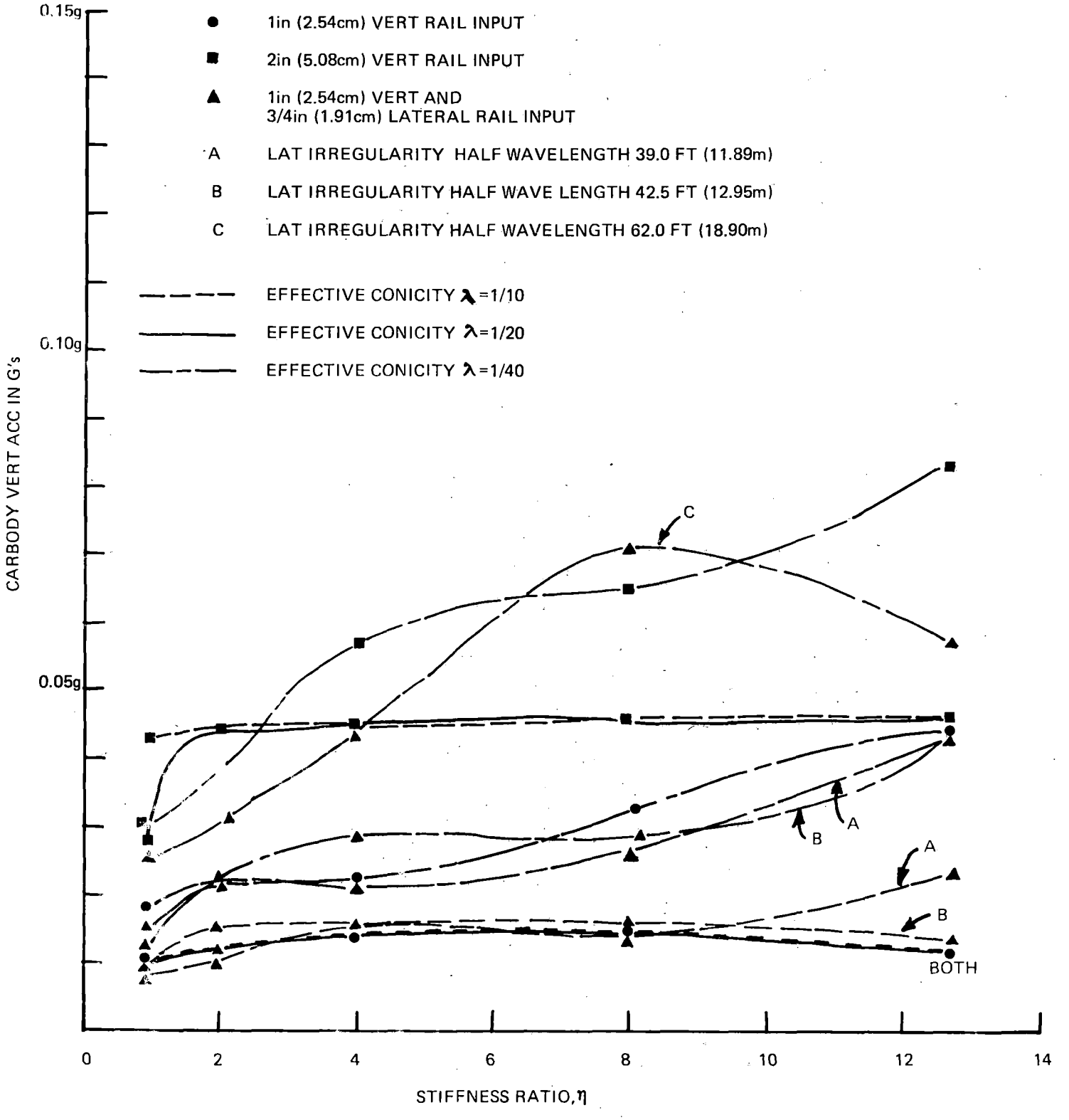

FIGURE 15C – MAXIMUM CARBODY VERTICAL ACCELERATION AT 80 MPH (128.72 KM/H) VS. STIFFNESS RATIO, η

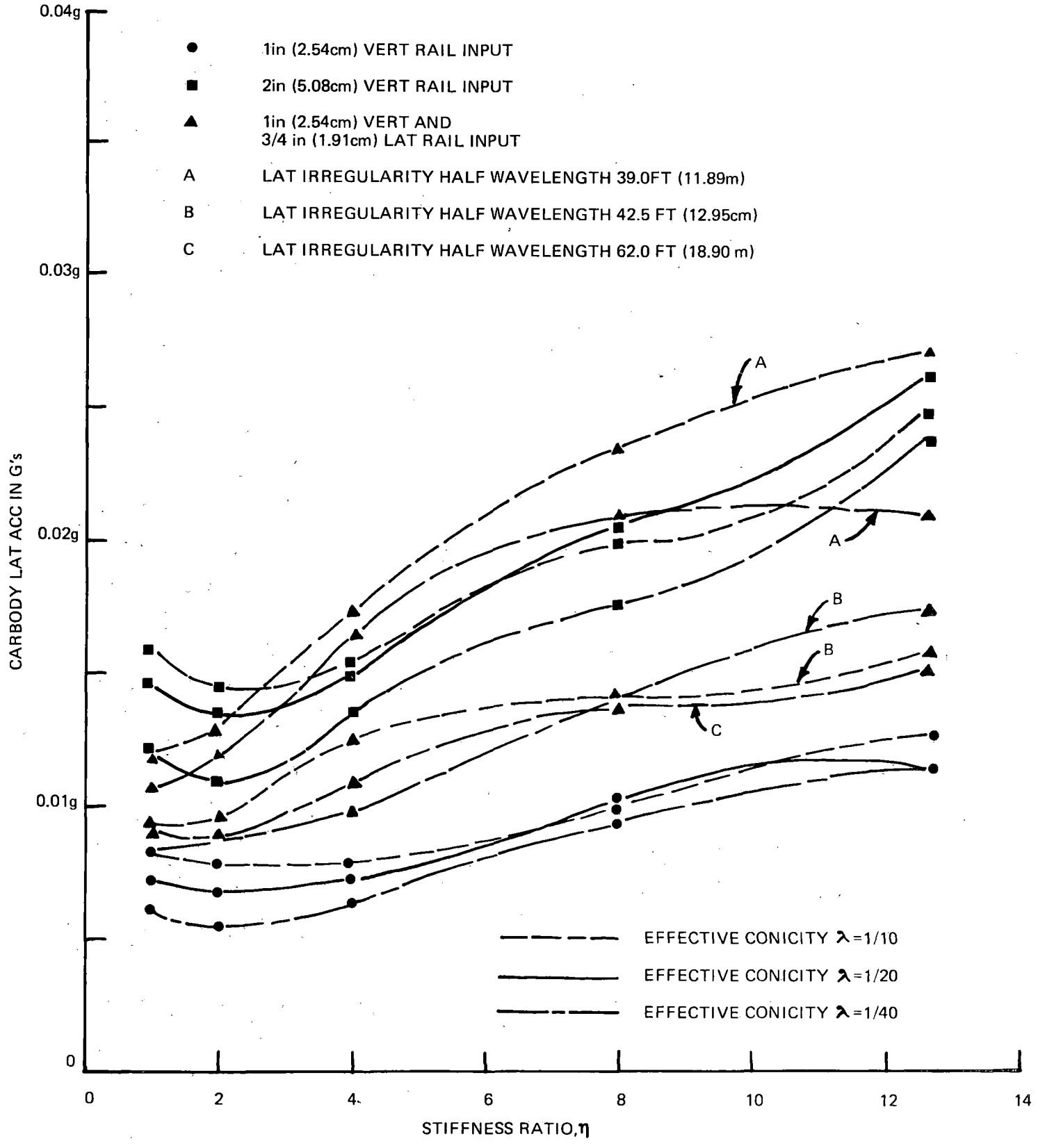

FIGURE 15D – MAXIMUM CARBODY LATERAL ACCELERATION AT 80 MPH (128.72 KM/H) VS. STIFFNESS RATIO, η

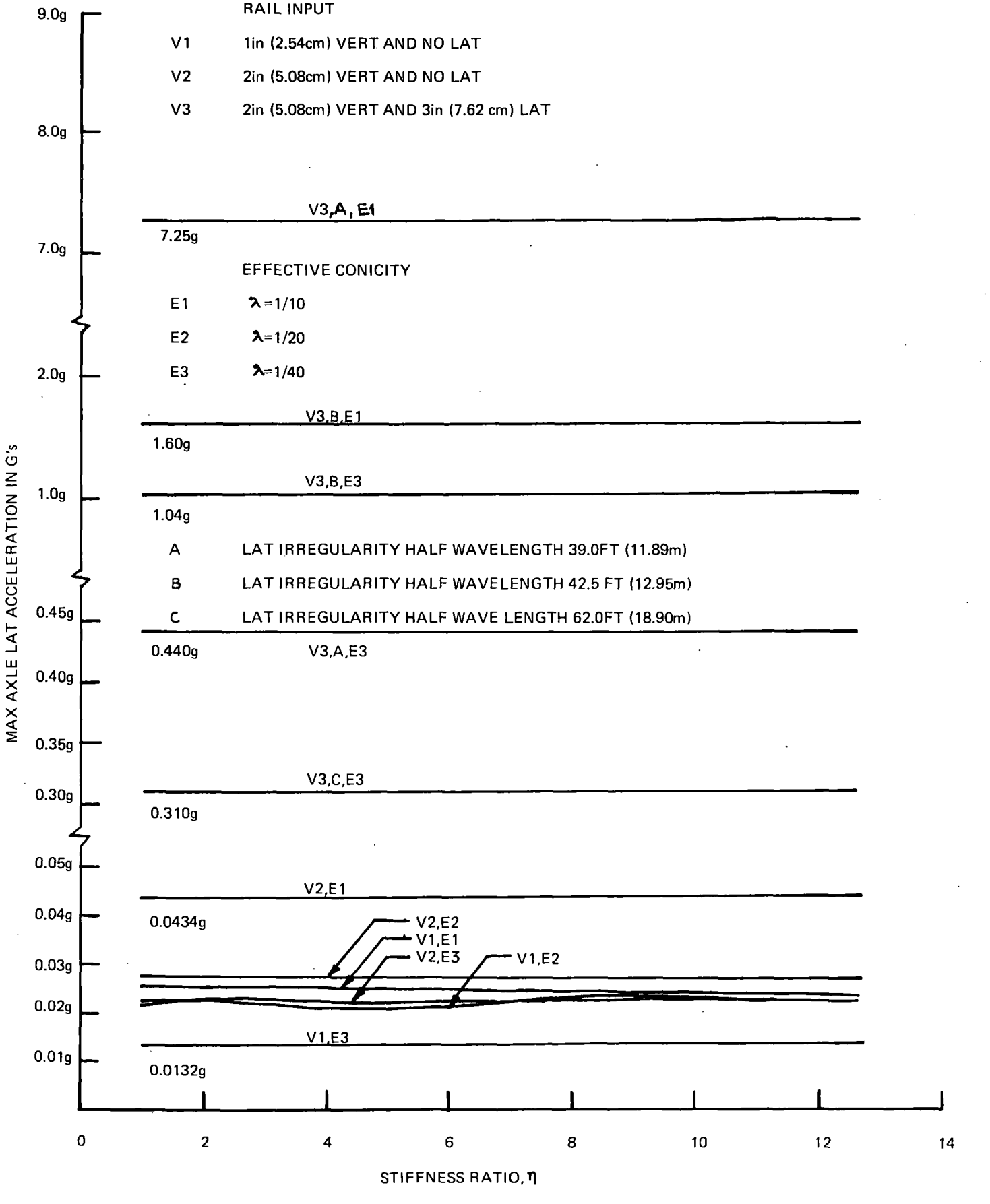

FIGURE 16A – MAXIMUM AXLE LATERAL ACCELERATION AT 18 MPH (28.96 KM/H) VS. STIFFNESS RATIO, η

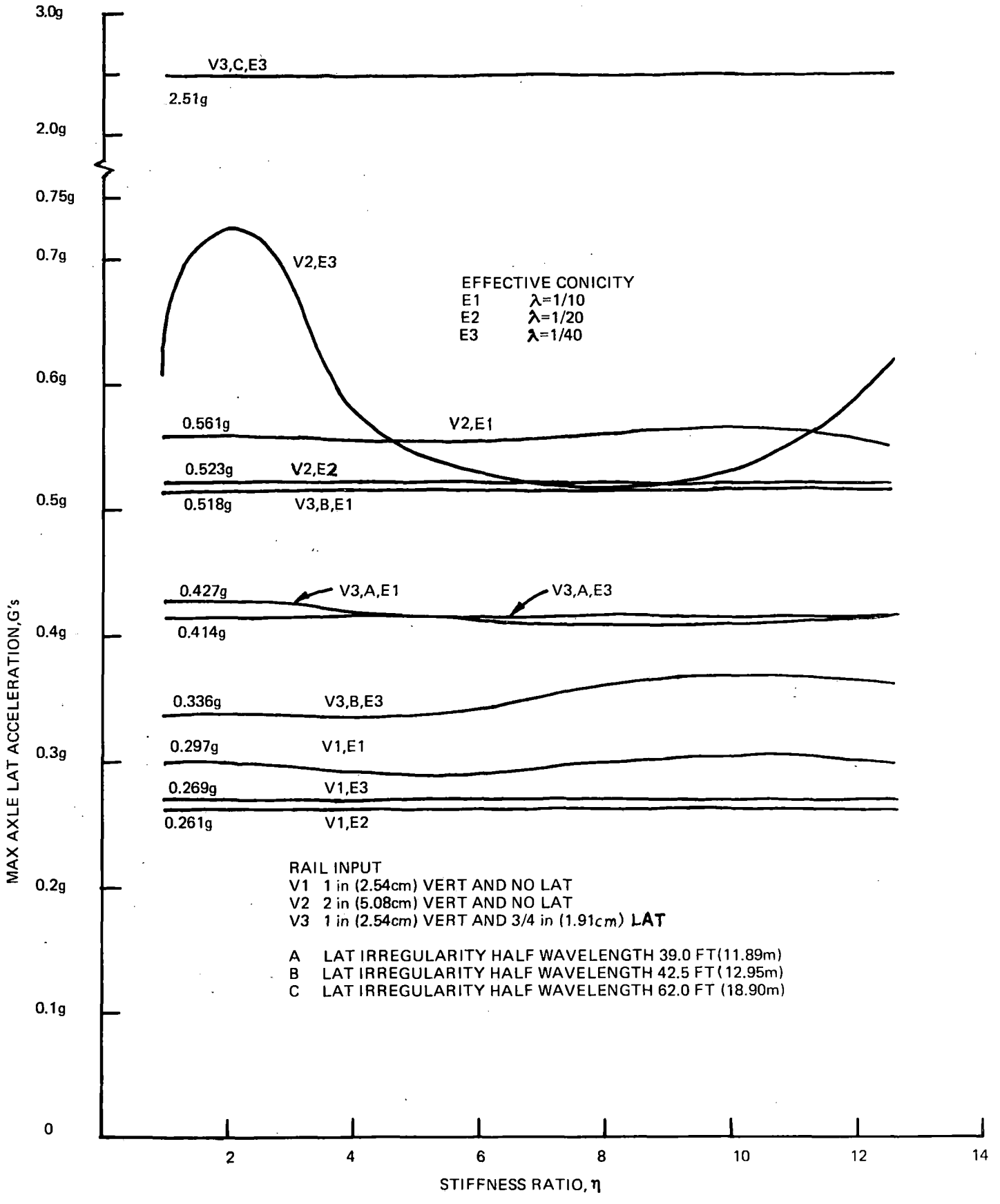

FIGURE 16B – MAXIMUM AXLE LATERAL ACCELERATION AT 80 MPH (128.72 KM/H) VS. STIFFNESS RATIO, η

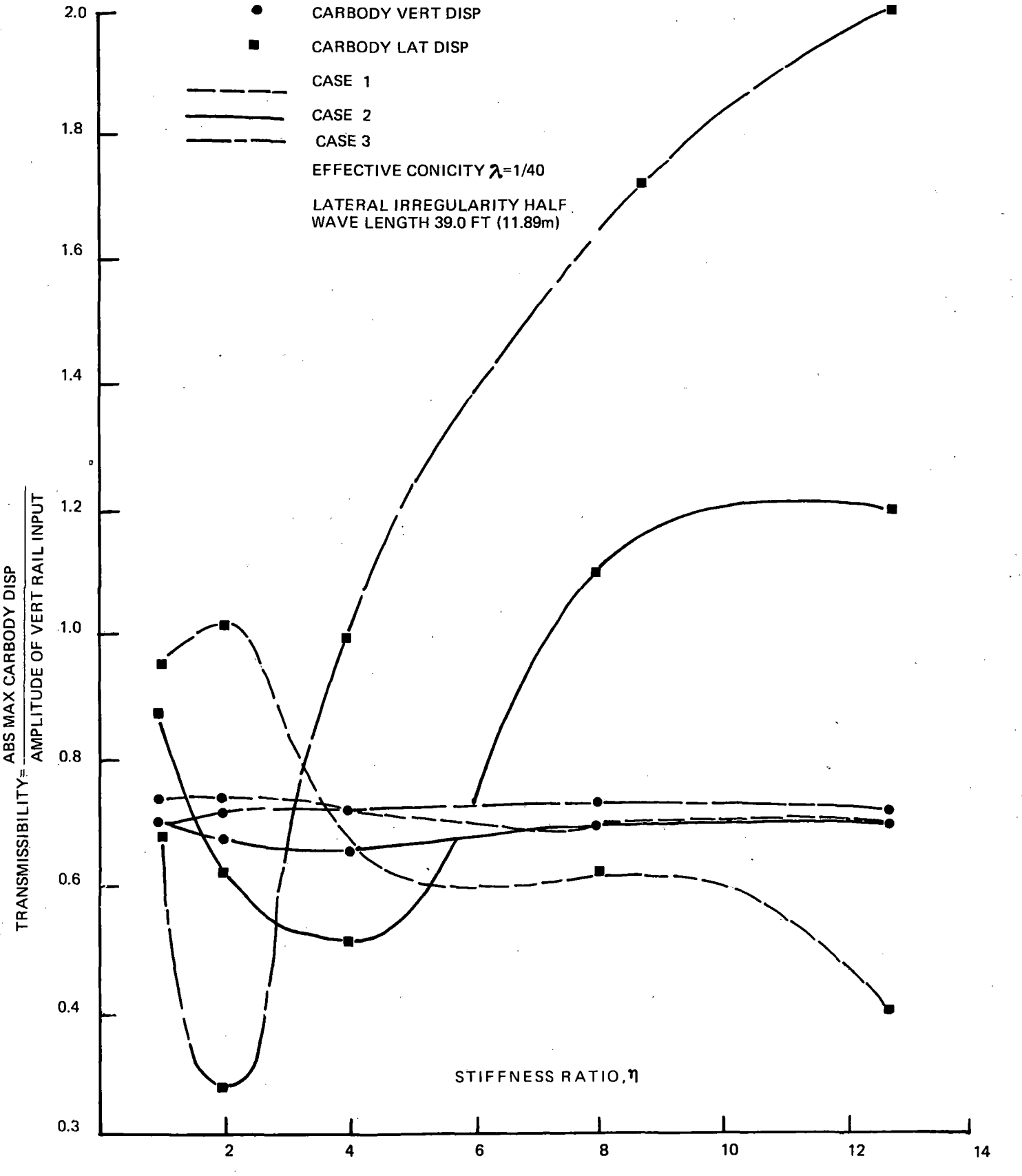

FIGURE 17 – EFFECTS OF PRIMARY SUSPENSION ON TRANSMISSIBILITY AT 18 MPH (28.96 KM/H) SPEED DUE TO 2 INCH (5.08 CM) VERTICAL AND 3 INCH (7.62 CM) LATERAL RAIL INPUT

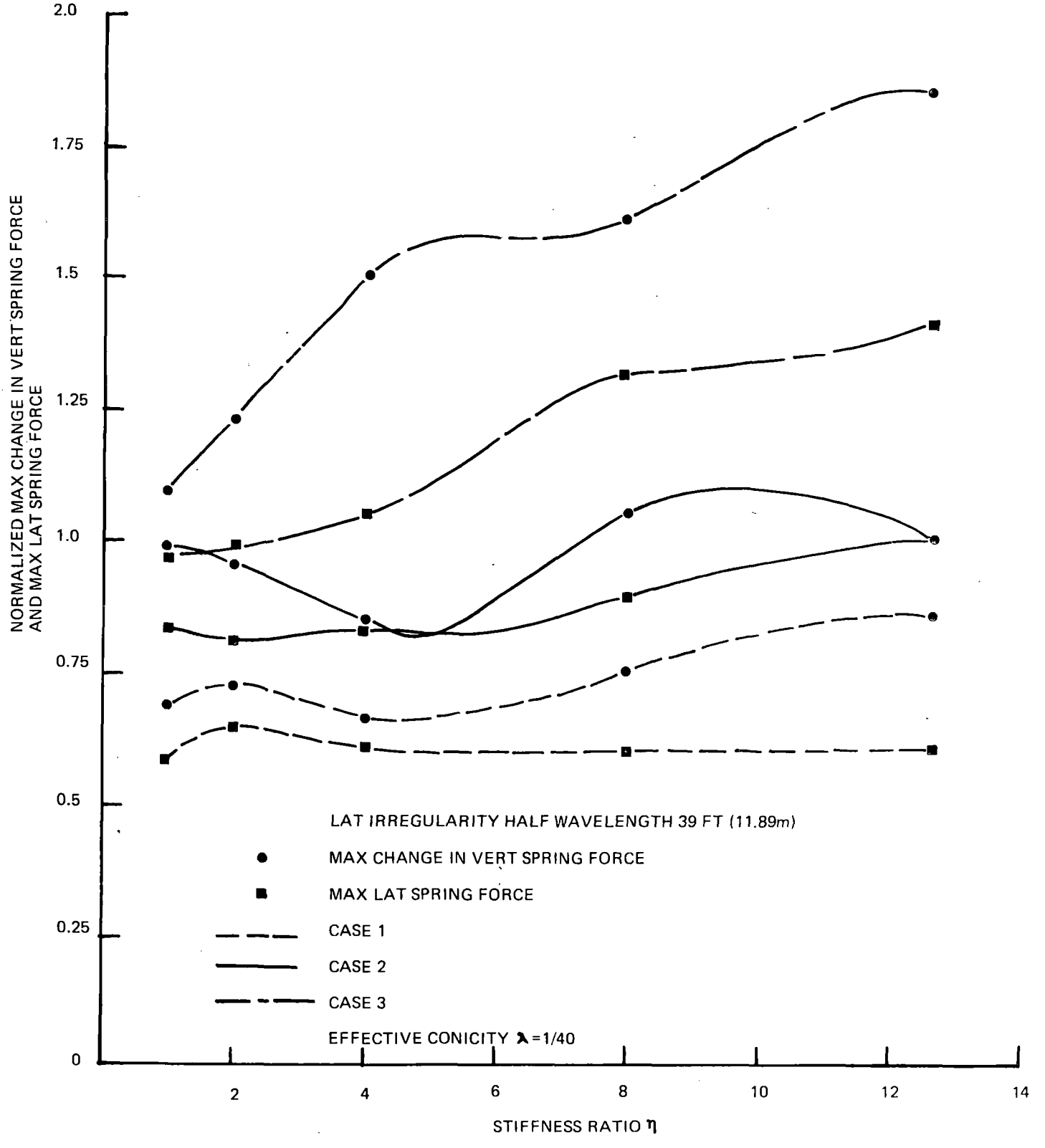

FIGURE 18- EFFECTS OF PRIMARY SUSPENSION ON THE NORMALIZED CHANGE IN VERTICAL SPRING FORCE AND MAXIMUN LATERAL FORCE AT WHEEL-AXLE SETS AT 18MPH(28.96KM/H) SPEED DUE TO 2INCH(5.08CM) VERTICAL AND 3 INCH(7.62CM) RAIL INPUT

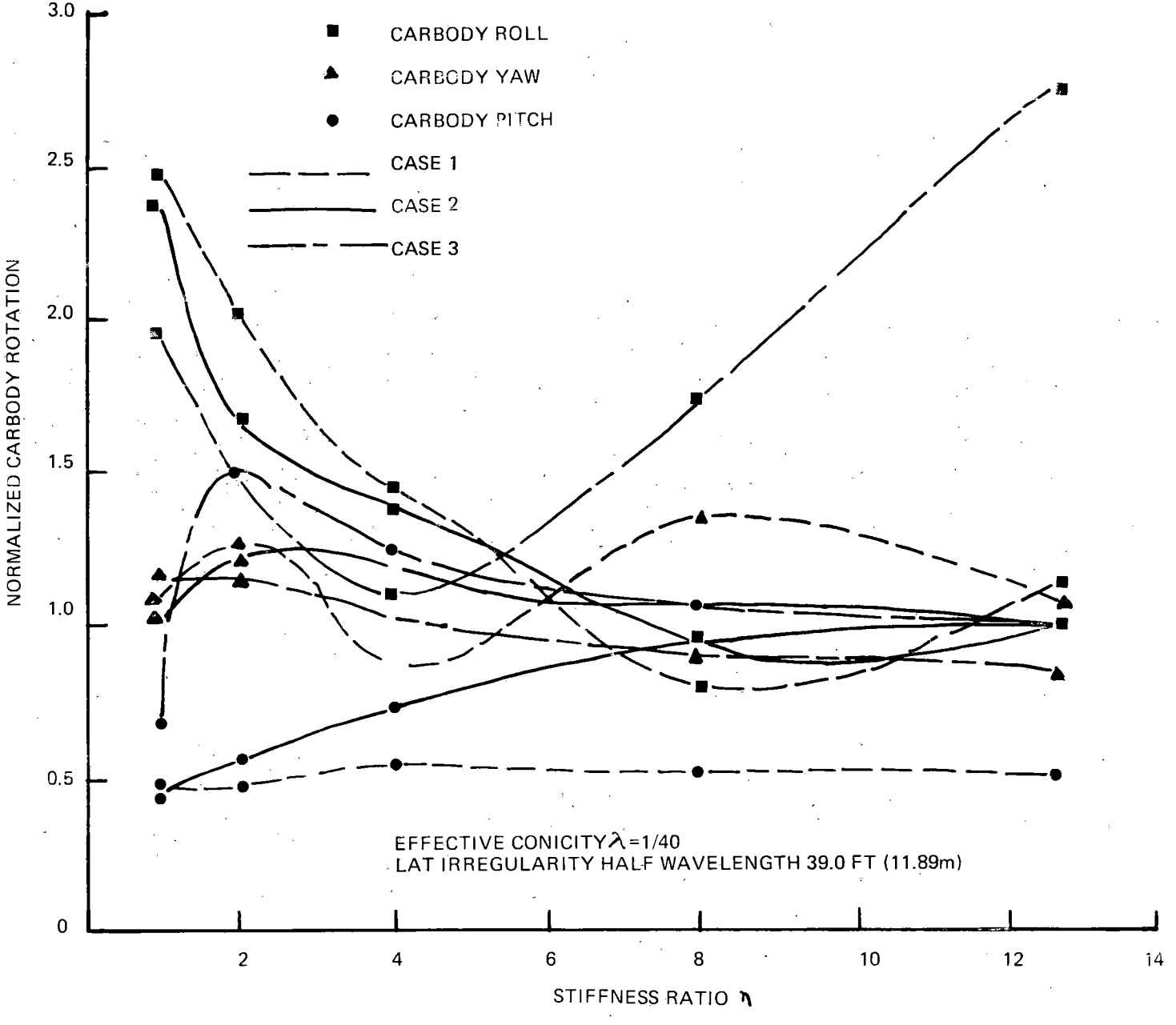

FIGURE 19 – EFFECTS OF PRIMARY SUSPENSION ON THE NORMALIZED CARBODY ROTATION AT 18 MPH (28.96 KM/H) SPEED DUE TO 2 INCH (5.08 CM) VERTICAL AND 3 INCH (7.62 CM) LATERAL RAIL INPUT

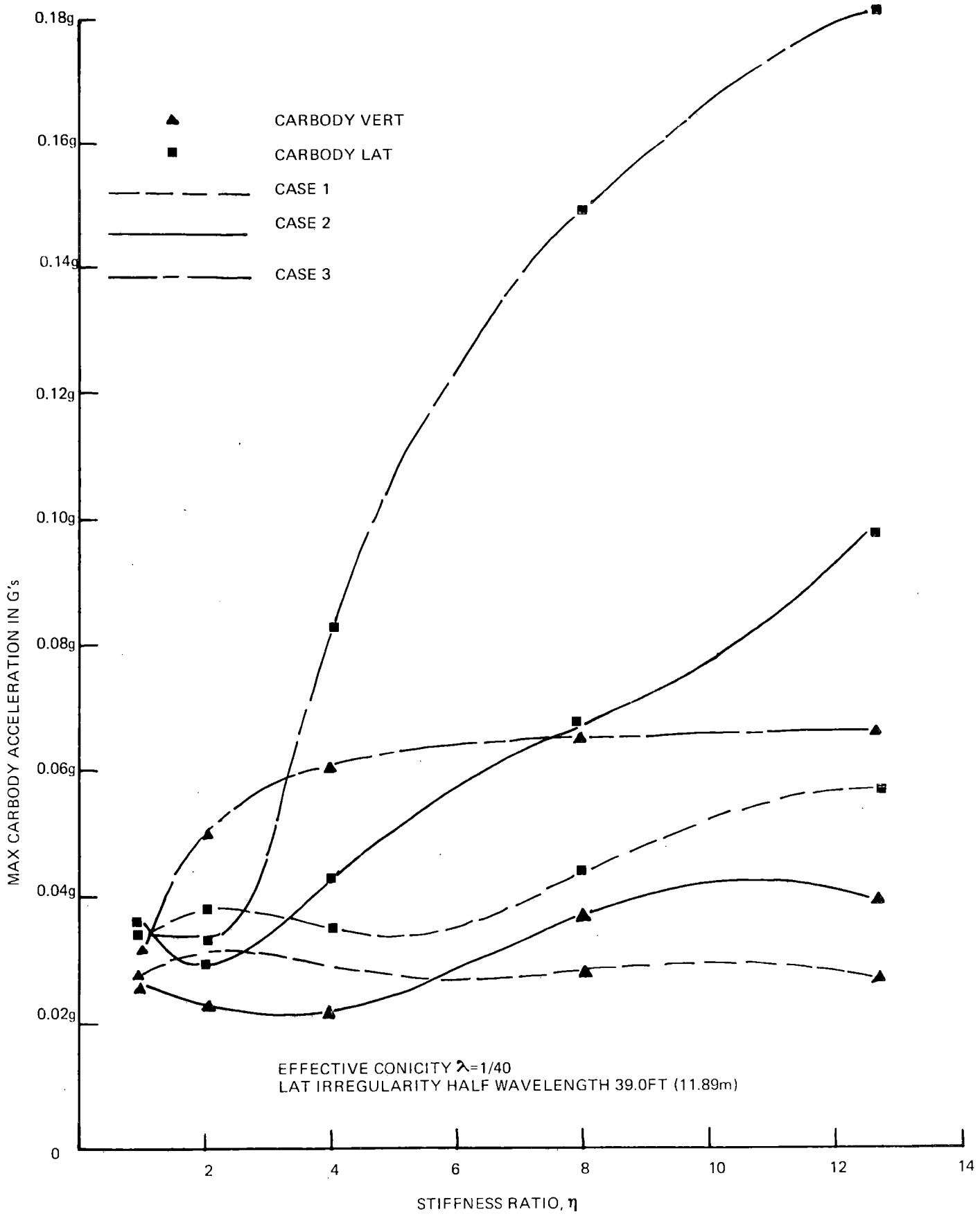

FIGURE 20 – EFFECTS OF PRIMARY SUSPENSION ON THE MAXIMUM CARBODY ACCELERATIONS AT 18 MPH (28.96 KM/H) DUE TO 2 INCH (5.08 CM) VERTICAL AND 3 INCH (7.62 CM) LATERAL RAIL INPUT

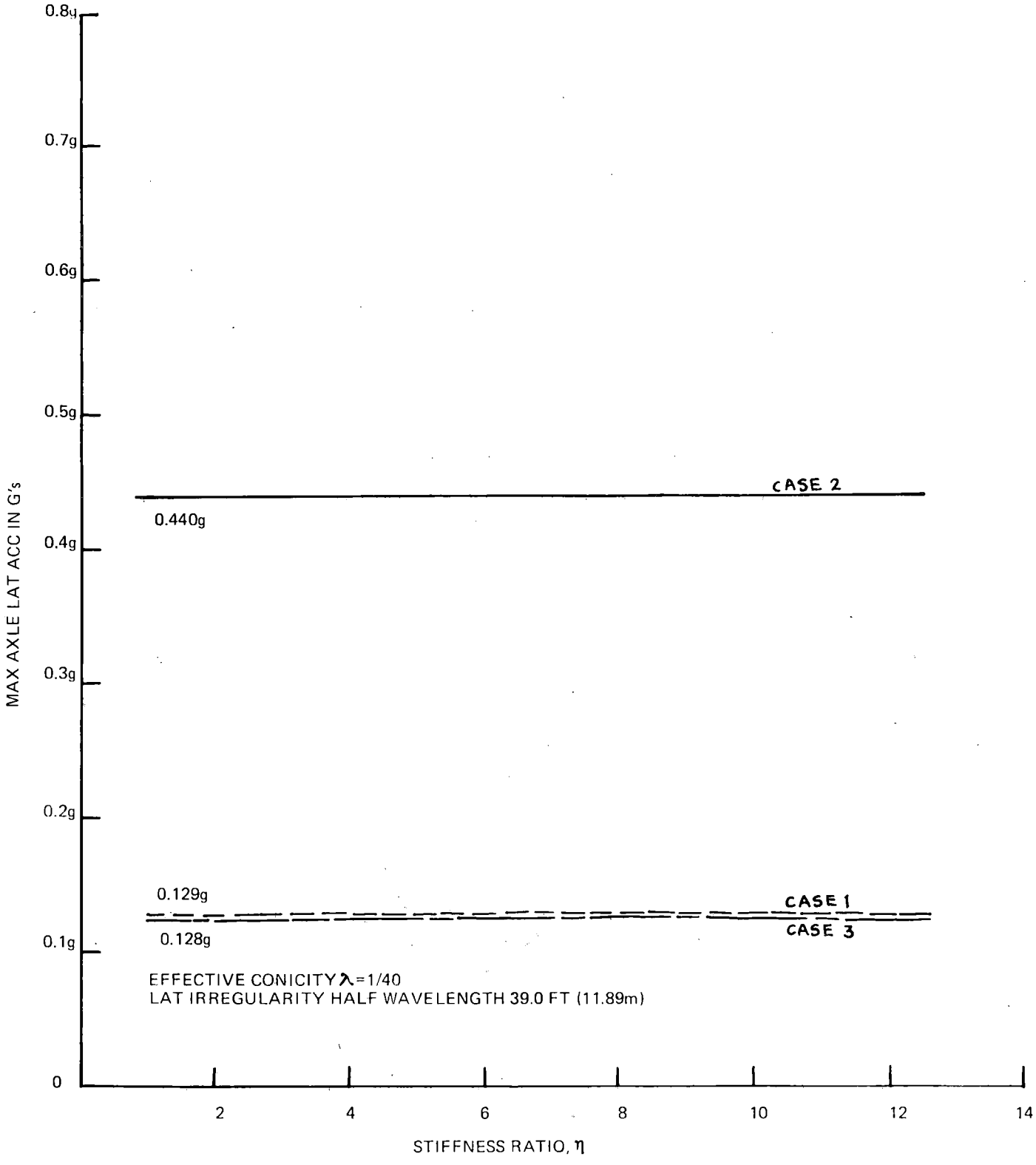

FIGURE 21 – EFFECTS OF PRIMARY SUSPENSION ON THE MAX AXLE LATERAL ACCELERATION AT 18 MPH (28.96 KM/H) DUE TO 2 INCH (5.08 CM) VERTICAL AND 3 INCH (7.62 CM) LATERAL RAIL INPUT

Technical Documentation; Locomotive Response Model, 1978
EH Chang, VK Garg, PW Hartman